To the Graduate Council:

I am submitting herewith a thesis written by Claudette Gail McKamey entitled "A Crystallization Study of Zr-Ni Metallic Glass in the Range 55-71 Atomic Percent Zirconium." I have examined the final copy of this thesis for form and content and recommend that it be accepted in partial fulfillment of the requirements for the degree of Master of Science, with a major in Metallurgical Engineering.

Ben F. Oliver, Major Professor

We have read this thesis
and recommend its acceptance:

Donald M Kroeger

Accepted for the Council:

The Graduate School

STATEMENT OF PERMISSION TO USE

In presenting this thesis in partial fulfillment of the requirements for a Master's degree at The University of Tennessee, Knoxville, I agree that the Library shall make it available to borrowers under rules of the Library. Brief quotations from this thesis are allowable without special permission, provided that accurate acknowledgment of source is made.

Permission for extensive quotation from or reproduction of this thesis may be granted by my major professor, or in his absence, by the Head of Interlibrary Services when, in the opinion of either, the proposed use of the material is for scholarly purposes. Any copying or use of the material in this thesis for financial gain shall not be allowed without my written permission.

Signature Claudette Gail McKamey

Date 5-17-85

A CRYSTALLIZATION STUDY OF Zr-Ni METALLIC GLASS IN THE RANGE 55-71 ATOMIC PERCENT ZIRCONIUM

A Thesis

Presented for the

Master of Science

Degree

The University of Tennessee, Knoxville

Claudette Gail McKamey

June 1985

ACKNOWLEDGMENTS

Many people have assisted in the research and support work for this thesis. The guidance of my research advisers, Dr. D. M. Kroeger of the Oak Ridge National Laboratory and Dr. B. F. Oliver of the University of Tennessee, is greatly appreciated. I would like to extend special thanks to D. S. Easton for his encouragement and helpful discussions and to J. O. Scarbrough for his guidance and assistance in the laboratory. I would also like to thank Drs. J. O. Stiegler, C. T. Liu, and C. C. Koch for giving me the chance to perform this work at ORNL. The guidance and assistance of O. B. Cavin and Dr. C. J. Sparks in performing the x-ray diffraction work is gratefully acknowledged. Also A. T. Fisher, J. L. Lehman, and Dr. J. A. Horton provided needed instruction in the use of the electron microscope. Special thanks are also extended to K. F. Russell, W. H. Smith, C. P. Haltom, and C. K. H. DuBose for allowing me to use their laboratory and equipment for TEM sample preparation and for their assistance in preparing the figures. Other contributors whose help was essential to the completion of this thesis include H. R. Livesey and J. P. Hickey for help with the drawings, Dr. M. K. Ferber and J. C. Ogle for assistance in using the computer and software for digitizing the DSC plots, V. L. Ridenour for photographing the splat-quencher, and P. T. Thornton and the Publications Office for their suggestions and encouragement in preparing this manuscript. I would also like to thank Drs. R. O. Williams and H. P. Lamparter for their helpful discussions.

A special thanks goes to Connie Dowker and Gwen Sims for typing the manuscript and to J. O. Scarbrough for assistance in preparing some of the drawings.

The financial support for this research project was provided by the U.S. Department of Energy, Division of Materials Sciences, under contract number DE-AC05-840R21400 with the Martin Marietta Energy Systems, Inc.

ABSTRACT

The crystallization of Zr-Ni metallic glasses between 55 and 71 at. % Zr has been investigated using differential scanning calorimetry (DSC), x-ray diffraction (XRD), and transmission electron microscopy (TEM). Transformation temperatures, effective activation energies, and enthalpy changes are reported as a function of composition. Results of x-ray diffraction patterns taken at different positions on the DSC traces are presented. A high temperature DSC peak and x-ray diffraction patterns are presented as evidence for the occurrence of a previously unreported metastable phase between 57 and 63.5 at. % Zr. Micrographs of the first crystals which form as a function of composition within the range of this study show different morphologies corresponding to the two equilibrium phases (ZrNi and Zr_2Ni) and the metastable phase. The possibility of phase separation around the eutectic at 63.5 at. % Zr and its relationship to the metastable phase is discussed.

TABLE OF CONTENTS

LIST OF TABLES

TABLE PAGE

LIST OF FIGURES

FIGURE PAGE

LIST OF SYMBOLS

A	area
C	constant
CSRO	chemical short range order
DRPHS	dense random packing of hard spheres
DSC	differential scanning calorimeter
D_v	diffusion coefficient
d	deviation
EXAFS	extended x-ray absorption fine structure
H	enthalpy
H_v	enthalpy of crystallization
I	nucleation rate
I	intensity
I_o	preexponential constant in the Becker-Volmer equation for the nucleation rate
I_{st}	solid-state nucleation rate
JMA	Johnson-Mehl-Avrami
k	the constant in the Johnson-Mehl-Avrami equation
k_o	preexponential constant in the equation which expresses the temperature dependence of the JMA constant k
M	metastable phase
m	the constant in the JMA equation which depends on the growth morphology
N	Loschmidt number

N	number of values
n	the total Avrami exponent
n_i	Avrami exponent for nucleation
n_u	Avrami exponent for crystal growth
Q	energy calibration constant for calibrating the energy axis of the DSC trace
R	gas constant
r	radius of a nucleus
r_c	radius of a critical size embryo
SAD	selected area diffraction
SAXS	small angle x-ray scattering
T	temperature (K)
$\dot{T}$	DSC heating rate (K/min)
T_c	superconducting transition temperature
TEM	transmission electron microscopy
T_g	glass transition temperature
T_{HT}	temperature at the maximum of the high-temperature DSC peak
T_m	melting temperature
T_p	temperature at the maximum of a DSC peak
T_{p_1}	temperature at the maximum of the first DSC peak
T_{p_2}	temperature at the maximum of the second DSC peak
T_{p_3}	temperature at the maximum of the third DSC peak
T_x	temperature at the onset of crystallization
t	time

t_o the time lag for solid state nucleation during which a steady state distribution of embryos is being established

u rate of crystal growth

u_o preexponential constant in the equation for crystal growth

u_o^{eff} preexponential constant involving the diffusion coefficient and the interlamellar spacing during eutectic crystallization

V_m molar volume

W weight

XRD x-ray diffraction

x a constant fraction of the volume of the sample which has crystallized

$x(t)$ the fraction of the sample crystallized after time t

y a measured quantity

α a crystalline phase

β a crystalline phase

ΔE the effective activation energy for the total crystallization process (includes nucleation and growth)

ΔE_1 effective activation energy for the transformation of the first DSC peak

ΔE_2 effective activation energy for the transformation of the second DSC peak

ΔE_3 effective activation energy for the transformation of the third DSC peak

ΔE^{eff} effective activation energy for eutectic crystal growth

ΔE_g activation energy for crystal growth

ΔE_{HT} effective activation energy for the transformation of the high-temperature DSC peak

ΔE_n activation energy for nucleation

ΔG difference in free energy per mole between the glass and crystal

ΔG_c change in free energy on forming a nucleus of critical size r_c

ΔG_g change in free energy per mole due to crystallization

ΔH enthalpy change for a transformation

$\overline{\Delta H}$ average enthalpy change for crystallization

$\overline{\Delta H}_{HT}$ average enthalpy change of the high-temperature DSC peak

$\overline{\Delta H}_{LT}$ average enthalpy change of the low-temperature DSC peaks

$\overline{\Delta H}_t$ average enthalpy change for the total crystallization process

ΔT undercooling needed to form a critical nucleus of size r_c

δ uncertainty in a measured or calculated quantity

σ solid-liquid interfacial energy used to calculate critical nucleus of size r_c

$\sigma_{\Delta H}$ standard deviation in ΔH

$\sigma_{\overline{\Delta H}}$ uncertainty in mean value of $\overline{\Delta H}$

CHAPTER I

INTRODUCTION

Since 1960, when William Klement, Ronald Willens, and Pol Duwez first demonstrated that a metal could be quenched from a molten state to a glassy one,[1] the interest in metallic glasses has escalated. At first only an academic curiosity, the combination of good metallurgical properties and economical production, along with the large number of metal alloys which can be made amorphous by rapid quenching from the liquid, makes metallic glasses attractive as engineering materials for the future.[2-4] Several articles describing their properties and uses can be found in the literature,[5-11] and recently several books dealing with metallic glasses have been published.[12,13]

Given the proper combination of temperature and time, a metallic glass will crystallize either directly to expected equilibrium phases (as expressed in an equilibrium phase diagram) or through complex stages involving intermediate metastable crystalline phases. The mechanical, magnetic, and electrical properties which were potentially useful in the metallic glass may be lost upon crystallization. For this reason alone, the study of the crystallization processes in metallic glasses seems warranted. However several other things can be gained from such a study:

1. One may acquire a deeper understanding of nucleation and growth processes in general.

2. A knowledge of the phases which appear upon crystallizing a metallic glass may aid in the study of the structure of the amorphous state.

3. Phases which are unobtainable by crystallizing from the melt may be discovered, thereby adding information to the equilibrium phase diagram.

The purpose of this thesis is to investigate the crystallization processes in the Zr-Ni metallic glass system between 55 and 71 at. % Zr. This alloy system lends itself well to such a study. It has been shown that it is possible to produce a glass in this system over a wide range of compositions, ideally from $Zr_{30}Ni_{70}$ to $Zr_{80}Ni_{20}$ (Ref. 14). The composition range of this study includes a "deep eutectic", which is known to enhance glass forming ability,[4,9] and two stable compounds (Zr_2Ni at $Zr_{66.7}Ni_{33.3}$ and ZrNi at $Zr_{50}Ni_{50}$) (Ref. 15). Interest in this system has increased lately due to the complex nature of the crystallization process around the eutectic at $Zr_{63.5}Ni_{36.5}$.

CHAPTER II

LITERATURE REVIEW

Crystallization Reactions in Metallic Glasses

As-quenched metallic glasses are metastable, not only with respect to the equilibrium crystalline phases, but with respect to a more stable glass. Therefore, given enough temperature and time, the glass will first relax to a more stable glassy state and then at higher temperatures will crystallize to stable equilibrium phases. Upon doing so, many of the interesting physical, mechanical, corrosion, and magnetic properties are lost or changed. It is therefore important to understand the crystallization process in metallic glasses, with the view toward using our knowledge to enhance the properties in which we are interested. Several investigators have already contributed to our knowledge of the kinetics and mechanisms of crystallization in metallic glasses.[16-21]

The annealing behavior of metallic glasses can be divided into two main topics: low-temperature structural relaxation in which a highly metastable glass structure relaxes toward a metastable glass structure of lower energy, and, at higher temperatures, crystallization to equilibrium phases. Relaxation is assumed to occur either by changes in both topological and compositional short-range order, by the annealing out of defects of unknown structure, or by annealing out of excess free volume.[18,22,23] This low-temperature process does not cause crystallization but does change many of the physical properties of interest

(e.g. magnetic anisotropy,[24] electrical resistivity,[25] Curie temperature,[26] diffusivity,[27] and ductility[28,29]). This thesis will not deal with structural relaxation at low temperatures but will concentrate its efforts toward studying the crystallization of metallic glasses to the equilibrium phases.

The mechanisms associated with crystallization in metallic glasses are quite complex but can be reduced to three fundamental reactions: polymorphic, eutectic, or primary crystallization.[18,21] All three proceed by nucleation and growth processes, but the occurrence of each depends on the glass composition, annealing temperature, and kinetics. The driving force for crystallization is the free energy difference between the glass and the crystalline phase(s) to which it tends to transform. This free energy difference is expressed hypothetically in Fig. 1 as a function of composition for the three types of reactions noted above.[21,30] In the following paragraphs the three types of reactions are described.

The polymorphous transformation of a glass to a crystalline phase of the same composition is the simplest of the three reactions because no long range movement of atoms is needed. Consequently, this type of reaction occurs at compositions near pure elements or intermetallic compounds, as shown by reactions 1 and 3 of Fig. 1, or at compositions where the formation of a metastable phase is thermodynamically more favorable, such as reaction 2 of Fig. 1. In metal-metalloid systems, the polymorphous reaction is usually not seen because the glass-forming regions are restricted to narrow composition regions around eutectics. However in metal-metal systems, where the glass-forming ranges are

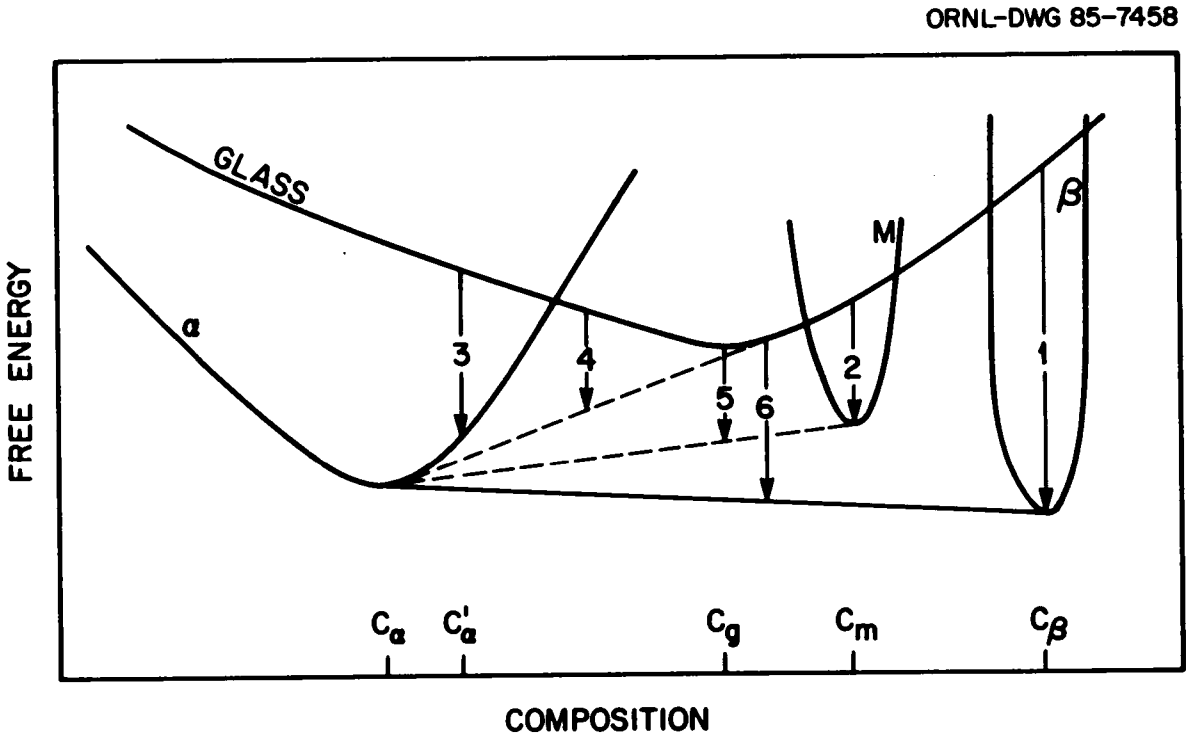

Figure 1. Hypothetical free energy versus composition for the crystallization of a metallic glass. Shown are the free energy curves for the glass, a metastable phase M, a terminal solid solution phase α, and a stable intermetallic phase β. The solid line indicates a stable equilibrium between phases α and β, while the broken lines represent metastable equilibria. Numbers refer to reactions described in the text.

wider, polymorphous reactions are more common, often producing phases well away from stoichiometry.[21] Studies on the polymorphous formation of intermetallic compounds from binary metallic glasses have shown that crystal growth is thermally activated and linear with time.[31,32] The morphologies of the crystals vary from unfaulted equiaxed single crystals in Ni_3P (Ref. 33) to heavily faulted polycrystals in Zr_2Ni (Ref. 31). Their shape is a function of the crystallographic dependence of growth rate since the crystals are growing in an isotropic medium and no long range diffusion is required.

Primary crystallization of a phase of different composition from that of the glass is illustrated by reaction 4 of Fig. 1 in which a supersaturated solid solution phase is formed. As can be seen, the formation of the α phase by this reaction results in an enrichment of the glass phase in solute. A later decomposition of the enriched glass produces the equilibrium phases. Morphologies for primary crystals may range from spherical to dendritic depending on alloy composition. The growth rate is diffusion controlled and is therefore parabolic with time. However this assumes that the crystals are spherical and remain so as growth progresses; if dendritic growth occurs, the growth of primary arms should be linear with time.[21,34]

The most complex crystallization reaction in metallic glasses is the eutectic reaction in which two crystalline phases form simultaneously (reactions 5 and 6 in Fig. 1). This reaction has a large driving force and in metallic glasses can occur over large composition ranges. Consequently it is a common reaction in the crystallization of metallic glasses. Lamellar as well as globular morphologies have been

observed, lamellar growth being the most common.[18] The growth rate is linear with time but much slower than polymorphous reactions because of the diffusion needed to separate into two phases in the reaction front. The linear kinetics has been confirmed by measurement of eutectic growth rates in Metglas 2826 (Ref. 35) and $Fe_{80}B_{20}$ (Ref. 36).

One aspect of the study of metallic glasses which relates the amorphous structure to the crystallization processes, and which has received much interest lately, is the concept of phase separation.[18,21] Phase separation occurs in systems where the free energy of a mixture of two amorphous phases is lower than that of a single amorphous phase. Relating this to Fig. 1, the curve for the glass, which shows a negative heat of mixing, would be interrupted in a narrow composition range by a positive heat of mixing. The first product of crystallization depends upon whether phase separation occurs. By studying the first products and relating those phases to the occurrence of phase separation, much can be learned about the amorphous structure itself. The following evidence for phase separation has already been reported:

1. The presence of two glass transition temperatures (T_g), which suggest the presence of two different amorphous structures, have been reported in as-quenched Ni-Pd-P glasses which were studied by differential scanning calorimetry (DSC).[37]

2. Two T_g's were found in DSC studies of $Ti_{24}Be_{40}Zr_{36}$. The morphology of this as-quenched glass, studied by transmission electron microscopy (TEM), also showed evidence of two amorphous phases.[38]

3. Two glassy phases have been seen in Fe-B alloys by TEM.[39]

4. For Zr-Ni glasses, two superconducting transition temperatures

(T_c),[40,41] two T_g's in DSC,[41] and two amorphous rings in selected area diffraction (SAD)[42] have been reported.

5. Small angle x-ray scattering techniques (SAXS) and DSC have shown evidence of two glassy phases in $Pd_{74}Au_8Si_{18}$ after low temperature anneals (low enough to cause no crystallization).[43,44]

Kinetics of Crystallization in Metallic Glasses

The kinetics of crystallization for metallic glasses depends on several parameters including the mode of crystallization, the number of quenched-in nuclei, the atomic diffusion coefficients, and the difference in free energy between the amorphous and crystalline phases. Interpretation of the kinetics can be done in terms of classical nucleation and growth theories,[45] with certain assumptions being made to relate the solid amorphous structure to the liquid amorphous structure. These assumptions include (1) homogeneous nucleation, (2) large undercoolings, and (3) steady-state nucleation.

The nucleation rate is expressed by a Becker-Volmer equation,

$$I = I_o \exp(-N\Delta G_c/RT) \exp(-\Delta E_n/RT) , \qquad (1)$$

where I_o is a preexponential constant, N is the Loschmidt number, R is the gas constant, T is temperature in degrees Kelvin, and ΔE_n is the activation energy for an atom to move from the amorphous matrix to the embryo. The free energy ΔG_c is the energy needed to form a spherical nucleus of critical size radius,

$$r_c = \frac{2\sigma}{H_v} \frac{T_m}{\Delta T} = \frac{2\sigma}{\Delta G} , \qquad (2)$$

where σ is the solid-liquid interfacial energy, T_m is the melting point, ΔT is the undercooling, H_v is the enthalpy of crystallization, and ΔG is the difference in free energy per mole between the glass and the crystal. For spherical nuclei, where the interfacial energies are isotropic,

$$\Delta G_c = \frac{16}{3} \pi \frac{\sigma^3 V_m^2}{\Delta G^2} , \tag{3}$$

where V_m is the molar volume. This equation expresses the fact that the phase which forms first may not be the equilibrium phase with the lowest free energy ΔG_c, but may be a metastable phase which has a lower interfacial energy than the stable one, thereby having a lower ΔG_c than the stable one.[18] The crystallization of metallic glasses is usually studied at such large undercoolings, $\Delta G_c \ll RT$, that Eq. (1) can be reduced to an Arrhenius-type equation:

$$I = I_o \exp (-\Delta E_n/RT) . \tag{4}$$

The use of these equations is complicated by the fact that we have assumed that steady-state nucleation exists for metallic glasses (i.e., that a steady-state concentration of embryos exists at all times). However, this may not always be the case, and at the beginning of crystallization there may be a finite period during which this steady-state distribution is being established.[47] Taking this time lag into account, the nucleation rate equation becomes[18]

$$I = I_{st} \left[1 + 2 \sum_{n=1}^{\infty} (-1)^n \exp [-n^2 (t/t_o)] \right] , \tag{5}$$

where I_{st} is given by Eq. (1), t is time, t_o is the time lag, and n is an exponent which depends on both nucleation and growth.

The temperature dependence for the rate of crystal growth is given by

$$u = u_o \exp(-\Delta E_g/RT)\,[1 - \exp(-\Delta G_g/RT)] \,, \tag{6}$$

where u_o is a preexponential term, ΔE_g is the activation energy for crystal growth, and ΔG_g is the change in free energy per mole due to crystallization. As with nucleation, assuming large undercoolings, the growth rate can be expressed as an Arrhenius-type equation:

$$u = u_o \exp(-\Delta E_g/RT) \,. \tag{7}$$

This means that the growth rate is linear, as in polymorphous crystallization where the radius of growing crystals is proportional to the time.

However in primary reactions grain growth is controlled by volume diffusion where

$$r = C\sqrt{D_v t} \tag{8}$$

and

$$u = \frac{1}{2} C^2 D_v r^{-1} \,, \tag{9}$$

where C is a constant, D_v is the diffusion coefficient, and t is time.[19]

Eutectic crystallization is even more complicated, involving either volume or interface diffusion, depending on the alloy and heating conditions. However growth by this process is usually reduced to

$$u \propto u_o^{eff} \exp\left(\frac{-\Delta E^{eff}}{RT}\right), \tag{10}$$

where u_o^{eff} is a constant involving the diffusion coefficient and the interlamellar spacing and ΔE^{eff} is the effective activation energy which is related to the activation energy for diffusion.[19]

The overall kinetics of the crystallization processes in metallic glasses have been explained in terms of the formal theory of transformation kinetics.[45-53] If one assumes that for crystallization of amorphous materials

1. isothermal transformation conditions exist (so the growth rate and nucleation rate are constant,

2. there is spatially random (homogeneous) nucleation, and

3. the growth rate is dependent only on temperature and not time (i.e., linear growth kinetics),

then

$$x(t) = 1 - \exp\left(\frac{-u^m I t^n}{4}\right), \tag{11}$$

where x(t) is the fraction of the transformation completed at time t, m is a constant depending on the growth morphology, and n is a constant which depends on both nucleation and growth.[50] This is the Johnson-Mehl-Avrami (JMA) transformation equation,[46,47] and is usually used in the form

$$x(t) = 1 - \exp\left[-k(t - t_o)^n\right], \tag{12}$$

where k is a function of temperature and includes both the nucleation and growth rates. The temperature dependence of the constant k is

expressed by an Arrhenius equation,

$$k = k_o \exp\left(\frac{-\Delta E}{RT}\right), \tag{13}$$

where k_o is a preexponential term and ΔE is the effective activation energy for the whole transformation.

The JMA equation [Eq. (12)] can be rearranged as follows:

$$\begin{aligned} x(t) &= 1 - \exp\left[-k(t - t_o)^n\right] \\ 1 - x(t) &= \exp\left[-k\,(t - t_o)^n\right] \\ \ln\left[1 - x(t)\right] &= -k\,(t - t_o)^n \\ \ln\left\{-\ln\left[1 - x(t)\right]\right\} &= \ln k + n \ln (t - t_o)\ . \end{aligned} \tag{14}$$

For isothermal conditions a plot of $\ln\{-\ln[1 - x(t)]\}$ against $\ln(t - t_o)$ can be used to find k and n. By substituting Eq. (13) into Eq.(14),

$$\ln\left\{-\ln\left[1 - x(t)\right]\right\} = \ln k_o - \frac{\Delta E}{RT} + n \ln (t - t_o)\ , \tag{15}$$

and taking measurements at different temperatures, a value for ΔE can be obtained from a plot of $\ln(t - t_o)$ versus T^{-1} at a constant fraction crystallized, x.

An alternative method for interpreting the kinetics of crystallization from data collected by differential scanning calorimetry (DSC) in which nonisothermal conditions exist was developed by Kissinger and has become the most used method by present researchers.[54] He assumed that the fraction crystallized with time at constant temperature obeys a first-order law. Then

$$\left(\frac{\partial x}{\partial t}\right)_T = k(1 - x)\ , \tag{16}$$

where x is the fraction crystallized and k is the rate constant expressed by Eq. (13). If the temperature is also changing with time, as in using a constant heating rate to crystallize an amorphous metal in the DSC, Kissinger was able to show that the rate can be expressed as

$$\frac{dx}{dt} = k_o\left(1 - x\right) \exp\left(\frac{-\Delta E}{RT}\right) . \tag{17}$$

This equation can be used as long as x and T are taken at the same t.

The reaction rate is assumed to be a maximum at the peak in the DSC curve. At this point

$$\frac{d}{dt}\left(\frac{dx}{dt}\right) = \frac{dx}{dt}\left[\frac{\Delta E}{RT^2}\frac{dT}{dt} - k_o \exp\left(\frac{-\Delta E}{RT}\right)\right] = 0 \quad . \tag{18}$$

Taking T_p as the temperature at the maximum of the DSC peak,

$$k_o \exp\left(\frac{-\Delta E}{RT_p}\right) = \frac{\Delta E}{RT_p^2}\frac{dT}{dt} \quad , \tag{19}$$

where dT/dt is the heating rate used (e.g. the heating rates used could be 5, 10, 20, 40, 80, etc. K/min). So by heating samples of the same composition at different rates in the DSC and measuring the temperature at the peak for each rate, the activation energy can be determined from a plot of $\ln (dT/dt)/T_p^2$ versus $1/T_p$, since

$$\frac{d[\ln (\dot{T}/T_p^2)]}{d(1/T_p)} = \frac{-\Delta E}{R} \quad , \tag{20}$$

where $\dot{T} = dT/dt$. Kissinger further showed mathematically that Eq. (20) can also be used for reactions that are not first-order, as long as the order remains constant through the greater part of the reaction.[54]

This interpretation of nonisothermal results in terms of isothermal kinetics has been discussed and debated by other researchers, especially by Henderson[49,50] and Yinnon and Uhlmann.[53] However no better method has yet been developed to interpret isochronal DSC data. From these techniques the important parameters necessary for the understanding of the crystallization process are obtained. These parameters include ΔE, n, t_o, k_o, and the enthalpy change of crystallization ΔH, which is obtained by measuring the area under the DSC curve. The ΔE obtained by either the isothermal method [Eq. (15)] or Kissinger's method [Eq. (20)] is an "effective" activation energy which reflects the activation energies for both nucleation [ΔE_n of Eq. (4)] and growth [ΔE_g of Eq. (7)]. Ranganathan and von Heimendahl[52] have shown that they are related by

$$\Delta E = \frac{(n_i \Delta E_i + n_u \Delta E_u)}{n} , \qquad (21)$$

where n is the total Avrami exponent of Eq. (12) and is equal to the Avrami exponent for nucleation n_i plus the exponent for growth n_u. Although theoretically it has been shown in Eq. (14) that n can be determined from the DSC data, an unambiguous determination can be obtained only by microstructural investigations in which nucleation and growth rates are measured.

Recent Research on Zr-Ni Metallic Glasses

The zirconium-nickel binary system has become a model system for the study of the production of metallic glasses, the glass structure, and the crystallization processes of metallic glasses. The phase

diagram (Fig. 2) shows several eutectics where glass forming ability has been shown to be enhanced.[4,9] Recently the range over which Zr-Ni can be made glassy has been extended to between 30 and 80 at. % Zr. This study will concern itself only with the crystallization reactions and kinetics for the composition range 55-71 at. % Zr, but a short listing of other studies on Zr-Ni glasses seems in order. Included are several studies on the electronic properties[41,55-59] and density and electrical resistivity measurements.[59-61] Karkut and Hake[61] report the values for many structure-related properties, as well as superconducting and electronic properties, for several compositions between 60 and 80 at. % Zr. An extensive study of the structure of amorphous and crystalline alloys with nominal compositions 63.5, 66.7, and 75.9 at. % Zr was conducted by Frahm, Haensel, and Rabe by means of extended x-ray absorption fine structure (EXAFS).[62] They studied differences in the nearest neighbor environment of the amorphous and crystalline state and related those differences to the subject of short-range order.

Buschow and Beekmans began investigating the crystallization processes in Zr-Ni metallic glasses, along with the magnetic and electronic properties, in the seventies.[63] Using a differential scanning calorimeter (DSC), they determined the crystallization temperatures of several $Zr_{100-x}Ni_x$ alloys (where x = 22, 24, 36, 60, 63, 90). From a more detailed study of the crystallization of $Zr_{78}Ni_{22}$, they determined that this alloy first transforms to a metastable bcc phase. Then, upon further heating, two stable crystalline phases appear. One of these they determined to be α-Zr, the other the tetragonal phase Zr_2Ni. The

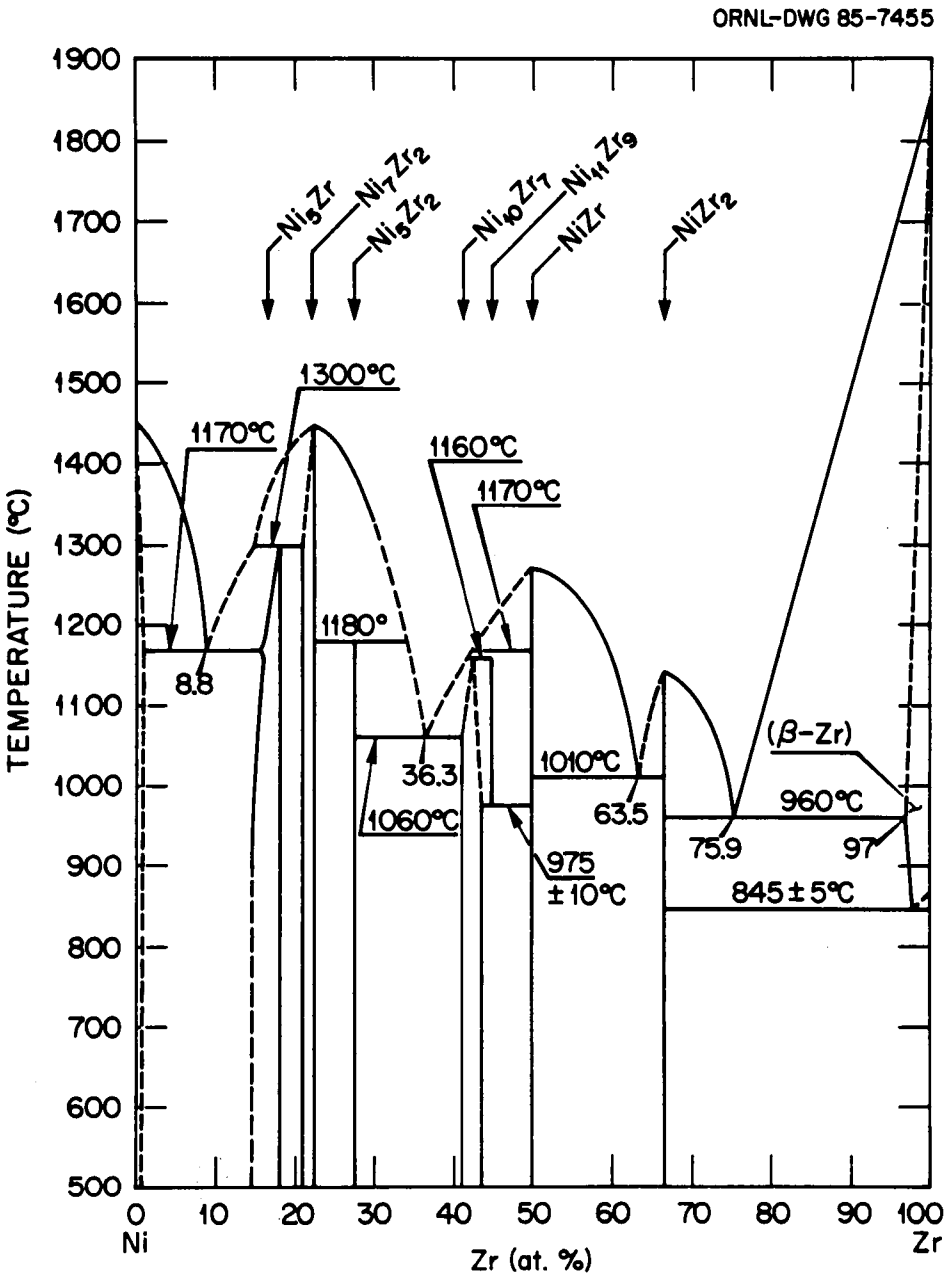

Figure 2. Phase diagram for the Zr-Ni binary system. The composition region of interest for this report is 55-71 at. % Zr which includes a eutectic at 63.5 at. % Zr and an equilibrium compound at 66.7 at. % Zr.

nature of the metastable bcc phase in other high zirconium alloys is still being investigated by Buschow and co-workers by using x-ray diffraction and Mössbauer spectroscopy.[64]

The first in-depth study of the composition dependence of thermal stability, crystallization morphology, density, and mechanical properties was conducted by Dong, Gregan, and Scott.[65] They reported crystallization temperatures, activation energies, crystallization morphologies, densities, Young's moduli, and x-ray diffraction data for Zr_xNi_{100-x} where x was from 33 to 42 and from 60 to 78 at. % Zr. Crystallization was accomplished by heating in a DSC and the kinetics were interpreted using the Kissinger method.[54] The morphologies were studied using transmission electron microscopy (TEM) and x-ray diffraction (XRD). The authors indicated, however, that the behavior of the compositions between 60 and 67 at. % Zr was complicated, and, especially near the eutectic at 63.5 at. % Zr, it was impossible to separate the processes or interpret the DSC peaks obtained.

Scott, Gregan, and Dong later did a TEM and DSC study of the 63.5, 66.7, 72 and 76 at. % Zr alloys and discussed further the nature of the transformations to the crystalline state.[31] It had been assumed that crystallization temperatures could be used to describe the thermal stability of metallic glasses, and that a discontinuity at a eutectic composition indicated a stable glass structure.[66] However Scott et al. concluded that, unlike in metal-metalloid glasses,[67,68] maximum stability of Zr-Ni metallic glasses was not associated with eutectic compositions. Instead, crystallization temperatures for Zr-Ni metallic glasses fell monotonically with increasing zirconium content through

eutectics at 63.5 and 76 at. % Zr. Their study also showed that only equilibrium phases occurred at various stages of crystallization.

Buschow, Verbeek, and Dirks[69] studied the crystallization of the $Zr_{63.5}Ni_{36.5}$ alloy by DSC, TEM, x-ray diffraction, and electrical resistivity measurements. They showed that, even though two strong exothermic effects are observed in the DSC trace, only the higher temperature effect is associated with crystallization of the sample. They suggest that the first transition of that alloy involves mainly short-range atomic rearrangements within the amorphous state. However, Frahm[70] reports different activation energies and a different DSC behavior for this same alloy.

Recently Altounian, Guo-hua, and Strom-Olsen[14] have presented research which contradicts some of the results of Buschow and co-workers. Altounian et al. identify the metastable phase present as the first transformation product of high zirconium alloys (e.g. $Zr_{78}Ni_{22}$) as being hexagonal ω-Zr, not a bcc phase as reported in Ref. 63. They do, however, support Buschow's findings in Ref. 69 of the absence of any crystallization due to the first peak in the DSC trace of $Zr_{63.5}Ni_{36.5}$, but can give no explanation. This thorough study of the Zr-Ni system between 30 and 80 at. % Zr resulted in several interesting conclusions.

1. They reported crystallization temperatures, activation energies, enthalpies, and electrical resistivities as a function of composition for the range of compositions studied.

2. They were able to extend the range of glass formation down to 30 at. % Zr.

3. They reported that at $Zr_{60}Ni_{40}$ and $Zr_{63.5}Ni_{36.5}$ the first peak in the DSC represents a change in the glassy structure, not a crystallization reaction.

4. A new peritectoid phase was confirmed at $ZrNi_2$. This phase had been studied previously by Polesya and Slipchenko.[71]

5. Peaks in the activation energy curve at eutectic compositions led the authors to speculate that the activation energy for crystallization would be a more sensitive measure for stability of the amorphous structure than the crystallization temperature.

6. Assuming that the enthalpy change on crystallization is almost entirely a change in internal energy between the glass and the equilibrium phases, they concluded that the enthalpy change curve could provide a guide to the crystalline phase diagram. They observed maxima at compositions corresponding to equilibrium phases (i.e. Zr_2Ni, ZrNi, and $ZrNi_2$), where it would be expected that the transformation from a metastable amorphous structure to a very stable, low energy, equilibrium phase would result in a large enthalpy change.

The absence of x-ray evidence for crystallization in the 62 and 63.5 at. % Zr alloys after heating to the top of the first exothermic peak in the DSC (the DSC traces of these alloys show two and three peaks, respectively) has caused an increased interest in the nature of the transformations at these compositions. As noted earlier, Buschow et al.[69] and Altounian et al.[14] have suggested that the first DSC peak represents a transition within the amorphous state and comprises mainly short range atomic rearrangements. On the other hand, Dong et al.[65] contends that for $Zr_{62}Ni_{38}$ the first DSC exotherm represents the

crystallization of Zr_2Ni and the second the crystallization of ZrNi from the nickel enriched glass. Other research has begun to relate the phenomena at these compositions to phase separation and chemical short range ordering (CSRO) in the glass. Van Swijgenhoven, Stals, and Buschow[72] have used TEM to show that as quenched $Zr_{63}Ni_{37}$ actually has two amorphous rings in its selected area diffraction pattern (SAD) and therefore is phase separated into two amorphous alloy phases during the liquid quenching operation, not on subsequent annealing in DSC. Crystallization of one of these phases occurs during the first DSC exotherm, but the phase separation in the glass is on such a fine scale that the complete crystallization of this phase is inhibited, resulting in an assembly of crystallites too small to be observable by x-ray diffraction. They believe the first crystallites to be ZrNi, but they note that the d-values determined from SAD patterns do not match exactly those of ZrNi in the same alloy after complete crystallization. Their study indicates that the first crystallites may not involve stoichiometric ZrNi but a compound somewhat richer in zirconium. They further note that the SAD rings are not far apart and speculate that the two amorphous phases are not very different in composition. They assume that these phases are precursors to the ZrNi and Zr_2Ni equilibrium crystalline phases, although they infer from values of the interatomic spacing calculated from the SAD ring radius that the Ni-rich amorphous phase is somewhat enriched in zirconium as compared to what would be expected for ZrNi.

Recent work by Schulz, Matijasevic, and Johnson[73] reporting a correlation between CSRO and electrical resistivity supports the general

conclusions of van Swijgenhoven et al. However, Schulz et al. believe that the precipitation of very fine grained microcrystalline Zr_3Ni is occurring during the first DSC exotherm.

From low-temperature specific heat data on a large number of compositions in the range 55 to 75 at. % Zr, Kroeger, Koch, Scarbrough, and McKamey[41] observed an unusual composition dependence of electronic properties. Specifically, evidence for two superconducting phases was observed in a liquid quenched (splat quenched) sample of composition $Zr_{62.9}Ni_{37.1}$. Low temperature annealing produced a large change in the volume fraction of these two phases. A glass of 61.2 at. % Zr, which showed no evidence of phase separation as quenched, did show two phases after annealing one hour at 200°C. From measurements of the density of states at the Fermi level, superconducting transition temperatures, and enthalpy change on crystallization, they concluded that the two phases have compositions of $Zr_{60}Ni_{40}$ (Zr_3Ni_2) and $Zr_{66.7}Ni_{33.3}$ (Zr_2Ni). The results of this work were interpreted in terms of an "association model" for liquid alloys developed by Sommer and Predel in which associations of atoms with definite stoichiometries exist in equilibrium with unassociated atoms.[74-76]

The relationship of chemical short range order (CSRO) to composition was investigated by Buschow for various Zr-based metallic glasses.[77] Crystallization temperatures and activation energies for the Zr-Ni, Zr-Co, Zr-Fe, and Zr-Cu systems were presented and discussed in relation to the occurrence of CSRO. He showed that activation energies for crystallization ΔE increased greatly for compositions where CSRO was suspected to occur, especially around the eutectic at $Zr_{63.5}Ni_{36.5}$. He

relates this increase to a stronger temperature dependence of the configurational entropy which is expected for compositions with strong CSRO.

CHAPTER III

EXPERIMENTAL PROCEDURES

Preparation and Characterization of Specimens

Alloy buttons for twenty-six compositions between 55 and 71 at. % Zr were made by arc-melting high purity zirconium and nickel in an argon atmosphere on a water-cooled copper hearth. Before and after casting, the weights of the alloy buttons were measured on a Fisher Scientific Co. Gramatic Balance (see Appendix A, Table A-I). The difference in weights (less than 0.05%) indicated that the compositions deviated from nominal values by no more than 0.2 at. %. The $Zr_{60}Ni_{40}$ alloy (ingot AAF) was analyzed for impurities and the results are presented in Table A-II. Total impurities were less than 420 ppm weight, indicating that the quality of the zirconium and nickel used to make the alloys was very good.

The amorphous samples were prepared by rapid quenching in an arc-hammer apparatus which is shown in Fig. 3. This apparatus rapidly cools a molten sample by "splatting" it between two massive, flat, copper plates in a process similar to that developed by Pietrokowsky in 1963.[78] The piece of alloy to be rapidly quenched is placed on the copper block inside the chamber which is evacuated and then backfilled with argon. After striking an arc on the electrode and melting the piece of alloy, a trigger at the top of the apparatus is released, allowing springs to propel the hammer and "splat" the sample between the two copper blocks. A microswitch triggers a timer which records the time it takes the

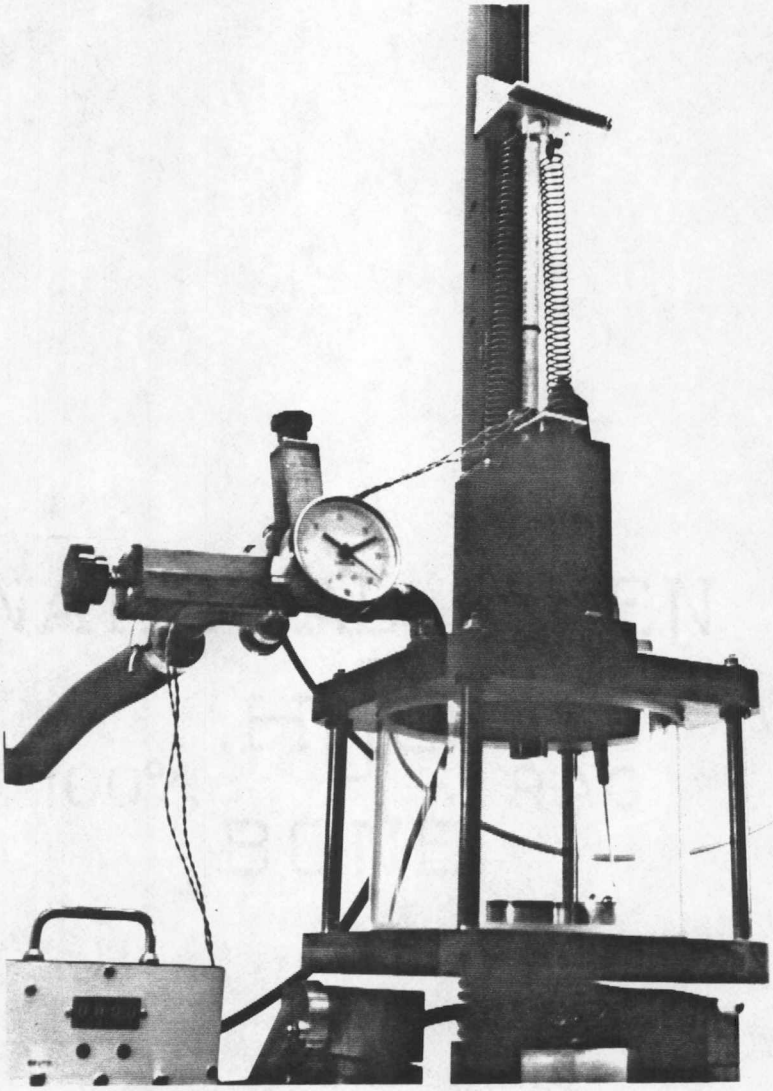

Figure 3. Arc-hammer apparatus used for preparation of rapidly-quenched metallic glass specimens. See text for a description of use.

hammer to fall. A velocity of about 8.4 m/sec was calculated for the Zr-Ni alloys, producing a quenching rate of about 10^6 K/sec.[79] All splat-cooled samples used in this research were prepared on this apparatus using approximately the same conditions: the same springs, the same power supply at the same voltage, copper quenching blocks, and approximately the same size piece of alloy for melting. Therefore splats of the same composition were assumed to possess a similar amorphous structure after quenching. The 20 to 30 μm thick foils produced were x-rayed on a Philips Norelco diffractometer using CuKα radiation and no splat was used which did not exhibit the broad diffuse pattern characteristic of an amorphous metal (as shown in Fig. 4).

Thermal Analysis of Crystallization Process

A Perkin-Elmer DSC-2 differential scanning calorimeter (DSC) was used for thermal analysis of the crystallization process. Basically this instrument records on a strip chart recorder the difference in power required to maintain the sample at the same temperature as a reference sample during heating at a constant rate or for an isothermal anneal. The ordinate then becomes a measure of the change in heat per unit time, and the abscissa is a measure of time for an isothermal anneal and both time and temperature for an isochronal anneal. Both axes are calibrated against known transformation temperatures and heats for standard samples. For a metallic glass, a typical data strip would appear as in Fig. 5, from which the crystallization temperature (T_x), peak temperatures (T_{p_1}, T_{p_2}, etc.), glass transition temperature (T_g), and heat of crystallization (ΔH) can be measured.

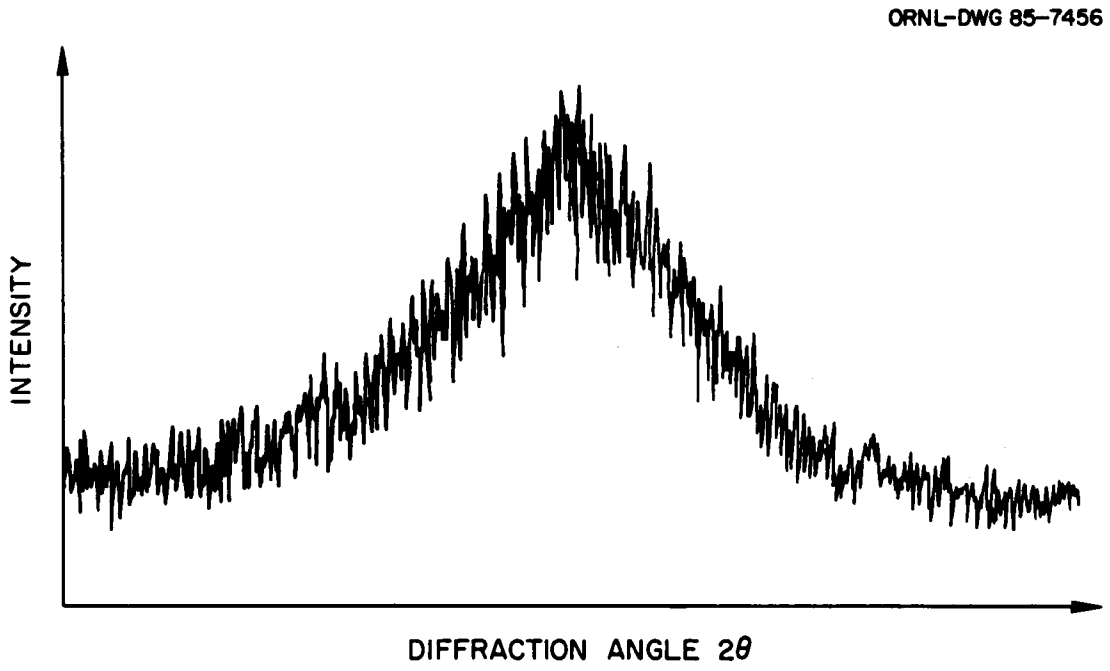

Figure 4. Characteristic x-ray diffraction pattern for an as-quenched metallic glass.

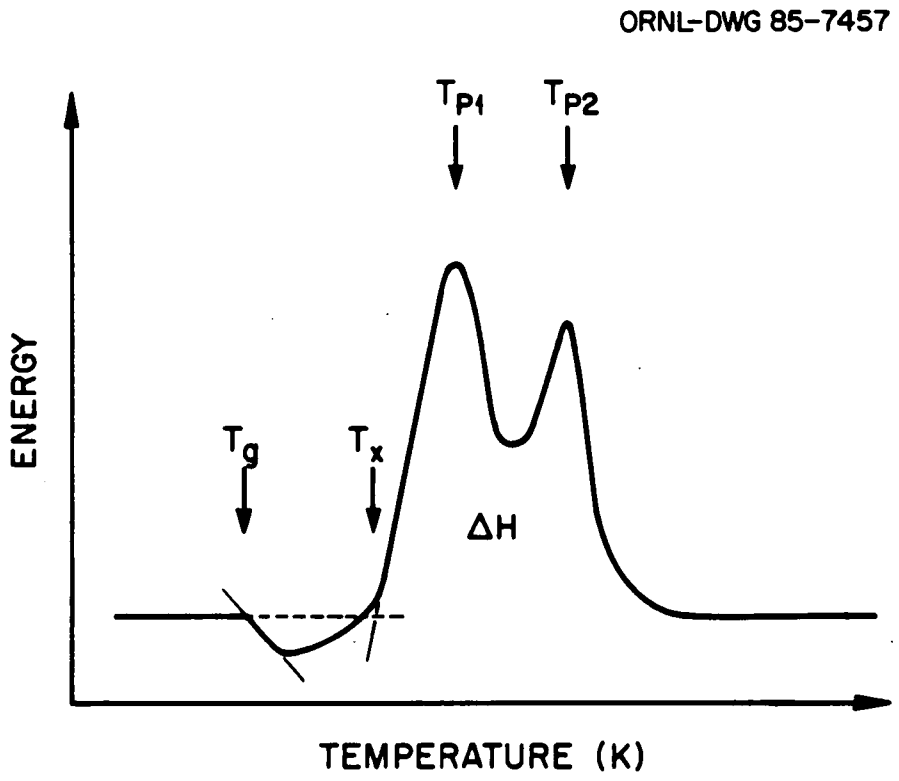

Figure 5. Characteristic differential scanning calorimeter (DSC) trace for the crystallization of a metallic glass with constant heating rate $\dot{T}$. Measurements of the glass transition temperature T_g, the onset of crystallization T_x, and the peak temperatures are shown. Measuring the area under the peaks leads to the calculation of the enthalpy change ΔH for the transformation.

For this project the temperature interval of the calorimeter was calibrated between the transformation temperatures of indium (429.75 K) and K_2CrO_4 (943.7 K) to within ±0.5°. Additionally, the temperature of the melting point of zinc at heating rates of 5, 10, 20, 40, and 80 K/min was determined to ±0.2°. The difference between the measured and actual melting temperature of 692.65 K was used as a correction for all measured temperatures. The heat given off during the melting of indium at 429.75 K was used to calibrate the ordinate. Samples weighing 2 to 4 mg were placed in gold pans (or aluminum if not going above 800 K) and heated at rates of 5, 10, 20, 40, and 80 K/min through the transformation peaks. The temperature at the onset of crystallization, T_x, was measured at the intersection of the extrapolated baseline and front slope of the first transformation peak, as shown in Fig. 5. Peak temperatures were recorded as T_{p1}, T_{p2}, T_{p3}, and T_{HT}. Temperatures were then corrected using the zinc calibration and the corrected temperatures were used to compute the activation energy for each peak (ΔE_1, ΔE_2, ΔE_3, and ΔE_{HT}) by the Kissinger method.[54] As described in Chapter 2, the Kissinger method involves measuring the transformation temperature of a particular DSC peak at various heating rates, $\dot{T}$, and after correcting the temperatures against the melting point of zinc, calculating $\ln (\dot{T}/T_p^2)$ and T_p^{-1}. As an example, this has been done for the two DSC peaks of $Zr_{59}Ni_{41}$ shown in Fig. 6. The calculations are presented in Table I and the slope of a plot of $\ln (\dot{T}/T_p^2)$ versus T_p^{-1} (Fig. 7) then gives the activation energy for that peak, ΔE. The glass transition temperature, T_g, was not measured in this study because for most samples it was obscured by the crystallization exotherms.

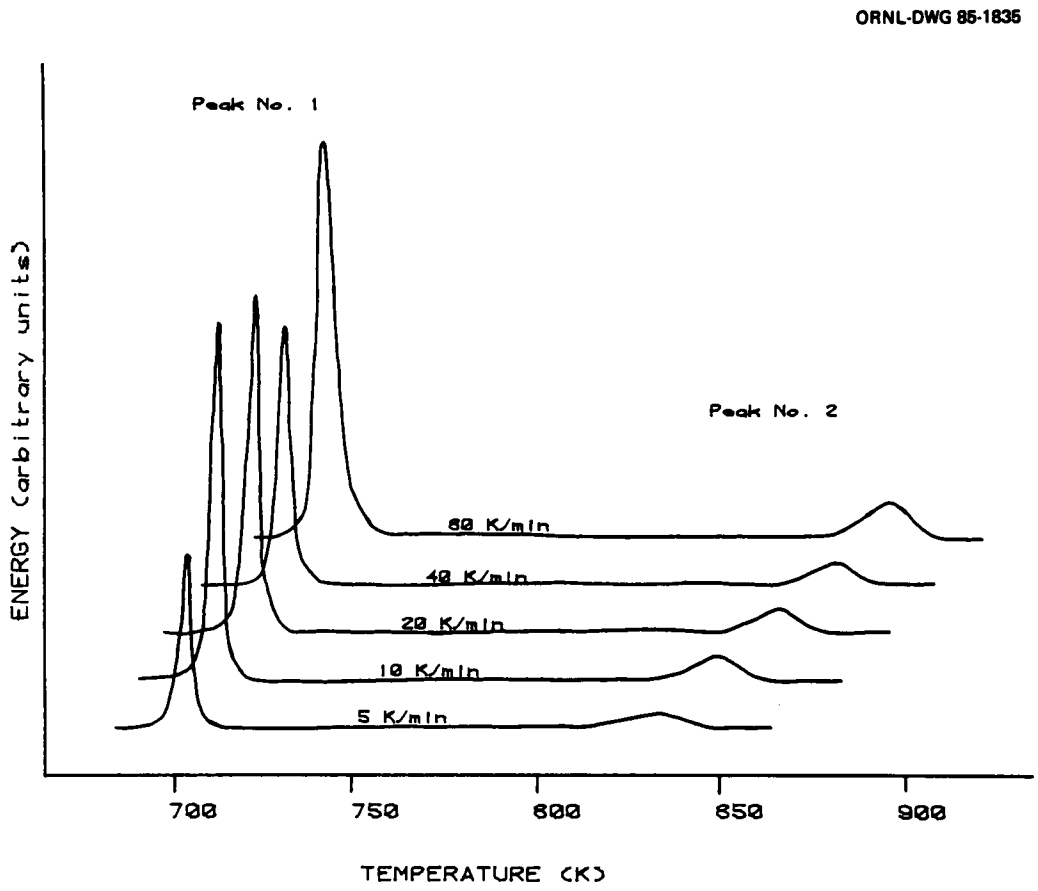

Figure 6. Change in crystallization peak temperature with DSC heating rate for $Zr_{59}Ni_{41}$. Heating rates of 5, 10, 20, 40, and 80 K/min were used. The peak temperatures measured from the original DSC trace are presented in Table I.

Table I. Calculation of Activation Energy of Crystallization ΔE for $Zr_{59}Ni_{41}$ Determined by Kissinger Method

Peak Number	Heating Rate T (K/min)	Temperature (K)		$\frac{10^3}{T}$ (K^{-1})	$\ln\left(\frac{\dot{T}}{T^2}\right)$	Slope $\Delta E/k^a$	ΔE (eV/atom)
		Apparent	Corrected				
1	5	705.2 ± 0.2	705.57	1.4173	−11.509		
	10	712.9 ± 0.2	712.67	1.4032	−10.835		
	20	722.2 ± 0.2	721.13	1.3867	−10.166		
	40	731.4 ± 0.2	728.64	1.3724	−9.493		
	80	742.6 ± 0.2	736.47	1.3578	−8.822	−44.807	3.86
2	5	832.3 ± 0.5	832.62	1.2010	−11.840		
	10	846.2 ± 0.5	845.97	1.1821	−11.178		
	20	862.6 ± 0.5	861.53	1.1607	−10.522		
	40	876.8 ± 0.5	874.04	1.1441	−9.857		
	80	892.6 ± 0.5	886.47	1.1281	−9.192	−35.880	3.09

[a]Boltzmann's constant $k = 8.6164 \times 10^{-5}$ eV/K.

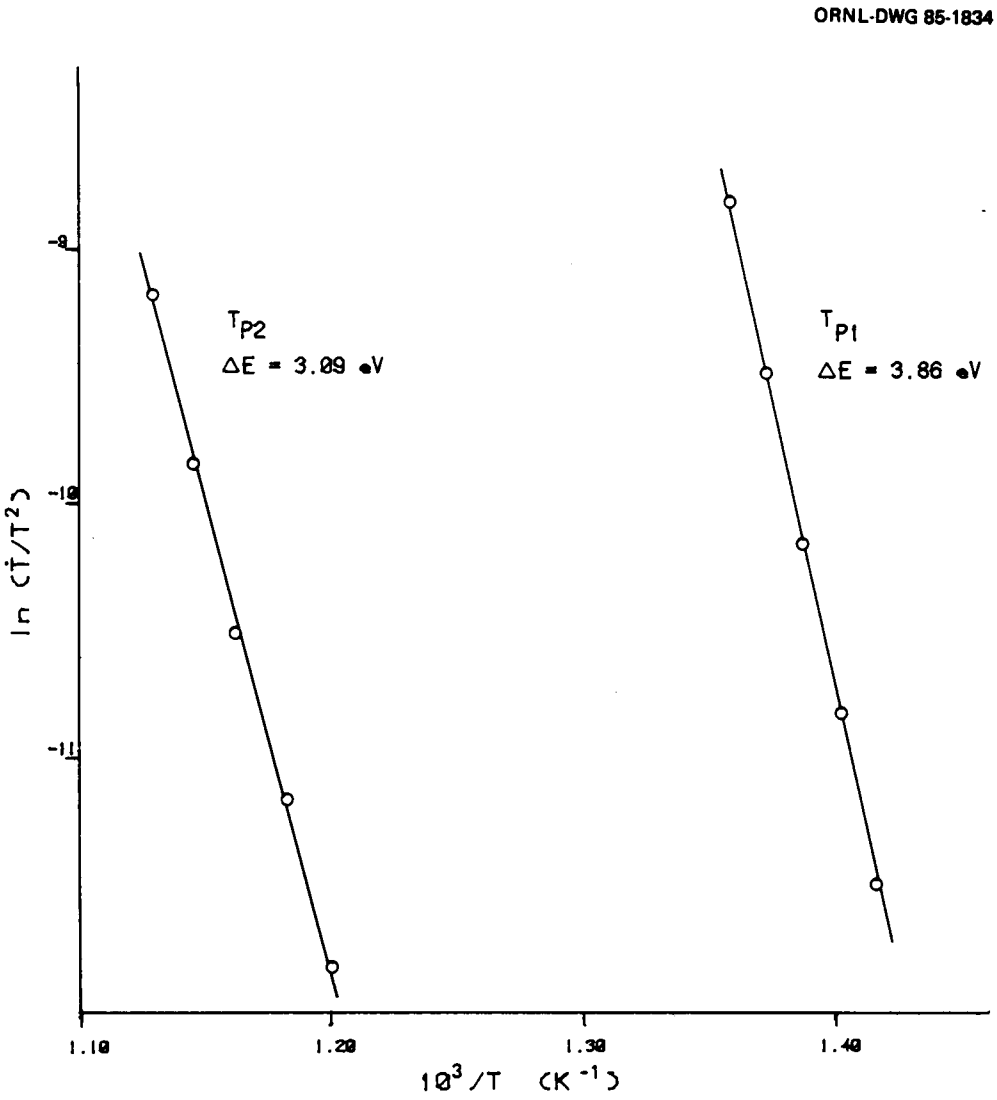

Figure 7. Kissinger plots for the two DSC peaks produced during the crystallization of $Zr_{59}Ni_{41}$. The slope of the line for each peak gives the activation energy for crystallization ΔE as calculated in Table I.

To determine the change in enthalpy during crystallization, ΔH, the areas under the DSC peaks were measured using a planimeter. The area for each sample was measured several times to get a good average value, and since five samples from each splat were annealed in the DSC, each at a different heating rate, an average of these five values was used to calculate the reported value of the change in enthalpy $\overline{\Delta H}$ for each splat.

Values for the change in crystallization enthalpy (in joules per mole) were calculated from the equation

$$\Delta H = \frac{\text{area}}{\text{area/chart square}} \times \frac{\text{H/chart square}}{Q} \times \frac{\text{molar wt}}{\text{specimen wt}} \times C \quad , \qquad (22)$$

where the area was measured in planimeter units, H/chart square was obtained from the range used on the DSC (0.1 to 20 mcal/sec) and the chart speed, weights were measured in milligrams, C was a conversion factor to convert calories to joules (4.186 cal/J), and Q ($\simeq$1) was an energy calibration constant determined from the ratio of the measured heat given off during the melting of indium at 429.75 K to the known value of 6.79 cal/gm. Several of the compositions tested produced more than one peak in the DSC, but due to the overlap of the peaks, it was not possible to measure the heat of the individual processes. All the peaks that occurred close together were measured together. However at some compositions a high temperature peak occurred as much as 140° above the lower temperature peaks and could be measured separately. Therefore the enthalpy change of crystallization was designated as $\overline{\Delta H_{LT}}$ for the low temperature peaks, $\overline{\Delta H_{HT}}$ for the high temperature peak, and $\overline{\Delta H_t}$ for

the total enthalpy change produced on going from the amorphous structure to the crystalline equilibrium phases.

X-Ray Diffraction Studies

In order to correlate phase transformations with peaks on the DSC trace, several compositions were selected for study by x-ray diffraction. Specimens were sealed in a gold pan and heated in the DSC at a rate of 80 K/min to the desired temperature corresponding to a point on the DSC trace, then immediately quenched to room temperature at 320 K/min (the fastest rate of which the DSC is capable). Using a Philips Norelco diffractometer with CuKα radiation, x-ray diffraction patterns were obtained on these specimens to determine which phases were appearing as the crystallization process proceeded.

Transmission Electron Microscopy

Several of the specimens that were prepared for x-ray diffraction studies by heating to specific points on the DSC trace were also studied by transmission electron microscopy (TEM). A JEOLCO 100C microscope operating at 120 kV was used. The specimens were prepared for TEM by electropolishing in a Tenupol electropolishing cell using a solution of 600 ml methanol, 495 ml isobutyl alcohol, and 105 ml perchloric acid at $-25°C$ and 20 V. Very low jet speeds were used due to the fragile nature of the specimens (they were very thin and brittle after annealing).

Curve Digitization by Computer

For purposes of presentation, the DSC traces generated in this research were digitized and redrawn using a personal computer system, which included an IBM-PC with 512 K memory, a Bausch and Lomb HIPAD digitizer, an Amdek Amplot II plotter, and an Okidata μ92 microline printer. The digitizing program, which was written by Matt Ferber,[80] allows one to digitize the curves, normalize them to the same size sample and same calorimeter parameters, and then redraw as many as six curves together on the same figure. The program is included as Appendix B of this thesis. For all the compositions studied, traces produced at 20 K/min were normalized to that of a 3 mg weight sample.

CHAPTER IV

EXPERIMENTAL RESULTS

Results of Thermal Analysis of Crystallization Process

The thermal characteristics of splat-quenched Zr-Ni samples of compositions between 55 and 71 at. % Zr were analyzed on a differential scanning calorimeter (DSC). The appearance of the exothermic response produced as the sample was heated through crystallization varied as a function of the composition. Figure 8 presents the peaks produced at a heating rate of 20 K/min as a function of temperature for the range of compositions studied. These peaks have been normalized to a 3 mg weight sample, so that the total area under the peaks for each composition represents the amount of heat given off when a 3 mg sample of that composition crystallizes at a constant heating rate. This figure makes the following suggestions:

1. Overall, the beginning of the crystallization process decreases in temperature as the alloy composition is increased in zirconium.

2. Beginning at the $Zr_{57.1}Ni_{42.9}$ composition and continuing right up to the eutectic composition at $Zr_{63.5}Ni_{36.5}$, the DSC pattern is characterized by a small exotherm which is more than 100° above the main transformation peak(s). This small peak appears to move toward higher temperatures as one goes from 57.1 to 59 at. % Zr, then decrease until it disappears after 63.2 at. % Zr. Likewise, it tends to increase and decrease in size following the same compositional dependence.

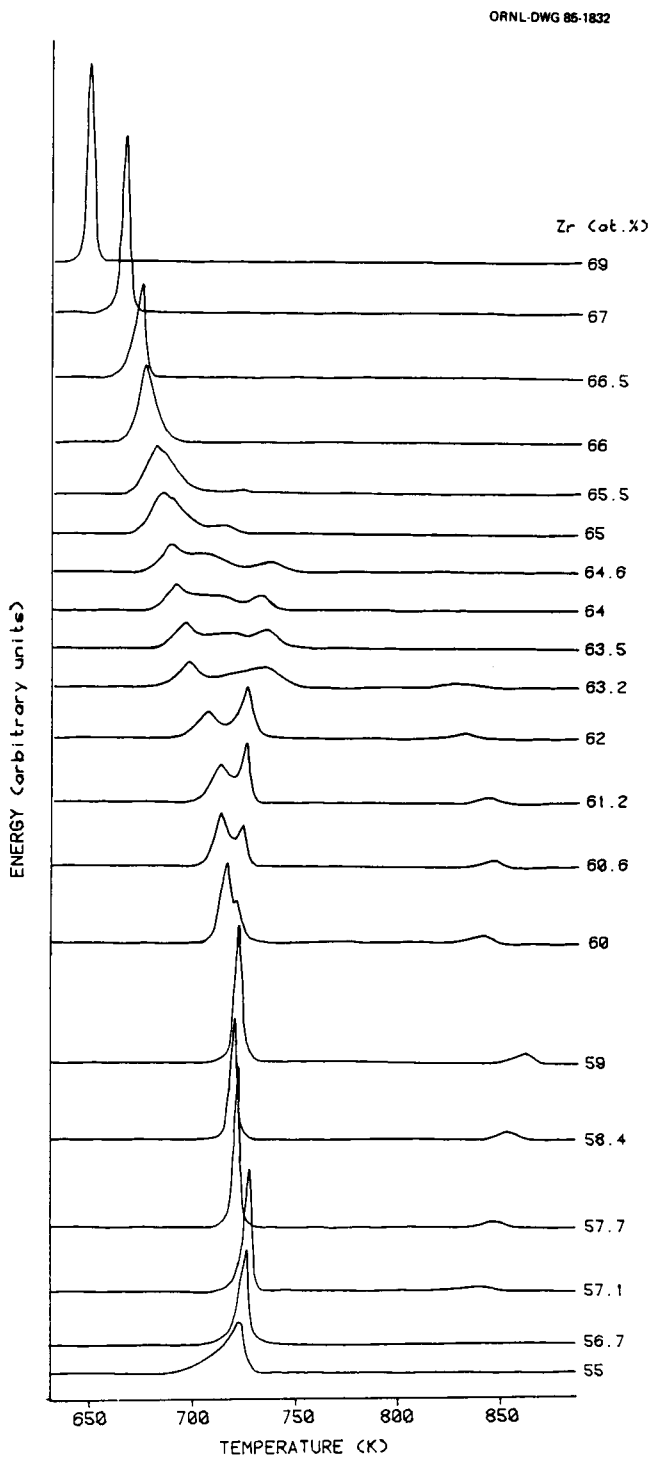

Figure 8. Differential scanning calorimeter (DSC) traces produced by the crystallization of Zr-Ni metallic glasses at a heating rate of 20 K/min, shown as a function of composition and temperature. All samples have been normalized to a weight of 3 mg.

3. Single sharp symmetric peaks appear as a consequence of the low-temperature transformation at compositions of 57.7—59 at. % Zr. Below this composition range, a leading shoulder gradually enlarges until the DSC peak is definitely asymmetric at 55 at. % Zr. Above 66.5 at. % Zr the trace again shows only one sharp peak.

4. At $Zr_{60}Ni_{40}$ a small second peak begins to appear during the low-temperature transformations. As the composition increases in zirconium content, this peak tends to separate in temperature from the first peak, and it becomes larger in size (as the first peak decreases in size) until, at 62 at. % Zr, the second peak dominates the total transformation process.

5. At $Zr_{63.2}Ni_{36.8}$ the second peak seems to flatten and separate into two broad peaks which are difficult to differentiate. From here through 65.5 at. % Zr there are definitely three peaks present, but it is difficult to relate them to the two peaks at $Zr_{62}Ni_{38}$. As the zirconium content increases, the second peak of the 63.2 at. % Zr alloy moves toward lower temperatures until at 66 at. % Zr it has merged with the first peak of that composition. Meanwhile, the third peak has decreased in size until it disappears above 65.5 at. % Zr.

6. The appearance of multiple peaks in the DSC trace occur at compositions which extend to approximately 3 at. % Zr on either side of the eutectic composition at 63.5 at. % Zr. At compositions near the equilibrium phase at 66.7 at. % Zr, a single sharp DSC peak is observed. Although no equilibrium phase has been reported in the 57—59 at. % Zr composition range, these alloys also show single sharp low-temperature peaks.

Calorimetry traces similar to those in Fig. 8 were obtained at 5, 10, 20, 40, and 80 K/min heating rates for twenty-six compositions between 55 and 71 at. % Zr. From these traces, temperatures T_x, T_{p1}, T_{p2}, T_{p3}, and T_{HT} were measured. These temperatures are recorded in Table II and are shown as a function of atomic percent zirconium at a heating rate of 20 K/min in Fig. 9. At most compositions, more than one splat-cooled sample was tested, producing more than one data point for each peak. However, because there were so many data points, and the data were so reproducible, only an average value was used in Fig. 9. The error in reading the temperature from the chart strip was estimated to be less than ±2° (see Appendix C). This figure confirms the tendency of the temperatures to decrease with increasing zirconium content, as was implied in Fig. 8. The temperatures recorded for the 55 and 56.7 at. % Zr alloys are believed to be a bit low and are probably due to crystallites quenched in during the splat-cooling process. During the TEM study, quenched-in crystals were actually observed in one of the 55 at. % Zr splats. This figure shows the DSC peak temperature of all peaks at each composition as well as the temperature, T_x, at the onset of the crystallization process. The occurrence of the multiple peaks, as discussed with regard to Fig. 8, is confirmed by this figure.

From the shift in the peak temperature as a function of heating rate, the effective activation energy ΔE for each peak was calculated as described in Chapter III. The ΔE values thus obtained are recorded in Table II and are shown as a function of composition in Fig. 10. Again there are as many as three data points for each peak for particular alloy compositions, indicating reproducible data values. The open

Table II. Transformation Temperatures as Measured from the DSC Traces and Corresponding Activation Energies Determined by the Kissinger Method

Composition (at. % Zr)	Specimen Number S2-	Peak Position[a]	Transformation Temperature (K ± 2°)[b] Heating Rate (K/min) 5	10	20	40	80	ΔE(eV) (±4 × 10^{-4} eV)[c]	Correlation Coefficient[d] r^2
55	63	X	679	682	710	718	725		
		1	701	698	722	731	739	3.11[e]	0.997
	89	X	--	704	714	726	735		
		1	--	713	723	732	742	3.23	0.999
56.7	93	X	701	709	720	730	739		
		1	709	718	727	735	745	3.43	0.999
	102	X	--	712	718	727	735		
		1	--	718	725	734	742	3.86	0.999
	163	X	--	712	720	729	737		
		1	--	718	727	735	743	3.75	0.998
57.1	54	X	703	714	722	730	738		
		1	711	719	727	735	744	3.79	0.999
		HT	?	835	846	857	871	3.48	0.999
	55	X	706	716	726	730	739		
		1	712	722	731	736	744	3.81	0.984
		HT	821	837	849	856	868	3.54	0.978
	92	X	--	714	722	731	739		
		1	--	720	727	736	744	3.74	0.999
		HT	--	828	840	853	866	3.28	0.999

Table II. (Continued)

Composition (at. % Zr)	Specimen Number S2-	Peak Position[a]	Transformation Temperature (K ± 2°)[b] Heating Rate (K/min) 5	10	20	40	80	ΔE(eV) (±4 × 10^{-4} eV)[c]	Correlation Coefficient[d] r^2
57.7	138	X	--	713	721	729	736		
		1	--	717	725	733	741	3.81	0.999
		HT	--	838	849	862	874	3.54	0.999
	141	X	--	712	720	728	736		
		1	--	716	724	732	740	3.86	0.999
		HT	--	839	849	861	873	3.64	0.999
58.4	91	X	--	709	717	724	733		
		1	--	713	721	729	738	3.68	0.999
		HT	--	841	855	868	882	3.12	0.999
	103	X	--	708	716	723	731		
		1	--	712	720	727	736	3.77	0.997
		HT	--	839	853	865	f	3.18	0.998
59	56	X	702	709	717	725	731		
		1	706	713	721	729	736	3.86	0.999
		HT	833	846	862	874	886	3.09	0.996
	156	X	--	712	719	727	733		
		1	--	717	724	732	739	4.06	0.999
		HT	--	848	861	874	885	3.42	0.998
59.5	90	X	--	706	714	721	727		
		1	--	710	718	726	733	3.85	0.999
		HT	--	839	853	872	880	2.90	0.976

Table II. (Continued)

Composition (at. % Zr)	Specimen Number S2-	Peak Position[a]	Transformation Temperature (K ± 2°)[b] Heating Rate (K/min) 5	10	20	40	80	ΔE(eV) (±4 × 10^{-4} eV)[c]	Correlation Coefficient[d] r^2
60	49	X	695	701	708	715	722		
		1	699	706	714	722	731	3.78	0.999
		2	?	711	721	731	741	3.00	0.999
		HT	807	825	838	857	874	2.38	0.997
	99	X	--	702	710	716	722		
		1	--	707	715	722	731	3.75	0.999
		2	--	711	721	731	741	3.02	0.999
		HT	--	830	845	859	874	2.82	0.999
60.6	162	X	694	701	707	713	718		
		1	700	707	714	722	729	4.11	0.999
		2	705	715	725	735	746	2.95	0.999
		HT	816	833	847	862	878	2.63	0.999
61.2	96	X	--	698	704	709	714		
		1	--	706	712	719	725	4.54	0.998
		2	--	715	725	735	746	2.92	0.999
		HT	--	828	844	861	876	2.56	0.999
	168	X	692	698	704	709	714		
		1	699	706	713	719	725	4.42	0.995
		2	706	716	727	737	747	2.93	0.998
		HT	814	830	848	863	879	2.48	0.997

Table II. (Continued)

Composition (at. % Zr)	Specimen Number S2-	Peak Position[a]	Transformation Temperature (K ± 2°)[b] Heating Rate (K/min) 5	10	20	40	80	ΔE(eV) (±4 × 10^{-4} eV)[c]	Correlation Coefficient[d] r^2
62	65	X	684	689	694	700	705		
		1	693	698	704	710	717	4.83	0.999
		2	703	714	723	734	745	2.92	0.999
		HT	799	813	829	847	865	2.31	0.999
	95	X	--	687	693	699	704		
		1	--	696	703	709	715	4.58	0.999
		2	--	713	724	734	745	2.89	0.999
		HT	--	811	829	841	865	2.20	0.986
62.8	98	X	--	682	689	694	700		
		1	--	693	699	704	711	4.63	0.999
		2	--	720	730	740	750	3.13	0.999
		3	--	?	?	?	760	g	
		HT	--	?	834	850	868	2.42	0.999
	111	X	--	683	689	694	699		
		1	--	693	699	705	711	4.82	0.999
		2	--	722	731	741	752	3.12	0.999
		3	--	?	?	?	763	f	
		HT	--	818	834	849	867	2.50	0.999
63.2	97	X	675	682	687	692	698		
		1	685	692	697	703	710	4.67	0.998
		2	?	?	732	742	753	2.91	0.999
		3	715	727	736	752	765	2.48	0.995
		HT	?	?	827	844	862	2.31	0.999

Table II. (Continued)

Composition (at. % Zr)	Specimen Number S2-	Peak Position[a]	Transformation Temperature (K ± 2°)[b] Heating Rate (K/min) 5	10	20	40	80	ΔE(eV) (±4 × 10^{-4} eV)[c]	Correlation Coefficient[d] r^2
63.5	38	X	673	678	684	688	695		
		1	682	687	693	699	706	4.70	0.999
		2	?	703	716	732	749	1.91	0.997
		3	710	722	733	745	756	2.63	0.999
	94	X	—	679	684	689	695		
		1	--	688	694	699	706	4.68	0.996
		2	--	702	718	731	748	1.94	0.998
		3	--	722	734	745	757	2.71	0.999
	166	X	--	678	684	690	695		
		1	--	688	694	701	706	4.52	0.998
		2	—	708	720	738	749	2.07	0.990
		3	--	725	736	750	760	2.63	0.995
64	87	X	--	676	681	686	694		
		1	--	685	690	696	705	4.82[h]	0.999
		2	--	696	709	722	740	2.18[h]	0.999
		3	--	721	734	746	760	2.51[h]	0.999
	101	X	--	675	680	685	692		
		1	--	684	690	696	704	4.36	0.991
		2	--	693	708	721	738	1.95	0.999
		3	--	720	732	743	757	2.53	0.999
64.6	107	X	--	672	677	682	690		
		1	--	681	687	692	701	4.23	0.988
		2	--	689	703	716	733	1.95	0.998
		3	--	726	736	746	762	2.63	0.984

Table II. (Continued)

Composition (at. % Zr)	Specimen Number S2-	Peak Position[a]	Transformation Temperature (K ± 2°)[b] Heating Rate (K/min) 5	10	20	40	80	ΔE(eV) (±4 × 10^{-4} eV)[c]	Correlation Coefficient[d] r^2
	157	X	--	673	679	684	691		
		1	--	683	689	693	702	4.52	0.987
		2	--	700	713	726	740	2.23	0.999
		3	--	738	749	761	772	2.81	0.999
65	129	X	--	668	674	680	685		
		1	--	676	683	690	696	4.21	0.999
		2	--	681	690	701	715	2.44	0.990
		3	--	703	715	727	740	2.42	0.999
65.5	106	X	--	666	671	676	682		
		1	--	673	680	687	693	4.14	0.999
		2	--	?	685	694	708	2.42	0.987
		3	--	?	722	734	745	2.66	0.999
	113	X	--	665	671	677	683		
		1	--	673	680	687	692	4.14	0.995
		2	--	673	686	694	709	2.35	0.993
		3	--	?	720	732	743	2.64	0.999
	167	X	658	665	671	677	682		
		1	666	673	681	687	694	3.90	0.998
		2	666	673	685	696	710	2.41	0.991
		3	?	?	726	738	749	2.63	0.999

Table II. (Continued)

Composition (at. % Zr)	Specimen Number S2-	Peak Position[a]	Transformation Temperature (K ± 2°)[b] Heating Rate (K/min) 5	10	20	40	80	ΔE(eV) (±4 × 10^{-4} eV)[c]	Correlation Coefficient[d] r^2
66	62	X	653	660	668	674	680		
		1	659	666	675	683	691	3.23	0.999
		2	658	666	676	687	697	2.61[i]	0.999
	104	X	--	660	667	674	681		
		1	--	667	675	683	692	3.15	0.999
		2	--	664	675	689	699	2.24[i]	0.994
66.5	34	X	649	657	664	671	678		
		1	654	662	671	680	691	2.85	0.998
67	41	X	642	650	659	668	676		
		1	646	654	663	673	684	2.65	0.999
	51	X	644	652	660	669	677		
		1	648	657	665	675	685	2.74	0.999
69	105	X	627	635	644	653	662		
		1	631	639	648	657	667	2.69	0.999
71	108	X	--	629	637	644	654		
		1	--	632	640	649	659	2.70	0.997

[a]Peak position refers to the numbered position of the peak in the DSC trace. For example No. 1 refers to the first DSC peak, etc.; HT refers to the high-temperature peak; X refers to the onset of crystallization.

Table II. (Continued)

[b]Reported temperatures were calibrated against the melting point of zinc (692.65 K). The values reported in this table are estimated to have a measurement error no larger than ±2° (see Appendix C). A dash indicates that no sample was run at that rate either due to time restraints or lack of enough sample. Where it was impossible to measure the temperature due to peak overlap, a question mark is used.

[c]See Appendix C for determination of error.

[d]The correlation coefficient is a statistical measure of how closely the data points fit the straight line determined by those points.

[e]The 10 K/min peak did not have the same appearance as the others and the temperature of the peak was much lower than it should have been, so it was not used in the determination of ΔE.

[f]Chart paper exhausted during test.

[g]A small third peak was seen only on the 80 K/min run. At other heating rates, it was obscured by the two large exotherms of this alloy.

[h]The 80 K/min temperature was not used to calculate ΔE because in the Kissinger plot that point fell much farther off the straight line than did the rest of the points.

[i]ΔE calculated from 20, 40, and 80 K/min runs only since this peak was obscured by the first peak at the slower heating rates.

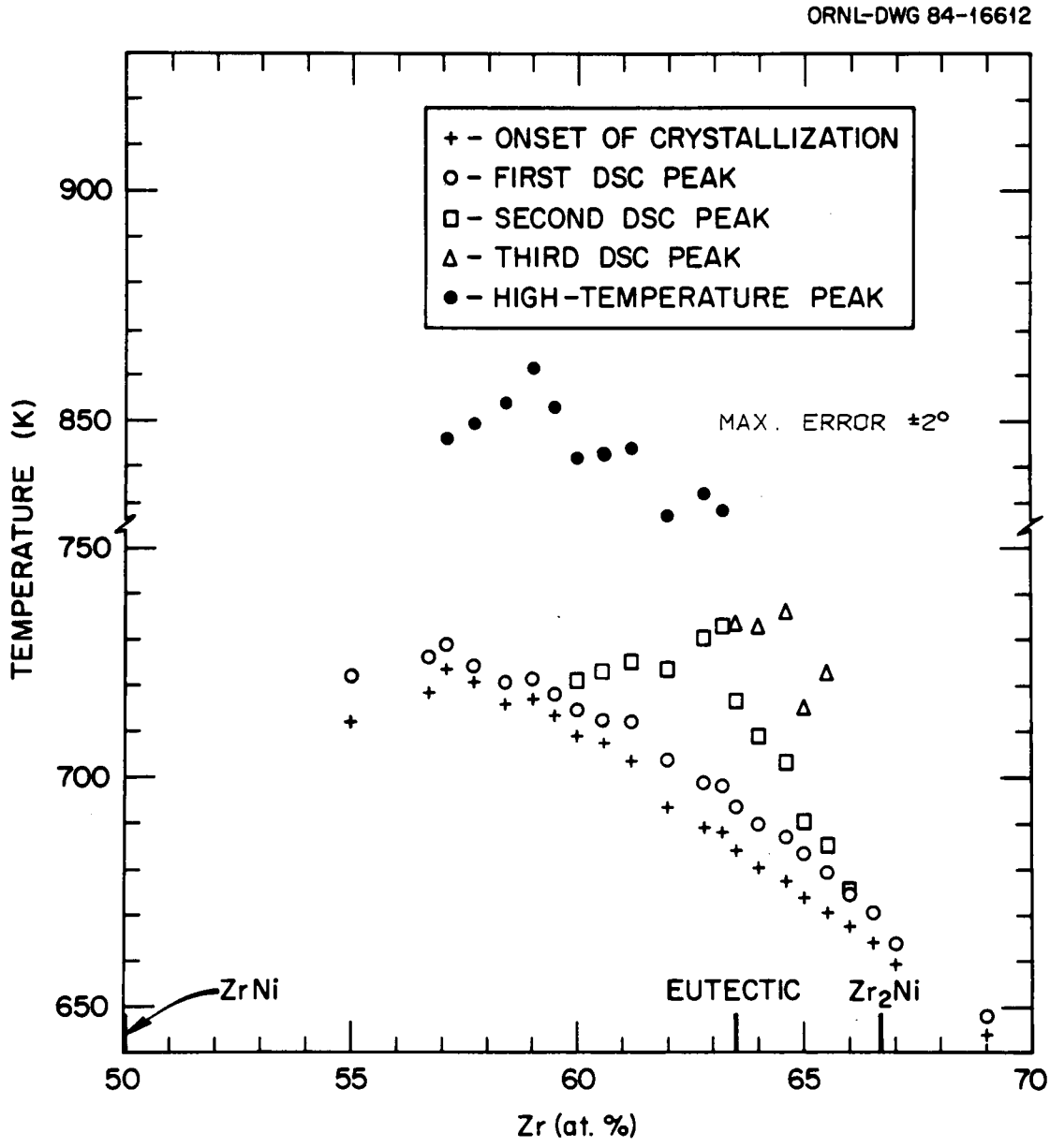

Figure 9. Transformation temperatures as a function of composition for the crystallization of Zr-Ni metallic glasses. The temperatures were taken from DSC traces in which the heating rate used was 20 K/min.

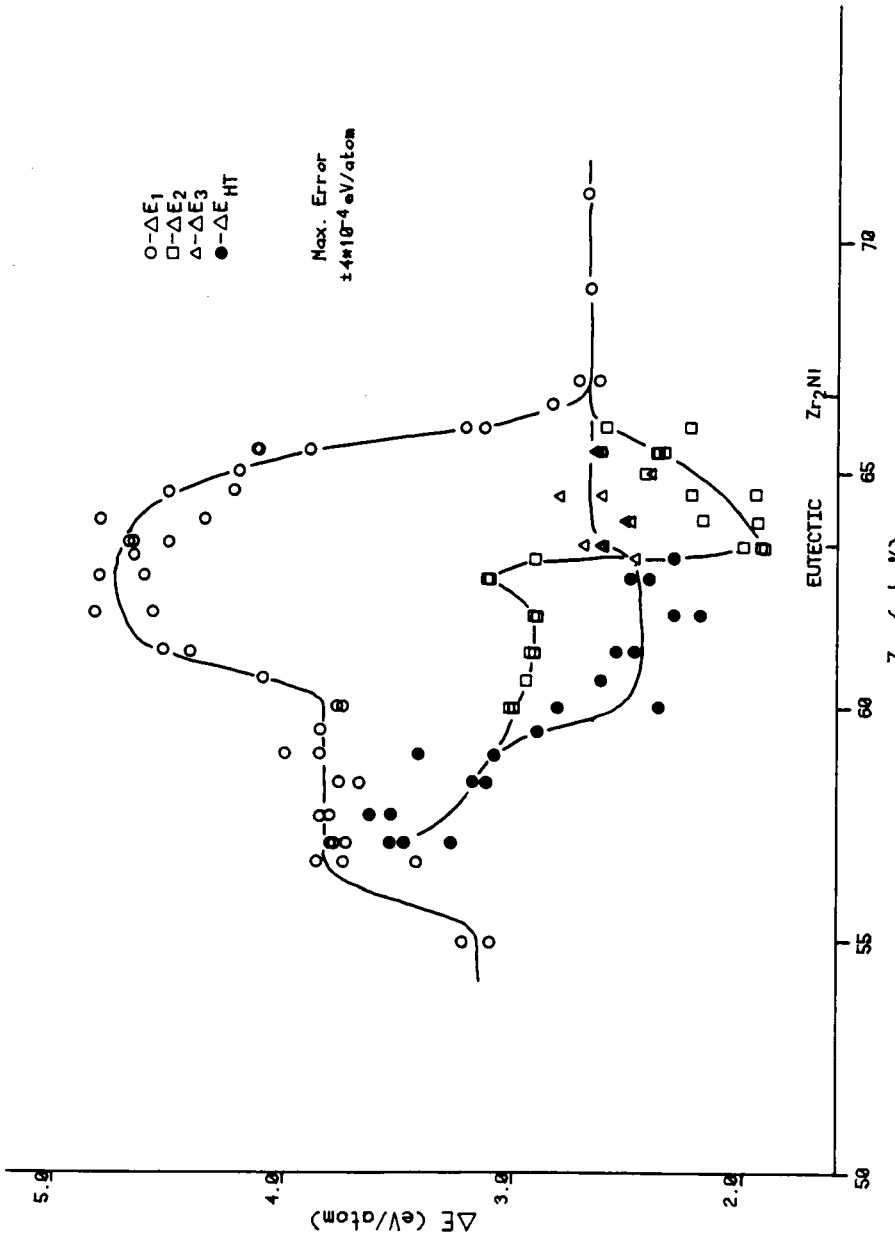

Figure 10. The activation energy as a function of composition for the DSC peaks produced during crystallization of Zr-Ni metallic glasses.

symbols represent the low-temperature DSC peaks; the darkened symbol represents the high-temperature peak. The lines have been drawn to serve as guides to following the trends in ΔE and do not represent any kind of mathematical fit to the data. Nor does a particular symbol always represent the same process. For example, as will be discussed below, the nature of the process represented by the first DSC peak changes as a function of composition. Several trends of this figure can be recognized.

1. The activation energy of the first peak, ΔE_1, changes as a function of composition. Below approximately 56.7 at. % Zr, its value is ~3.2 eV/atom; between 56.7 and 60 its value exhibits a plateau at ~3.8 eV/atom; there is a broad peak reaching to ~4.65 eV/atom between 61.2 and 66 at. % Zr; from 66.5 to 71 at. % Zr its value has decreased and leveled off at ~2.65 eV/atom. The reproducibility of the data points shows that these changes of ΔE_1 with composition definitely exist, and, if one compares these composition ranges with the appearance of additional DSC peaks in Fig. 8, one can conclude that there are definite relationships between the appearance of extra DSC peaks and the nature of the first crystallization process. It is believed that the changes in ΔE_1, as shown in this figure, indicate compositions where the process of the first DSC peak changes.

2. The activation energy of the high-temperature peak is about the same as the low-temperature peak for the 57.1 at. % Zr alloy (~3.6 eV/atom), where it is first discernible. With increasing zirconium, ΔE_{HT} decreases approximately linearly until it disappears at the eutectic composition, where its value is ~2.3 eV/atom.

3. The second DSC peak, which first appears as a shoulder on the high temperature side of the large transformation peak of $Zr_{60}Ni_{40}$, has a ΔE_2 of ~3 eV/atom and remains at about this value as one adds zirconium until the eutectic is reached. However the alloy at 62.8 at. % Zr exhibited a slightly higher ΔE_2 which could not be explained. At the eutectic ΔE_2 decreased drastically to ~2 eV/atom, exhibiting a decrease of 33% within a composition change of only 0.5 at. % Zr. From the eutectic composition to near the equilibrium compound, ΔE_2 increased to ~2.7 eV/atom. Only one DSC peak was seen above 66 at. % Zr.

4. The activation energy of the third DSC peak ΔE_3 remains at about 2.7 eV/atom for the composition range where it occurs (63.5-65.5 at. % Zr).

5. The activation energies of all three DSC peaks seem to come together at the equilibrium compound Zr_2Ni.

The amount of heat given off during a transformation is determined from a measure of the area under the DSC peak, as was described in Chapter III. Ideally, one hopes that the area of each peak can be measured separately giving a $\overline{\Delta H}$ for each process. However, many of the samples in this study produced multiple peaks which overlapped making it impossible to get separate determinations of $\overline{\Delta H}$. Instead a $\overline{\Delta H}$ value corresponding to the area under all the peaks added together was obtained and designated as $\overline{\Delta H}_t$. At the compositions where a high-temperature DSC peak occurred, $\overline{\Delta H}_t$ is equal to the enthalpy change of the low-temperature (ΔH_{LT}) and high-temperature (ΔH_{HT}) peaks added together. Where no high-temperature peak occurred, $\overline{\Delta H}_t$ equals $\overline{\Delta H}_{LT}$. These data values are listed in Table III for all alloy compositions

Table III. Experimental Enthalpy Change Data Determined From the Measure of the Area Under the DSC Peaks

Composition (at. % Zr)	Specimen Number S2-	Peak Position[a]	ΔH (kJ/mole) Heating Rate (K/min) 5	10	20	40	80	$\overline{\Delta H}$	$\overline{\Delta H_t}$
55	63	LT	--	4.499	5.277	5.042	5.385	5.05 ± 0.20	5.05 ± 0.20
	89	LT	--	5.122	5.106	5.033	5.079	5.08 ± 0.02	5.08 ± 0.02
56.7	93	LT	4.779	4.382	4.802	4.719	4.741	4.68 ± 0.08	4.68 ± 0.08
	102	LT	--	4.596	4.715	4.393	b	4.57 ± 0.09	4.57 ± 0.09
	163	LT	--	4.691	4.646	4.704	4.986	4.76 ± 0.08	4.76 ± 0.08
57.1	55	LT	4.766	4.694	4.716	5.185	4.886	4.85 ± 0.09	
		HT	0.255	0.183	0.272	0.129	0.444	0.26 ± 0.05	5.11 ± 0.10
	92	LT	--	4.781	4.746	4.913	5.089	4.88 ± 0.08	
		HT	--	0.397	0.362	0.268	0.263	0.32 ± 0.03	5.20 ± 0.08
57.7	138	LT	--	4.712	4.960	5.107	5.099	4.97 ± 0.09	
		HT	--	0.740	0.776	0.766	0.740	0.76 ± 0.01	5.73 ± 0.09
	141	LT	--	4.663	4.726	4.813	5.005	4.80 ± 0.07	
		HT	--	0.777	0.788	0.673	0.716	0.74 ± 0.03	5.54 ± 0.08
58.4	91	LT	--	4.443	4.529	4.747	4.688	4.60 ± 0.07	
		HT	--	0.783	0.810	0.913	1.090	0.90 ± 0.07	5.50 ± 0.10
	103	LT	--	4.500	4.561	4.561	4.840	4.62 ± 0.08	
		HT	--	0.766	0.896	0.916	b	0.86 ± 0.05	5.48 ± 0.09

Table III. (Continued)

Composition (at. % Zr)	Specimen Number S2-	Peak Position[a]	ΔH (kJ/mole) Heating Rate (K/min) 5	10	20	40	80	$\overline{\Delta H}$	$\overline{\Delta H_t}$
59.0	56	LT	4.408	4.510	4.582	4.667	4.580	4.55 ± 0.04	
		HT	0.764	0.720	0.792	0.979	0.788	0.81 ± 0.04	5.36 ± 0.06
	156	LT	--	4.124	4.539	4.618	4.811	4.52 ± 0.14	
		HT	--	0.784	0.812	0.949	0.782	0.83 ± 0.04	5.36 ± 0.14
59.5	90	LT	--	4.724	4.839	4.709	4.720	4.75 ± 0.03	
		HT	--	0.768	0.758	0.704	0.823	0.76 ± 0.02	5.51 ± 0.04
60.0	49	LT	4.592	4.675	4.843	4.711	4.956	4.76 ± 0.06	
		HT	0.482	0.697	0.524	0.657	0.604	0.59 ± 0.04	5.35 ± 0.07
	99	LT	--	4.628	4.649	4.871	4.975	4.78 ± 0.08	
		HT	--	0.520	0.736	0.654	0.736	0.66 ± 0.05	5.44 ± 0.09
60.6	62	LT	4.898	5.071	4.934	5.107	5.085	5.02 ± 0.04	
		HT	0.503	0.540	0.649	0.664	0.664	0.60 ± 0.03	5.62 ± 0.05
61.2	96	LT	--	5.010	4.980	5.178	b	5.06 ± 0.06[c]	
		HT	--	0.546	0.565	0.610	b	0.57 ± 0.02	5.63 ± 0.06
62.0	65	LT	5.036	5.428	5.290	5.412	5.477	5.33 ± 0.08	
		HT	0.276	0.346	0.535	b	0.475	0.41 ± 0.06	5.74 ± 0.10
	95	LT	--	5.419	5.178	5.464	5.341	5.35 ± 0.06	
		HT	--	0.270	0.343	0.372	0.250	0.31 ± 0.03	5.66 ± 0.07

Table III. (Continued)

Composition (at. % Zr)	Specimen Number S2-	Peak Position[a]	ΔH (kJ/mole) Heating Rate (K/min) 5	10	20	40	80	$\overline{\Delta H}$	$\overline{\Delta H}_t$
62.8	98	LT	--	5.481	5.269	5.283	5.652	5.42 ± 0.09	
		HT	--	b	0.205	0.264	0.256	0.24 ± 0.02	5.66 ± 0.09
	111	LT	--	4.988	5.416	5.583	5.541	5.38 ± 0.14	
		HT	--	b	0.164	0.288	0.173	0.21 ± 0.04	5.59 ± 0.14
63.2	97	LT	4.983	5.205	5.572	5.591	5.768	5.42 ± 0.14[c]	
		HT	b	b	0.180	0.207	0.242	0.21 ± 0.02	5.64 ± 0.14
63.5	38	LT	0.350	5.155	5.391	5.450	5.695	5.41 ± 0.09	5.41 ± 0.09
	94	LT	--	b	5.601	5.570	5.729	5.63 ± 0.05	5.63 ± 0.05
	166	LT	--	5.278	5.322	5.822	5.978	5.60 ± 0.18	5.60 ± 0.18
64	87	LT	--	b	5.674	5.568	5.757	5.67 ± 0.05	5.67 ± 0.05
	101	LT	--	5.300	5.664	5.644	5.984	5.65 ± 0.14	5.65 ± 0.14
64.6	107	LT	--	5.309	5.759	5.605	5.595	5.57 ± 0.09	5.57 ± 0.09
	157	LT	--	5.024	5.442	5.797	5.984	5.56 ± 0.20	5.56 ± 0.20
65.0	129	LT	--	5.574	5.714	5.923	5.851	5.77 ± 0.08	5.77 ± 0.08
65.5	106	LT	--	b	5.699	5.975	5.981	5.88 ± 0.09	5.88 ± 0.09
	113	LT	--	5.229	b	5.500	5.619	5.45 ± 0.12	5.45 ± 0.12
	167	LT	b	5.643	5.473	5.476	5.565	5.54 ± 0.04	5.54 ± 0.04

Table III. (Continued)

Composition (at. % Zr)	Specimen Number S2-	Peak Position[a]	ΔH (kJ/mole) Heating Rate (K/min) 5	10	20	40	80	$\overline{\Delta H}$	$\overline{\Delta H_t}$
66.0	62	LT	5.094	5.423	5.371	5.477	5.767	5.43 ± 0.11	5.43 ± 0.11
	104	LT	--	5.435	5.364	5.454	5.715	5.49 ± 0.08	5.49 ± 0.08
66.5	34	LT	5.733	5.395	5.447	b	5.813	5.60 ± 0.10	5.60 ± 0.10
67.0	41	LT	5.880	6.081	6.082	5.648	5.691	5.88 ± 0.09	5.88 ± 0.09
	51	LT	5.880	5.902	5.887	b	b	5.89 ± 0.01	5.89 ± 0.01
69.0	105	LT	5.424	5.476	5.646	5.711	5.722	5.60 ± 0.06	5.60 ± 0.06
71.0	108	LT	--	5.284	5.512	5.841	5.481	5.53 ± 0.12	5.53 ± 0.12

[a]Due to peak overlap, it was not possible to measure the enthalpy change of the individual peaks. They were therefore designated as low-temperature (LT) and high-temperature (HT) peaks for this measurement.

[b]The range of the DSC determines the y-axis. For this sample, the wrong range was selected, causing the transformation peak to go off the chart.

[c]The baselines of the DSC traces for these samples were not level and did not match up to the traces themselves. The position of the true baseline was therefore not known.

studied. As noted in Chapter III, the bar over ΔH indicates that the enthalpy change recorded for that particular sample is an average of three to five pieces of that sample which were heated at different rates in the DSC. Figure 11 shows experimental $\overline{\Delta H}_{LT}$ values for the low-temperature transformations of all compositions studied (open circles) and, where the high-temperature peak occurred, $\overline{\Delta H}_t$ values for both the low- and high-temperature peaks combined (dark circles) as a function of zirconium composition. The line has been drawn in to serve as an aide in following the trends of the data and does not represent any kind of mathematical fit to the data. This figure shows the following features:

1. A small maximum in $\overline{\Delta H}_t$ is seen at compositions of 67 at. % Zr (near the composition of the Zr_2Ni equilibrium phase) and at 57.7 at. % Zr.

2. A high plateau in $\overline{\Delta H}_t$ exists between 60.6 and 64 at. % Zr.

3. In the composition region where the high-temperature peak is observed, there is a minimum near 59 at. % Zr in the $\overline{\Delta H}_{LT}$ value.

4. The scatter in $\overline{\Delta H}$ values is larger than for the ΔE values of Fig. 10 because of the nature of the determination of baselines for measurement of the area under the curves. (See Appendix C for determination of uncertainties in the data.) However for most alloy composition the methods used produced data points of enough reproducibility to assume that the data trends seen as a function of zirconium content are real.

Figure 12 shows $\overline{\Delta H}_{HT}$ for the high-temperature peak as a function of zirconium content. It is seen that the peak is first detected at 57.1

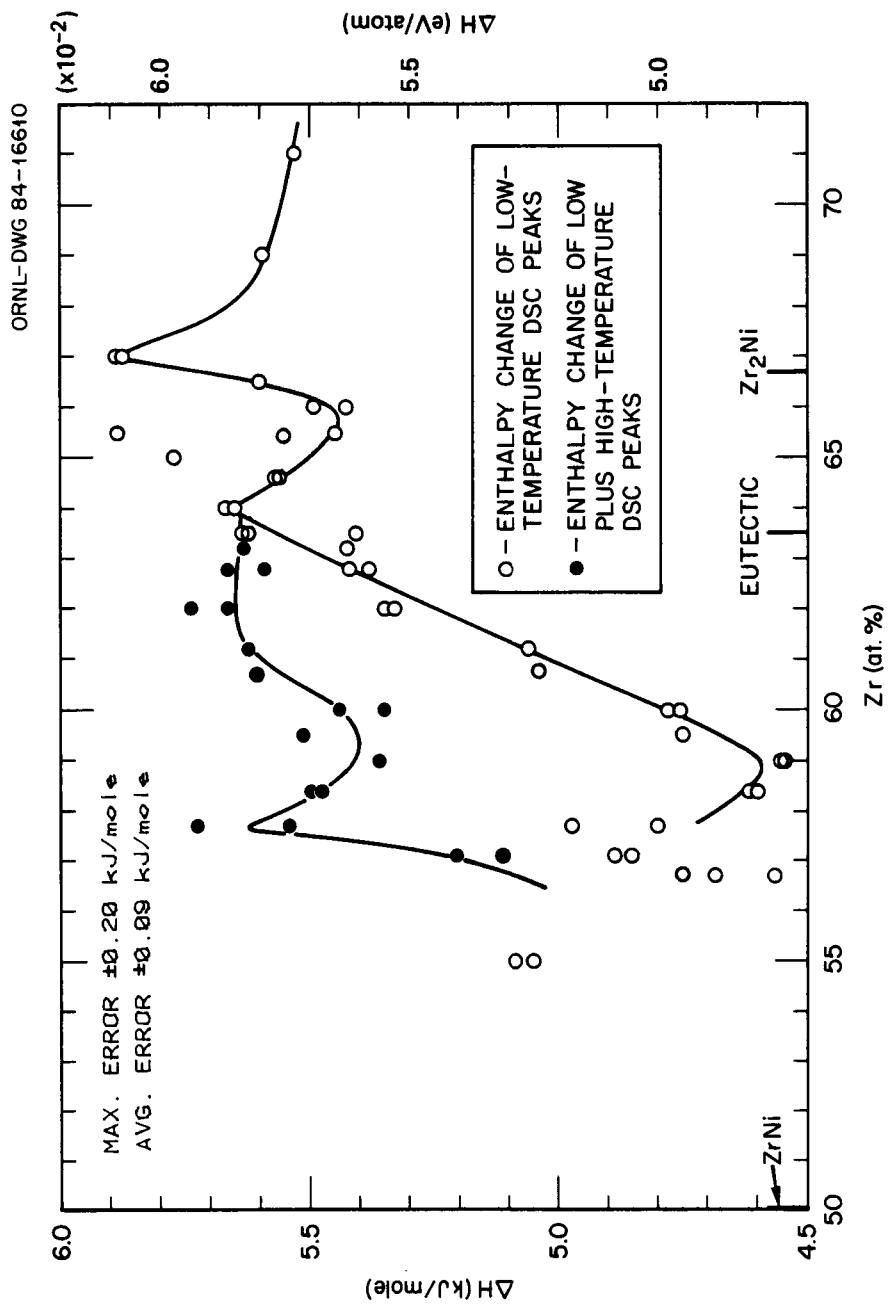

Figure 11. The enthalpy of crystallization as a function of composition for Zr-Ni metallic glasses. The open circles represent values determined by measuring the areas of all low-temperature DSC peaks involved in crystallization. The dark circles represent the values obtained by including the high-temperature peak where it occurred.

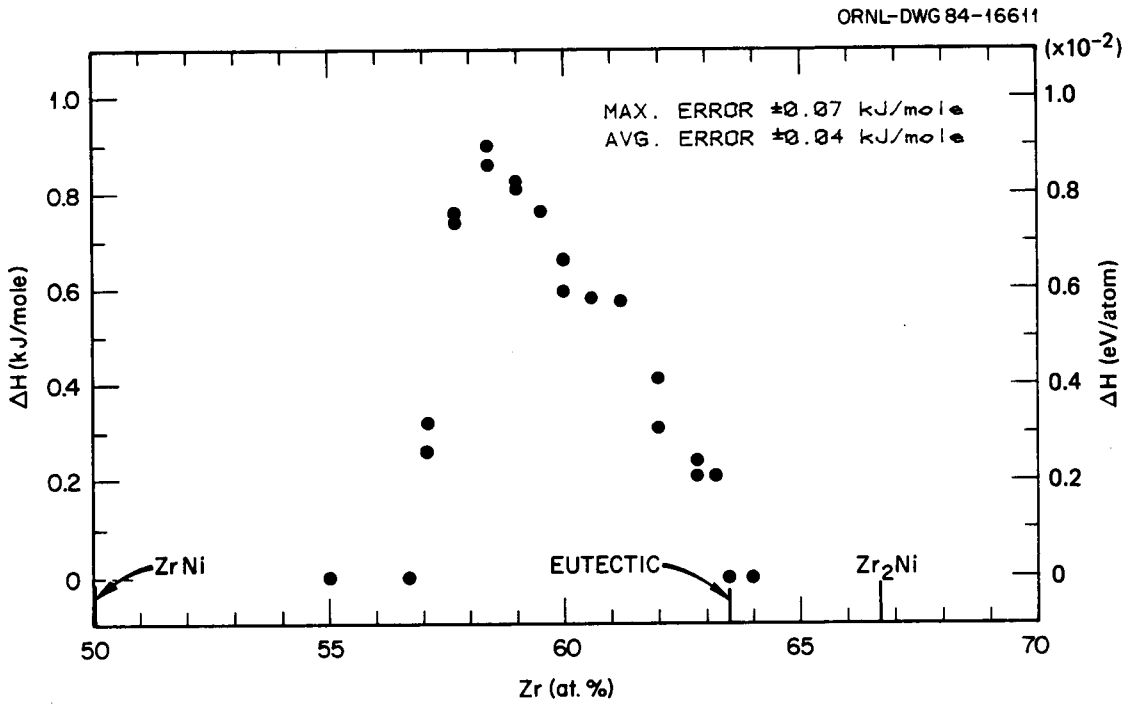

Figure 12. The enthalpy of the high-temperature peak showing its composition range and its heat content as a function of composition.

at. % Zr and increases rapidly to a maximum at 58.4 at. % Zr. The peak then decreases more gradually until it disappears above 63.2 at. % Zr.

Phase Identification by X-Ray Diffraction

The thermal study by DSC indicated that the crystallization process for Zr-Ni metallic glasses around the eutectic composition at 63.5 at. % Zr was very complicated. Assuming that each DSC peak represents a separate transformation, the total crystallization process for a particular composition involves as many as four different transformations. Realizing that it was necessary to identify the transformation represented by each DSC peak, several alloy compositions were selected for further study by x-ray diffraction (XRD). Pieces of the samples were heated at 80 K/min in the DSC to particular points on the DSC curve. In order to determine the transformation products present at that stage in the crystallization process, the samples were then quenched at 320 K/min to room temperature and x-rayed using CuKα radiation. Figures 13–19 show the compositions studied, their DSC traces at 80 K/min, and the x-ray pattern produced as a function of the point on the DSC trace to which the sample was heated. As-quenched and equilibrium x-ray patterns are also included where space is available, as well as a bar identifying the x-ray lines characteristic of the two equilibrium phases to which these compositions transform. The length of the marks on the bar represent the intensity of the characteristic x-ray lines for each phase. For some alloys, where one x-ray pattern appeared and persisted through a range of higher temperatures, only the higher temperature pattern, which exhibited sharper lines, is shown. For

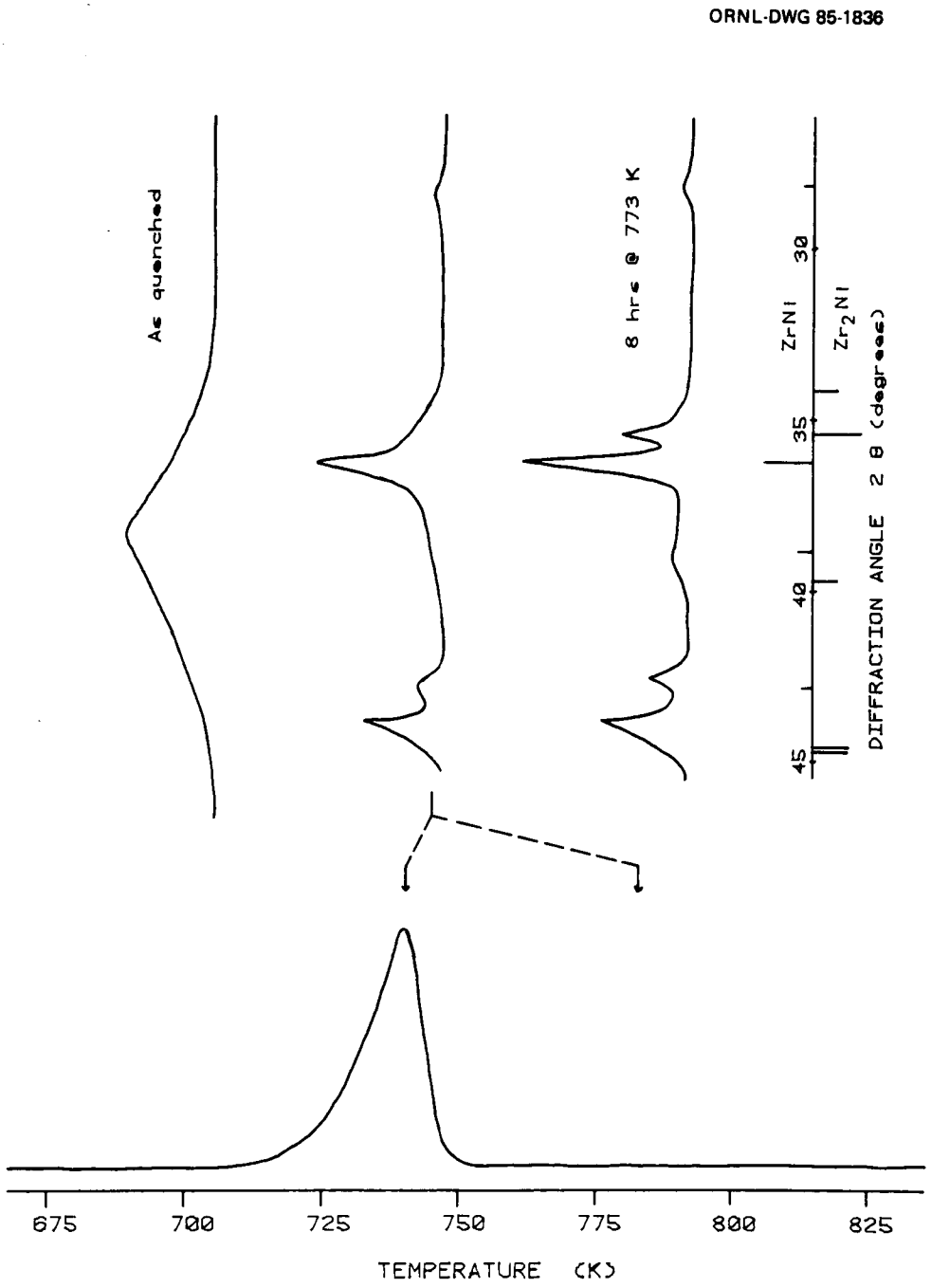

Figure 13. X-ray diffraction patterns obtained for $Zr_{55}Ni_{45}$ as a function of the progression of the crystallization process. Samples were heated in the DSC at 80 K/min to temperatures indicated by the arrows. Dashed lines connect those temperatures to the x-ray patterns obtained. A scale showing the major x-ray lines for ZrNi and Zr_2Ni is also presented to aid in the analysis of the x-ray patterns.

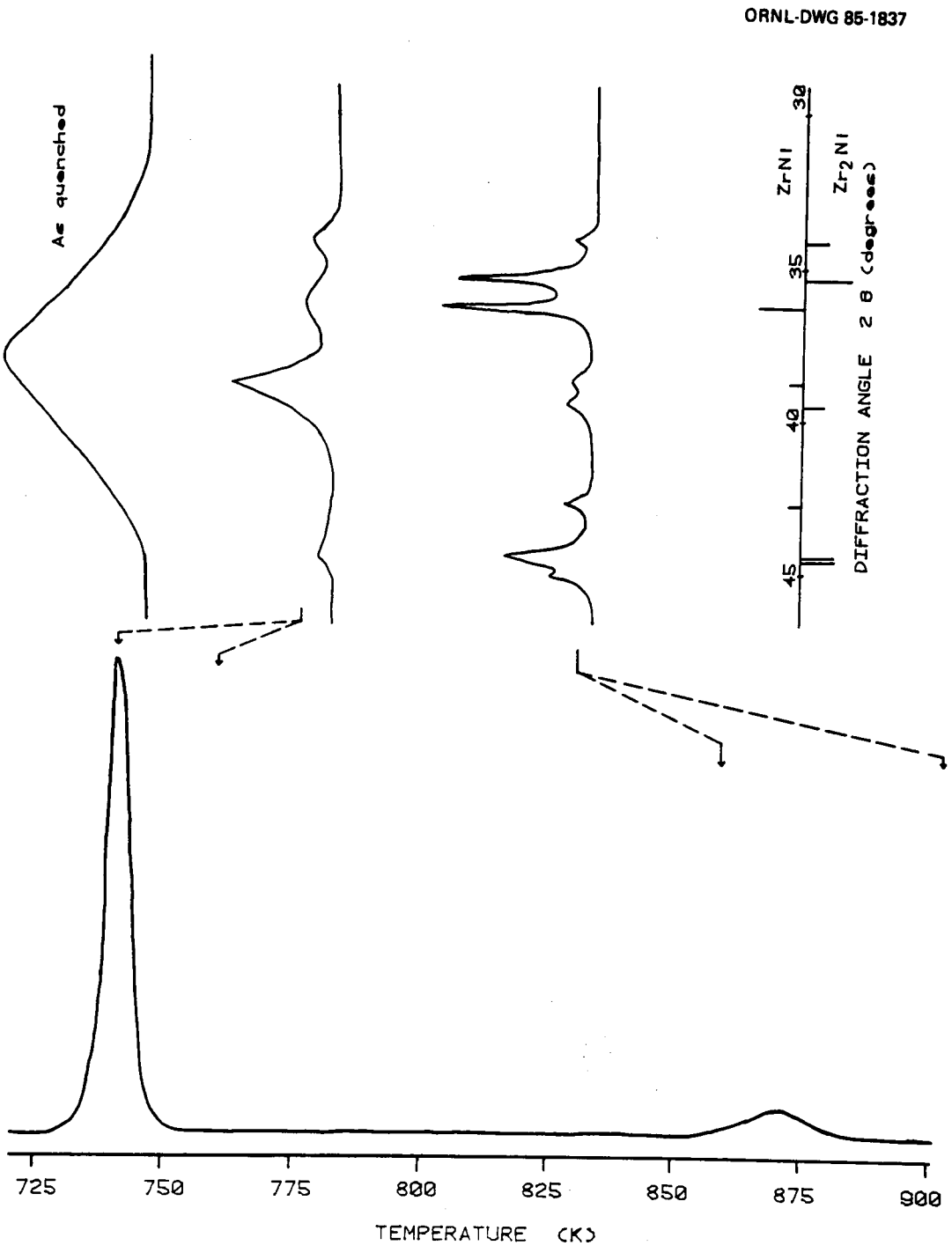

Figure 14. X-ray diffraction patterns obtained for $Zr_{57.7}Ni_{42.3}$ as a function of the progression of the crystallization process. Samples were heated in the DSC at 80 K/min to temperatures indicated by the arrows. Dashed lines connect those temperatures to the x-ray patterns obtained. A scale showing the major x-ray lines for ZrNi and Zr_2Ni is also presented to aid in the analysis of the x-ray patterns.

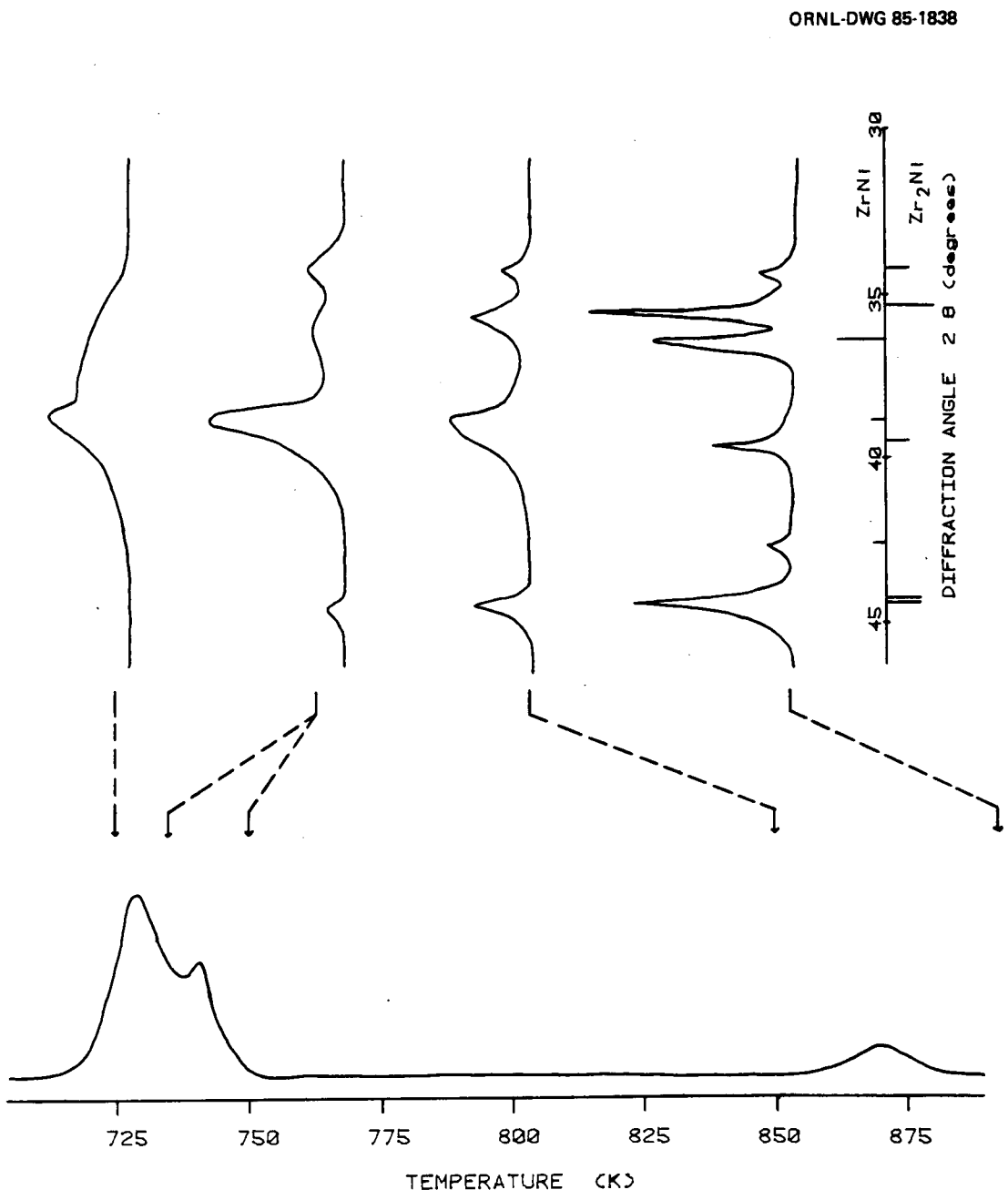

Figure 15. X-ray diffraction patterns obtained for $Zr_{60}Ni_{40}$ as a function of the progression of the crystallization process. Samples were heated in the DSC at 80 K/min to temperatures indicated by the arrows. Dashed lines connect those temperatures to the x-ray patterns obtained. A scale showing the major x-ray lines for ZrNi and Zr_2Ni is also presented to aid in the analysis of the x-ray patterns.

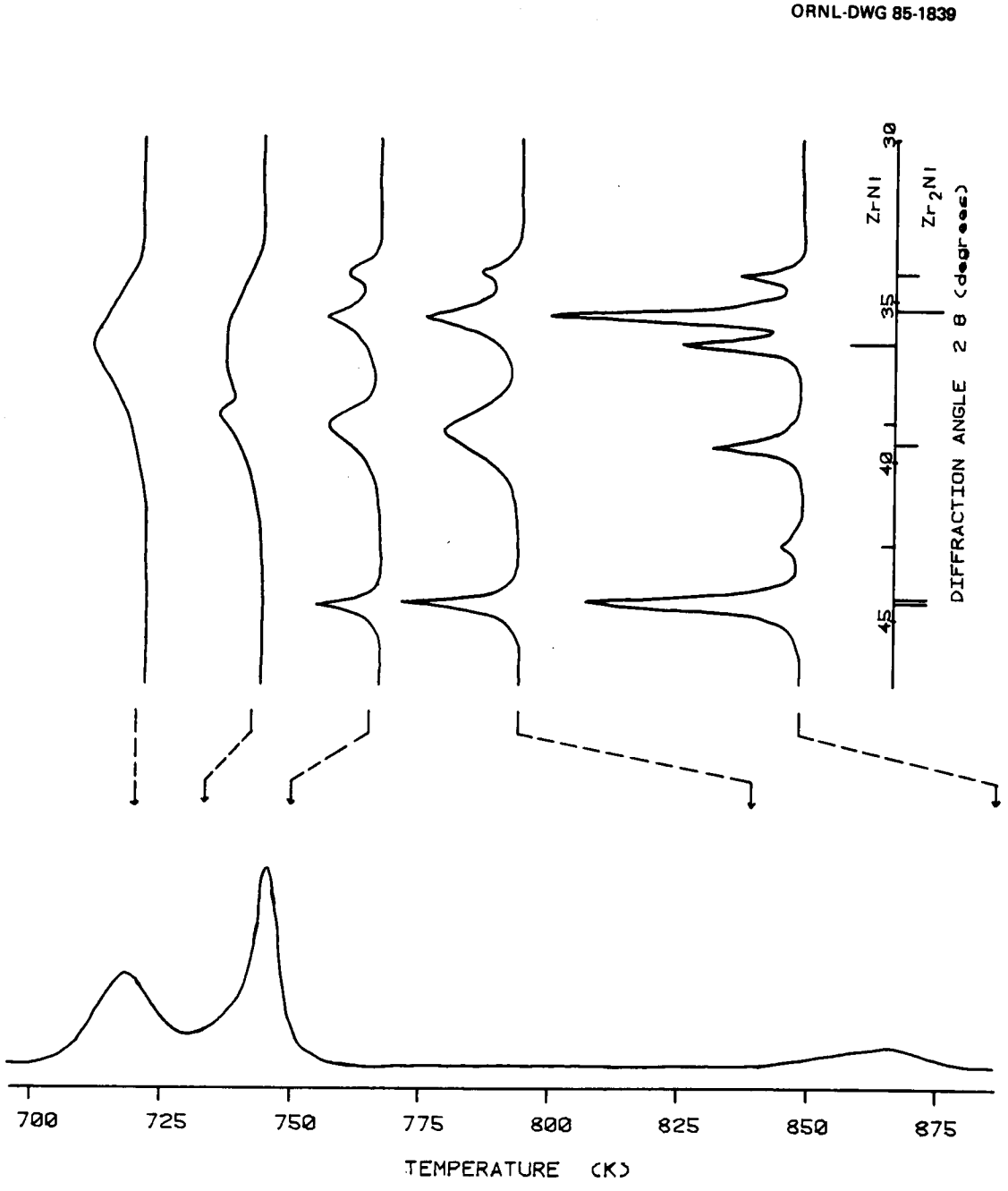

Figure 16. X-ray diffraction patterns obtained for $Zr_{62}Ni_{38}$ as a function of the progression of the crystallization process. Samples were heated in the DSC at 80 K/min to temperatures indicated by the arrows. Dashed lines connect those temperatures to the x-ray patterns obtained. A scale showing the major x-ray lines for ZrNi and Zr_2Ni is also presented to aid in the analysis of the x-ray patterns.

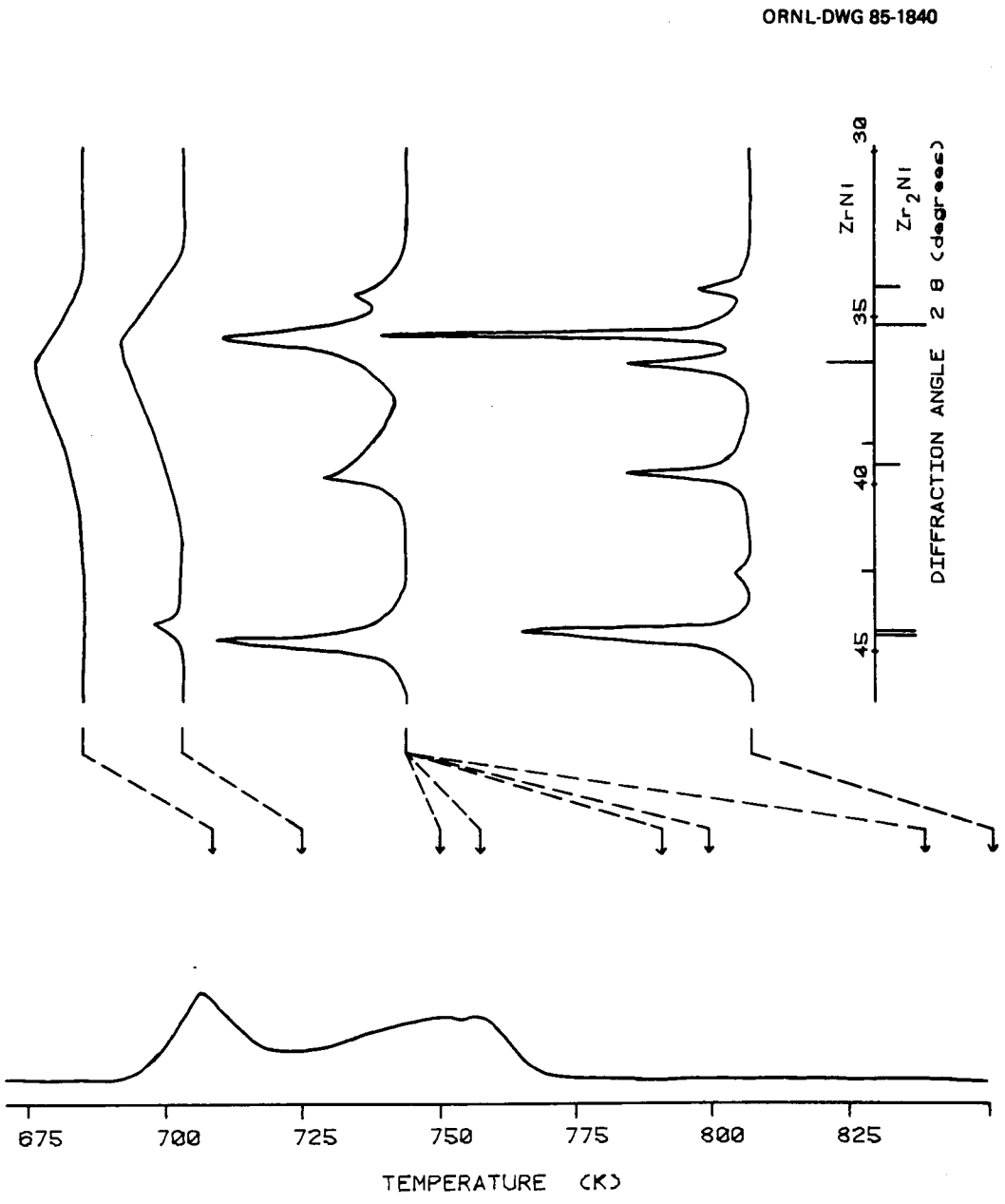

Figure 17. X-ray diffraction patterns obtained for $Zr_{63.5}Ni_{36.5}$ as a function of the progression of the crystallization process. Samples were heated in the DSC at 80 K/min to temperatures indicated by the arrows. Dashed lines connect those temperatures to the x-ray patterns obtained. A scale showing the major x-ray lines for ZrNi and Zr_2Ni is also presented to aid in the analysis of the x-ray patterns.

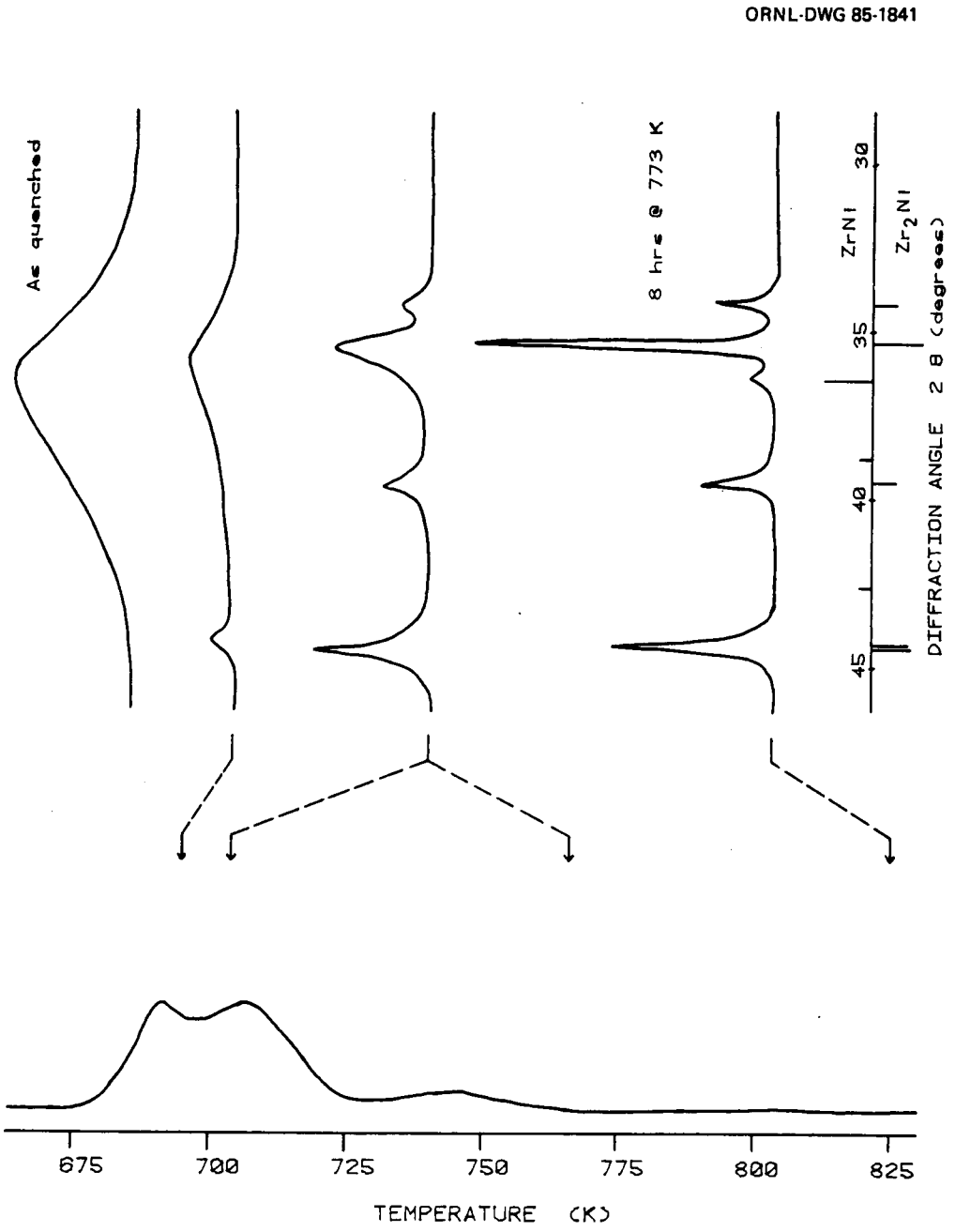

Figure 18. X-ray diffraction patterns obtained for $Zr_{65.5}Ni_{34.5}$ as a function of the progression of the crystallization process. Samples were heated in the DSC at 80 K/min to temperatures indicated by the arrows. Dashed lines connect those temperatures to the x-ray patterns obtained. A scale showing the major x-ray lines for ZrNi and Zr_2Ni is also presented to aid in the analysis of the x-ray patterns.

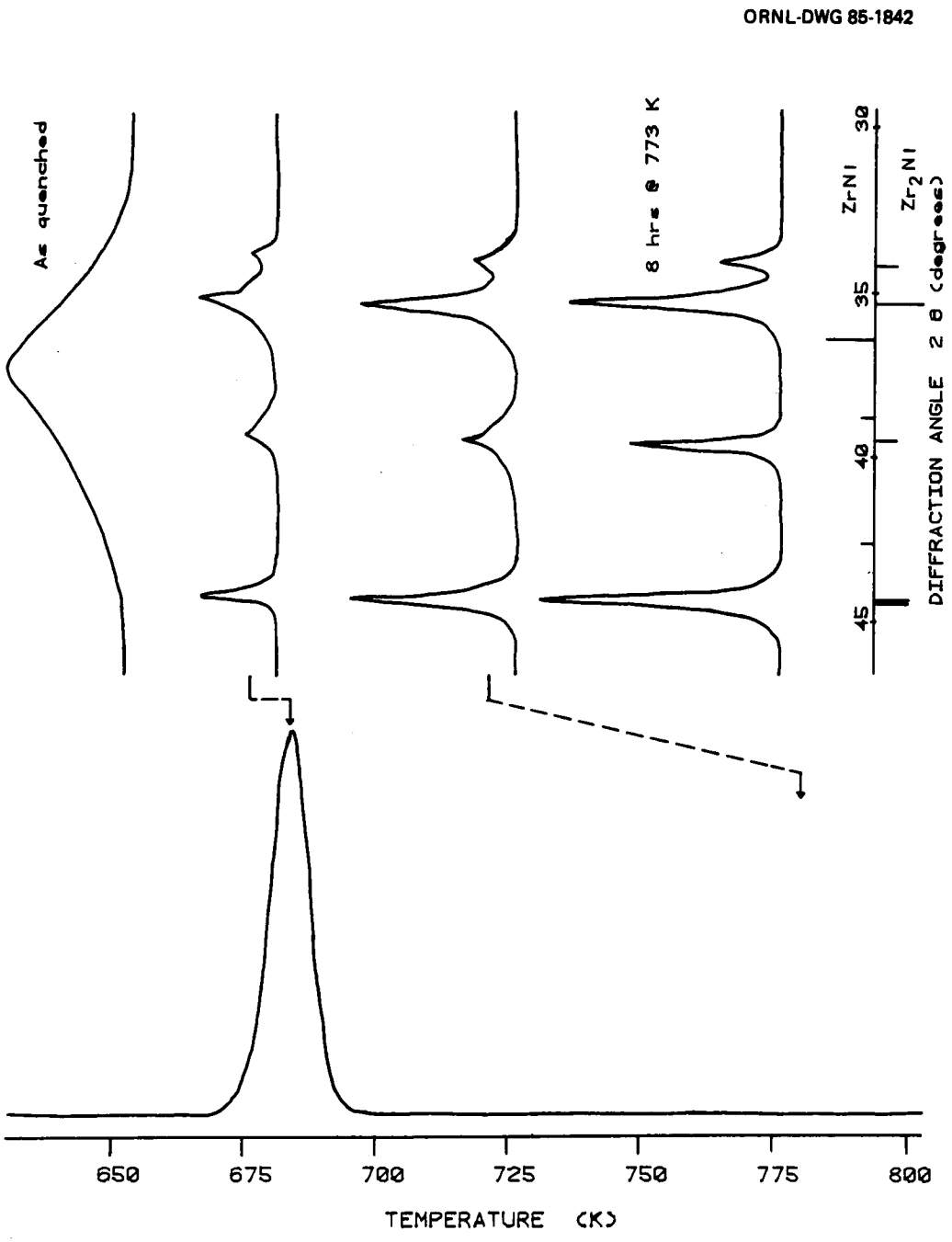

Figure 19. X-ray diffraction patterns obtained for $Zr_{67}Ni_{33}$ as a function of the progression of the crystallization process. Samples were heated in the DSC at 80 K/min to temperatures indicated by the arrows. Dashed lines connect those temperatures to the x-ray patterns obtained. A scale showing the major x-ray lines for ZrNi and Zr_2Ni is also presented to aid in the analysis of the x-ray patterns.

example, Fig. 13 shows that at the top of the one DSC peak for $Zr_{55}Ni_{45}$ (T_{p_1} = ~740 K at $\dot{T}$ = 80 K/min), an x-ray pattern indicating the presence of mostly ZrNi with some Zr_2Ni was seen. This pattern sharpened in other pieces of this alloy which were heated to 750 and 785 K. So, in order to get the whole figure in the space provided, only the higher temperature x-ray patterns were included. A summary of the transformation products observed by x-ray diffraction as a function of temperature for the selected alloys are listed in Table IV. From a study of this table and the x-ray diffraction patterns in Figs. 13–19, the following observations are made.

1. The one DSC peak of $Zr_{55}Ni_{45}$ actually represents two processes occurring at almost the same time. As seen in Fig. 13 (as well as Fig. 8), the peak is asymmetric on the low temperature side, indicating the presence of another peak underneath the main one. An x-ray diffraction pattern of an isothermal anneal at 773 K shows lines for both equilibrium phases ZrNi and Zr_2Ni, but it was not possible to tell which phase appeared first. So, at this composition, either ZrNi begins to transform first, enriching the amorphous matrix in zirconium, and thus allowing the almost simultaneous formation of Zr_2Ni, or Zr_2Ni transforms first, followed by ZrNi from the Ni rich matrix.

2. As shown earlier in this chapter, the DSC trace for $Zr_{57.7}Ni_{42.3}$ showed a large exotherm at ~740 K followed by a small high temperature peak above 850 K. The x-ray diffraction pattern taken after annealing to the top of the DSC peak at 740 K showed a strong x-ray line at ~38.9° 2θ and a few weaker lines (see Fig. 14). These

Table IV. Transformation Products of Zr-Ni Metallic Glasses Heated in the DSC at a Constant Heating Rate of 80 K/min to Different Points of the DSC Curve and Analyzed by X-Ray Diffraction

Alloy Composition (at. % Zr)	Temperature to Which Heated (K)	Phases Observed
55	740	Amorphous + ZrNi + Zr_2Ni
	750–785	ZrNi + Zr_2Ni
57.7	740–760	Metastable
	860–925	ZrNi + Zr_2Ni
60	725	Amorphous + metastable just starting
	735–750	Metastable
	850	Metastable + Zr_2Ni
	910	Zr_2Ni + ZrNi
62	720	Amorphous
	735	Amorphous + metastable just starting
	750	Metastable + Zr_2Ni
	840	Metastable + Zr_2Ni
	900	Zr_2Ni + ZrNi
63.5	710	Amorphous
	725	Amorphous + Zr_2Ni just starting
	750–840	Zr_2Ni
	860	Zr_2Ni + ZrNi
65.5	695	Amorphous + Zr_2Ni just starting
	705–765	Zr_2Ni
	850	Zr_2Ni + ZrNi
67	685–780	Zr_2Ni

lines could not be indexed to either of the two equilibrium phases. This same x-ray pattern persisted as other pieces of the same splat were annealed to higher temperatures. Only after annealing to or above the high-temperature peak (860 K or above) were x-ray lines of Zr_2Ni and ZrNi seen. In order to determine its structure, much more x-ray diffraction and electron diffraction work is being done on this possible metastable phase. This work will be published separately.[81-83] However, Table V, which lists the x-ray diffraction lines for the metastable phase (as taken from a CuKα Debye-Scherrer pattern with Straumanis film arrangement) along with those of the ZrNi and Zr_2Ni equilibrium phases, and Fig. 20, which shows the x-ray diffraction patterns of a sample of $Zr_{60}Ni_{40}$ which was annealed for 20 min at 430°C to produce the metastable phase and then annealed at 700°C, indicate that a metastable crystalline phase does exist.

3. At $Zr_{60}Ni_{40}$ (Fig. 15) the first crystalline phase to appear is the metastable phase associated with the first DSC peak. This alloy has a small second DSC peak at ~740 K, but the x-ray diffraction patterns at 740 or 750 K did not identify it. However, after heating to 850 K, which is just below the high-temperature peak, the diffraction pattern showed a weakening of the strong line of the metastable phase at ~38.9° 2θ and a strengthening of the strong Zr_2Ni lines at ~35.5 and ~44.4° 2θ. This phenomenon indicates that the second DSC peak at 740 K could represent the forming of Zr_2Ni after the initial formation of the metastable phase. Only after heating to higher temperatures did the Zr_2Ni crystals become large enough to produce detectable peaks in the x-ray diffraction pattern. Heating into or above the high-temperature

Table V. X-Ray Diffraction Lines for the Equilibrium Phases ZrNi and Zr_2Ni as Compared to Lines of a Metastable Phase Near $Zr_{60}Ni_{40}$

ZrNi		Zr_2Ni		Metastable	
deg 2θ	I (relative)	deg 2θ	I (relative)	deg 2θ	I (relative)
28.49	10	34.18	10	28.96	VW
36.50	100	35.44	100	34.05	M
38.93	20	39.43	10	35.15	MW
42.81	18	39.53	30	37.11	W
44.35	25	44.23	60	38.59	S
44.94	44	44.38	60	41.97	W
				44.35	MW

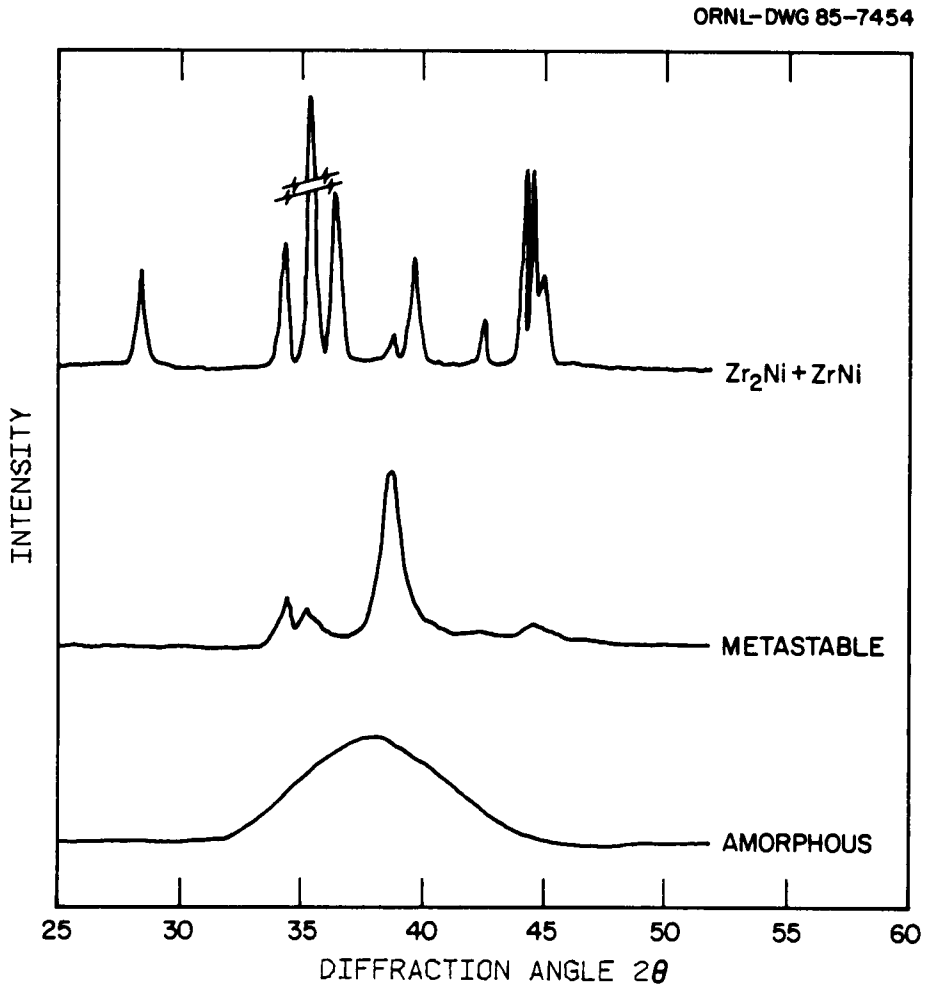

Figure 20. A comparison of x-ray diffraction patterns obtained for $Zr_{60}Ni_{40}$. The sample was initially amorphous as shown by the bottom pattern. Heating to just below the high-temperature peak produced the metastable pattern, followed by the characteristic patterns for Zr_2Ni and ZrNi after heating through the high-temperature peak.

peak again produced the equilibrium pattern for this alloy, showing only lines of Zr_2Ni and ZrNi.

4. At $Zr_{62}Ni_{38}$ (Fig. 16) another characteristic enters the crystallization process. The x-ray pattern taken after heating to the top of the first DSC peak does not indicate that any crystallization has taken place. Instead, the broad diffuse peak typical of an amorphous structure is seen. The first crystalline x-ray peak to appear is the strong line of the metastable phase which occurs after heating into the trough between the two low-temperature DSC peaks. Just after the second DSC peak, the two strongest x-ray lines of Zr_2Ni (~35.5 and ~44.4° 2θ) appear. Heating to higher temperatures tends to sharpen the Zr_2Ni lines but does not seem to sharpen the strong line of the metastable phase. After heating to above the high-temperature peak, only Zr_2Ni and ZrNi are seen.

5. Again in the $Zr_{63.5}Ni_{36.5}$ alloy (Fig. 17), no crystalline x-ray peaks appear until after heating well into the trough following the first DSC peak. When this first crystalline peak appears, it is not one of the peaks of the metastable phase, but is the strong double peak of Zr_2Ni at ~44.4° 2θ. From 750-840 K the other Zr_2Ni x-ray lines appear and continue to sharpen. Not until heating to 860 K do the strong lines of ZrNi appear. There appears to be no high-temperature DSC peak produced by this alloy.

6. The DSC trace for the $Zr_{65.5}Ni_{34.5}$ alloy (Fig. 18) shows that the third DSC peak is almost gone. According to the x-ray diffraction patterns, Zr_2Ni is the first phase to form, followed by ZrNi. However

crystalline x-ray lines are not detected until heating to just above the first DSC peak.

7. At $Zr_{67}Ni_{33}$ only one DSC peak occurs (Fig. 19), which according to the x-ray diffraction pattern represents the formation of Zr_2Ni from the glass.

Results of Transmission Electron Microscopy

It was hoped that a transmission electron microscopy (TEM) study of samples as a function of the DSC anneal each received would accomplish three things:

1. According to the DSC and XRD results, three different phases participate in the crystallization processes for the composition range studied. Transmission electron microscopy may show three different types of crystals. That is, the morphology of the crystals may be different, thereby aiding in their identification.

2. It was hoped that characteristic selected area diffraction (SAD) patterns could be obtained for each phase which would alloy one to follow the appearance and disappearance of each phase as crystallization progressed. Since the crystals of each phase form in random orientations with respect to the electron beam of the microscope, the SAD pattern would appear as a series of rings, the spacing of which would indicate the d-spacings of the planes of the unit cells of the crystals. The identification of phases present at any composition and annealing temperature could then be made by comparison of its SAD pattern with those of the three phases.

3. As reported in Chapter II, previous investigators of this alloy system have reported the presence of two amorphous SAD rings instead of one as evidence for the occurrence of phase separation within the glass.[72] If this supposition is correct, then a TEM study of the "as-splat" samples between 55 and 67 at. % Zr would indicate the composition range in which the phase separation occurs.

With these objectives in mind, most of the compositions and annealing conditions discussed in Figs. 13–19, plus as-splat samples of several other compositions in the range of this study, were looked at in transmission. It was found that the three phases did indeed exhibit a different physical appearance. Figure 21 shows the first crystals which form from splats of $Zr_{55}Ni_{45}$, $Zr_{60}Ni_{40}$, and $Zr_{65.5}Ni_{34.5}$ upon heating at 80 K/min in the DSC. The initial crystals from $Zr_{55}Ni_{45}$ are diamond-shaped and retained their shape and general appearance through the entire crystallization process until they impinged upon one another. Those from $Zr_{60}Ni_{40}$ are needle-shaped with many showing internal striations in the long direction. These needle-like crystals were the first crystals to appear in the 57.7, 60, and 62 at. % Zr alloys. However, after annealing to above the high-temperature DSC peak, they were gone (Fig. 22). The first crystals from $Z_{65.5}Ni_{34.5}$, which were also seen at 63.5 and 66.5 at. % Zr, exhibit internal striations and are only slightly longer in one direction. As will be discussed in the next chapter, these crystals match those identified by other researchers as Zr_2Ni.

The attempts to obtain a characteristic SAD ring pattern for each phase were not successful. As shown in Table V, the three phases

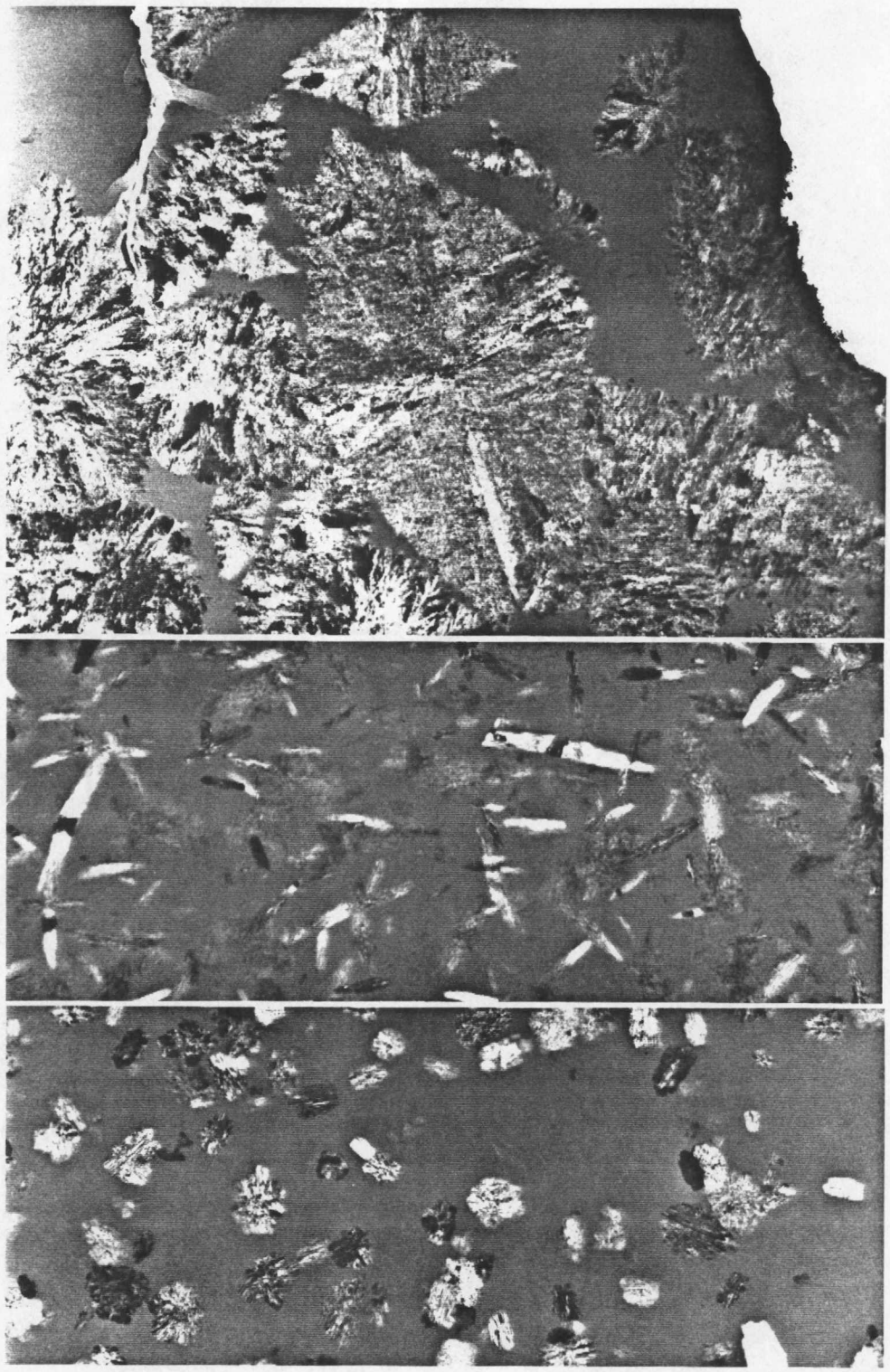

Figure 21. Transmission electron micrographs of the initial crystals which form upon heating at 80 K/min in the DSC from (a) $Zr_{55}Ni_{45}$, (b) $Zr_{60}Ni_{40}$, and (c) $Zr_{65.5}Ni_{34.5}$. All three are printed at 40,000X.

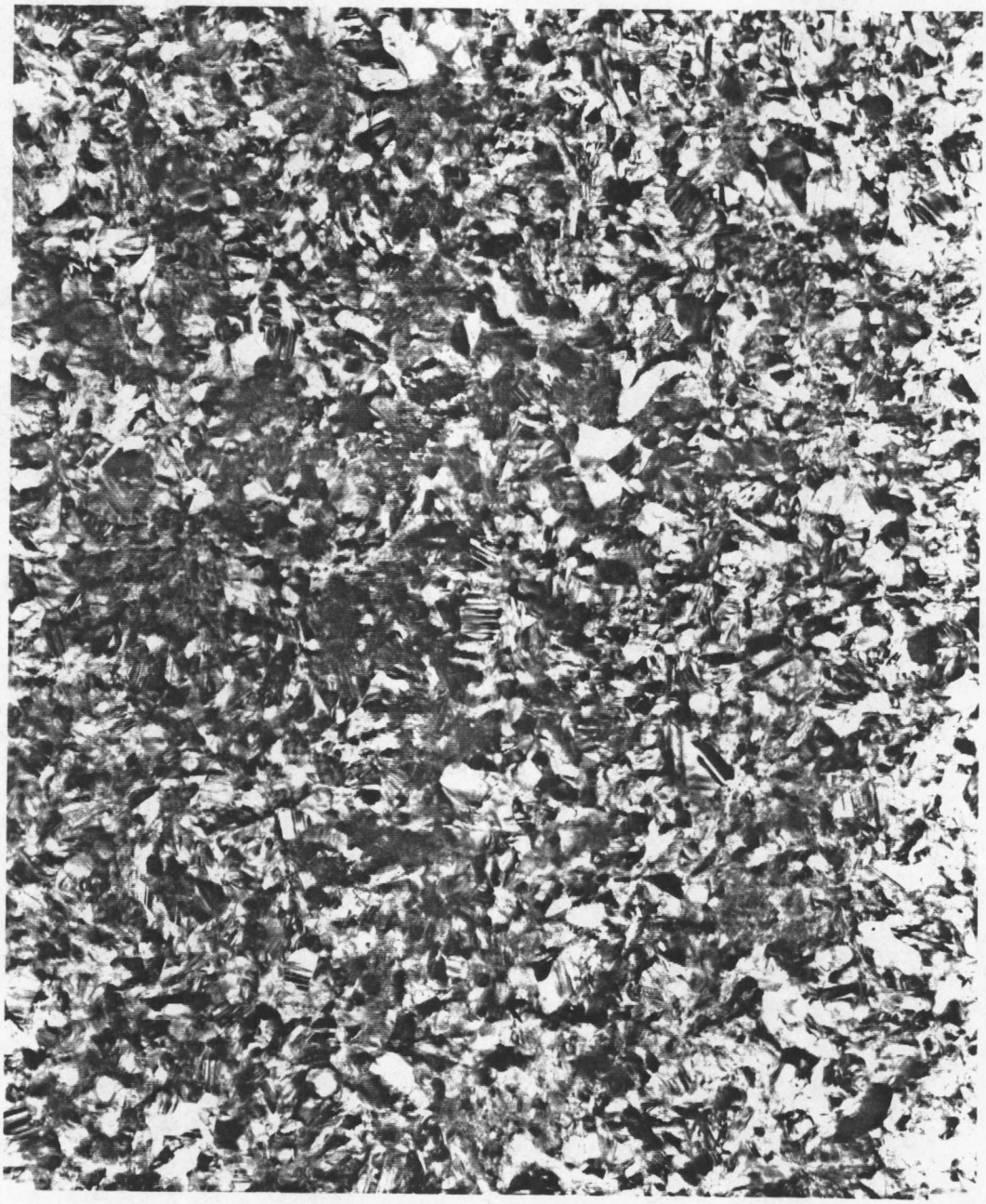

Figure 22. Transmission electron micrograph of $Zr_{57.7}Ni_{42.3}$ after heating in the DSC to 925 K. 40,000X.

exhibit many x-ray lines at nearly the same Bragg angle. In terms of SAD ring spacings, this means that many rings are so close as to make it impossible to determine which phase they represent. In Fig. 23 is shown the ring patterns for a partially crystallized (DSC anneal to 760 K) and a fully crystallized (DSC anneal to 925 K) sample of $Zr_{57.7}Ni_{42.3}$. The rings are so numerous and, in some cases, so diffuse that accurate measurement was impossible. It was determined that only with much more TEM could this approach to phase identification be utilized.

A TEM survey of as-splat samples across the composition range of this study produced some double ring SAD patterns as shown in Fig. 24 for $Zr_{62}Ni_{38}$ and $Zr_{63.5}Ni_{36.5}$, but results were inconsistent. For example, Fig. 24(b) shows a single ring for $Zr_{63.5}Ni_{36.5}$, while another area of the same TEM sample shows the double ring (c). Still another area of the same sample shows two rings (d), but the outer ring is much more diffuse and the spacing between the two rings is not the same as in (c). Double rings were also seen in samples of 57.1, 58.4, 59, 61.2, and 65 at. % Zr, but, as for those in Fig. 24, single rings could be produced by simply moving the electron beam to an adjacent area.

(a)

(b)

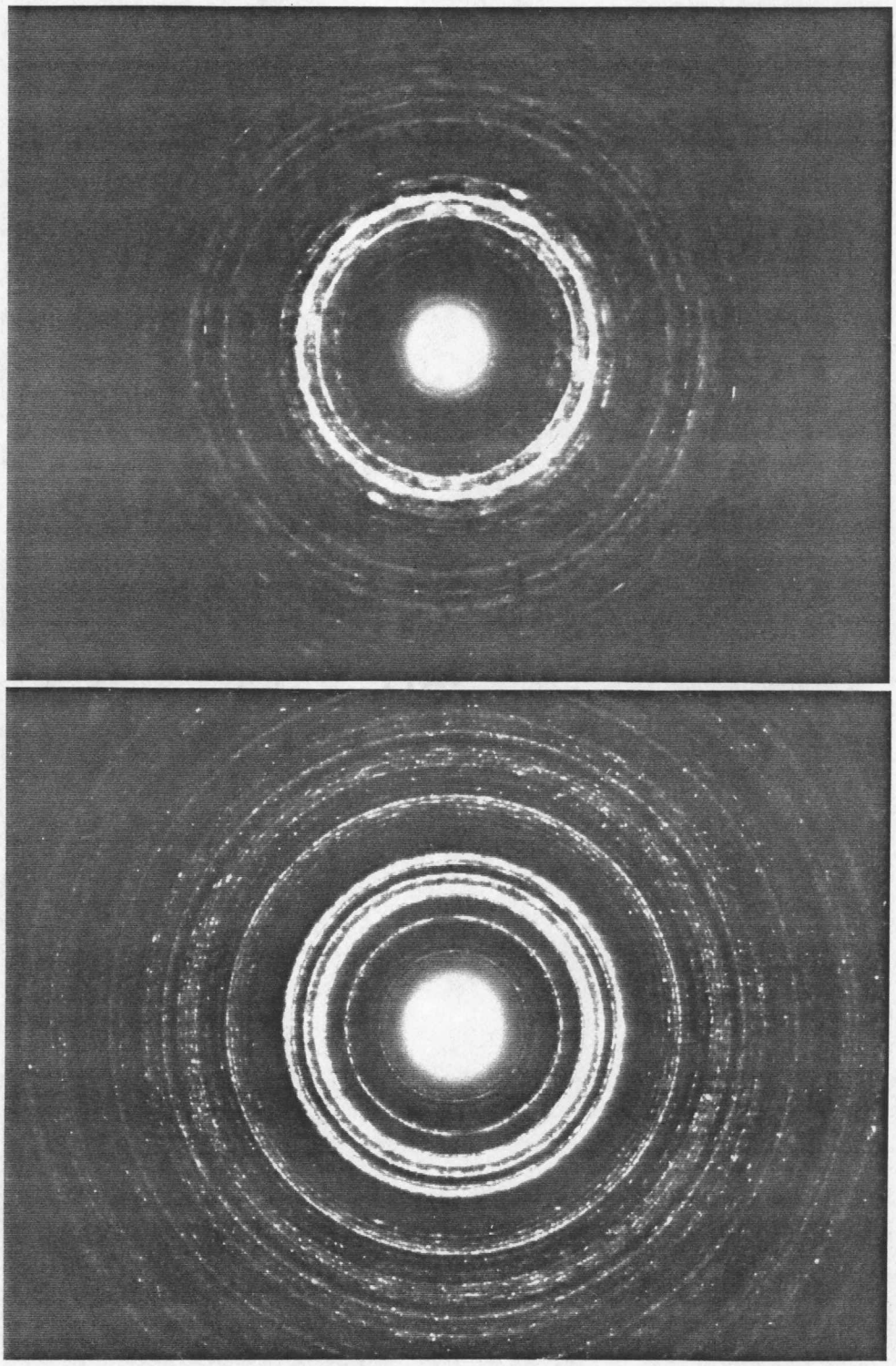

Figure 23. Selected area diffraction (SAD) ring patterns of $Zr_{57.7}Ni_{42.3}$ after annealing in the DSC to (a) 760 K and (b) 925 K.

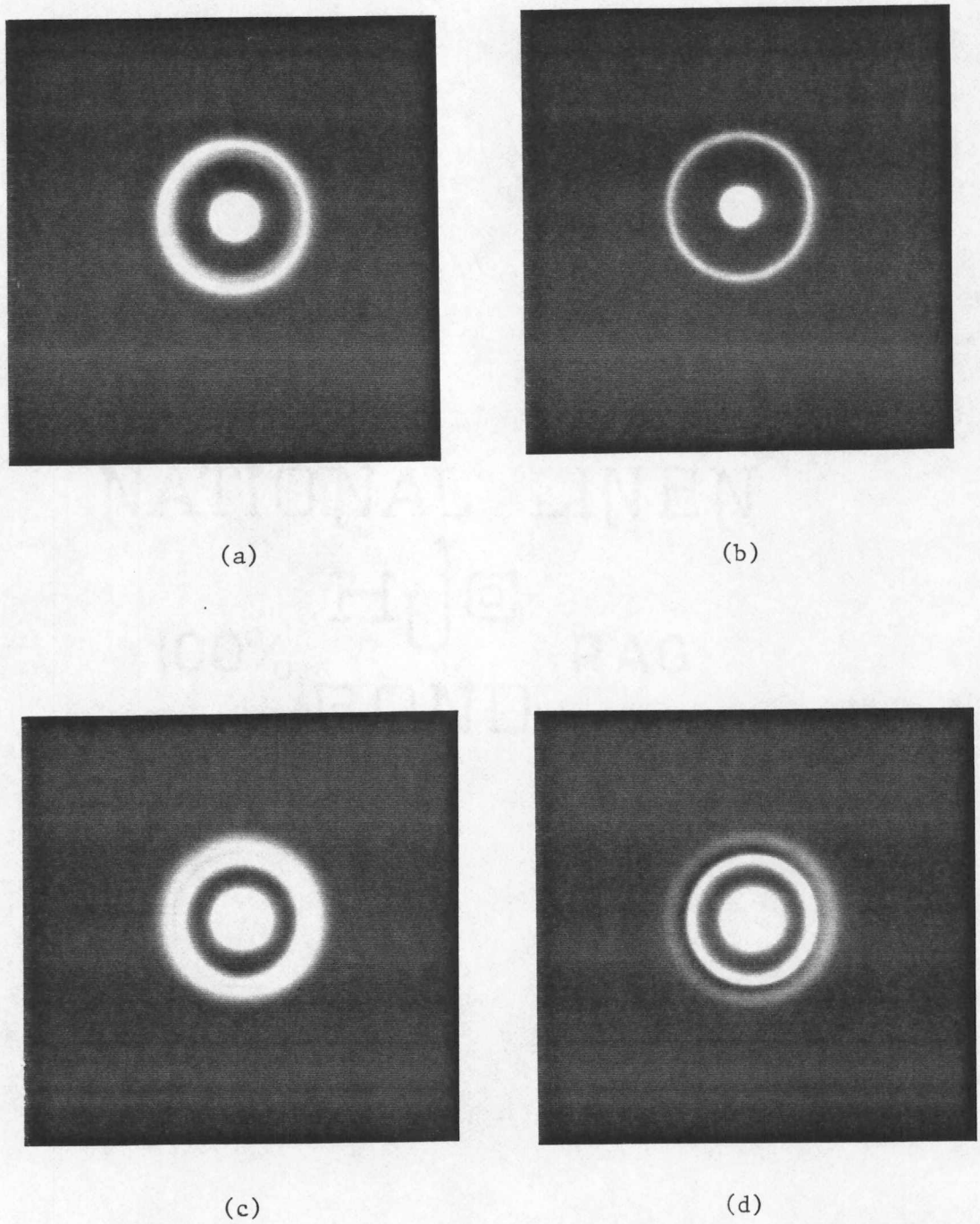

Figure 24. Selected area diffraction (SAD) ring patterns for as-quenched (a) $Zr_{62}Ni_{38}$ and (b), (c), and (d) $Zr_{63.5}Ni_{36.5}$.

CHAPTER V

DISCUSSION OF RESULTS

Comparison of Results to Previous Investigations

Three groups of investigators have produced the bulk of the data available on the crystallization of Zr-Ni metallic glasses. These investigators, whose studies have covered the whole composition range over which Zr-Ni can be made glassy, are Dong, Gregan, and Scott,[31,65] Buschow et al.,[63,69,72,77] and Altounian et al.[14] Other investigators have added data on individual alloy compositions,[70,73] reproducing data already presented by the three groups cited above. For the purposes of this discussion, comparison is made to the results of Refs. 14, 65, and 77, where most of the previous results in the composition range of this study have been presented. It must be borne in mind that all previous investigators have conducted their studies on melt-spun ribbon, whereas the samples used in this study were prepared by splat-quenching. No information is available concerning the comparison of thermal data from the two methods. Possible sources of any difference could involve the different quench rates (splat-quenching is usually considered to be faster, 10^6 K/sec compared to 10^4 to 10^5 K/sec for melt spinning), the degree of superheat (can be higher for the melt-spinning process), or the amount and kind of contaminants added during the quenching process. During the melt-spinning process, the melt is held for varying periods of time in the crucible before being ejected onto the quenching wheel. The hot melt could react with elements in the crucible material or contaminants in the atmosphere (such as oxygen or hydrogen). On the other

hand, the splat-quenching process involves much smaller charges of sample and is heated only long enough for melting to occur.

The most often reported data on the crystallization of metallic glasses is the crystallization temperature. Table VI shows the DSC peak crystallization temperatures, T_{p_1}, T_{p_2}, T_{p_3}, reported by Refs. 14, 65, and 77, as a function of the composition range of this study. For comparison, the peak temperatures reported in this study are included. For the most part, they compare quite well. However, because the previous studies involved such large composition ranges (Dong et al. studied glasses of 33-42 and 60–78 at. % Zr, Altounian et al. studied the range from 30 to 80 at. % Zr, and Buschow et al. studied the range from 9 to 78 at. % Zr), none of the three concentrated their efforts in a small composition range. It should also be noticed that Dong et al. and Altounian et al. report data that was taken at a DSC heating rate of 10 K/min, and the data of Buschow et al. was taken at 50 K/min. Only the 50 K/min data would need a noticeable correction for heating rate in order to compare it to the data of this study (taken at 20 K/min). Judging from the experience this researcher has had in using the DSC, the correction should be no more than $-5^{\circ}K$. Both Dong et al., who studied compositions from 60 to 67 at. % Zr, and Altounian et al., who covered the range from 50 to 70 at. % Zr, show a steady increase in T_{p_1} with increasing nickel content. The high value reported by Dong et al. at 60 at. % Zr is probably due to the fact that they experienced difficulty in producing good quality melt-spun ribbon at this composition. Altounian et al. reported a maximum in the T_{p_1} at approximately 55 at. % Zr. The closer spacing of the compositions studied in this thesis also

Table VI. Reported Crystallization Temperatures for Zr-Ni Metallic Glasses

Composition (at. % Zr)	T_{p_1} (K)				T_{p_2} (K)				T_{p_3} (K)	
	This Study[a]	Reference			This Study[a]	Reference			This Study[a]	Reference
		14[b]	77[c]	65[b]		14[b]	77[c]	65[b]		65[b]
50		695				--				
55	722	725			--	--			--	
57	728		745		--		--		--	
58	720		749		--		754		--	
60	714	715	726	740	721	730	740	750	--	--
61	712		727		726		751		--	
62	704	705	727	700	723	720	763	740	--	--
63	697		734		731		778		736	
63.5	694	695	722	690	717	735	770	720	734	740
65	683		695	680	690		736	700	715	750
67	664	665	702	670	--	--	733	--	--	--
70		650				--				

[a]Values reported in this table are averages of values reported in Table II and are for comparison purposes only. The DSC heating rate used was 20 K/min.

[b]References 14 and 65 presented their data in the form of figures. The values presented in this table are the best values measured from the figures and the error in reading the value from the figure is estimated to be no better than ±5°.

[c]Values were taken directly from Table I of Ref. 77.

indicate a peak in T_{p_1}, but at 57 at. % Zr. Both Dong et al. and Altounian et al. show temperatures for a second DSC peak, T_{p_2}, which compare favorably with the results of this study. But again the previous reports involve only a few compositions and do not report a maximum in this peak near the eutectic. As seen in the table, Buschow's data seems to suggest a maximum in both T_{p_1} and T_{p_2} near the eutectic. However, the general trend of T_{p_1}, increasing with an increase in nickel, is the same as that of the other researchers. His study involved more samples in the composition range of interest and does show the maximum in T_{p_2} at the eutectic. Generally his reported values for T_{p_1} and T_{p_2} are much higher than the values reported in this study, even after correcting for the different heating rate. A third DSC peak occurring between 63.5 and 65.5 at. % Zr is reported in this thesis. Only Dong et al. previously reported values for a third DSC peak, which they indicate as occurring at 63.5 and 65 at. % Zr. Their values for T_{p_3} are 6 and 35° higher than the values reported here for the same compositions. Buschow does state in several references that he saw three DSC peaks in this same composition region,[69,77] and Altounian et al. show a figure of the DSC trace for the 63.5 at. % Zr alloy which clearly shows three peaks, although they do not discuss it in their paper. All the previous researchers agree that multiple DSC peaks occur in a composition range between 60 and 66 at. % Zr, but no one reports a high-temperature peak in compositions between 57 and 63.5 at. % Zr such as the one reported here.

In Table VII is presented a comparison of the effective activation energies, ΔE_1 and ΔE_2, and the enthalpy change on crystallization ΔH as

Table VII. Reported Values of ΔE and ΔH for Zr-Ni Metallic Glasses

Composition (at. % Zr)	ΔE_1 (eV/atom)				ΔE_2 (eV/atom)			ΔH (kJ/mole)	
	This Study[a]	Ref. 14[b]	Ref. 77[c]	Ref. 65[b]	This Study[a]	Ref. 14[b]	Ref. 77[c]	This Study[a]	Ref. 14[b]
50		2.40							7.30
55	3.17	3.45			--			4.99	5.60
57	3.78		3.65		--			5.16	
58	3.73		4.43		--		4.43	5.49	
60	3.76	4.80		4.75	3.01	3.40		5.40	5.50
61	4.48		5.57		2.92		3.50	5.63	
62	4.70	5.20	6.81	4.35	2.90	3.20		5.70	
63	4.67		5.03		2.91		3.50	5.63	
63.5	4.69	4.65	4.72	3.95	1.92	2.75	2.61	5.62	5.50
65	4.21		4.96	3.90	2.44		3.43	5.76	
67	2.69	3.25		3.35	--			5.89	6.15
70		2.85	3.04						5.80

[a]Values reported in this table are averages of values reported in Tables I and II and are for comparison purposes only.

[b]References 14 and 65 presented their data in the form of figures. The values presented in this table are the best values measured from those figures and the error reading the value from the figure is estimated to be no better than ±0.05.

[c]Values were taken directly from Table I of Ref. 77.

reported in Refs. 14, 65, and 77. In general all the previous researchers report a maximum in ΔE_1 at 62 at. % Zr. None of the structure as seen in Fig. 10 of this study is seen in their data because they did not investigate enough compositions in this range. Only Altounian et al. report values of ΔH and, again, not enough values for a good comparison. However their data values for 60, 63.5, and 67 at. % Zr agree well with the values reported here. They do show a maximum in ΔH at 67 at. % Zr and again at 50 at. % Zr, which are the compositions of the equilibrium crystalline phases for the composition range of this study.

Dong et al.[65] also used x-ray diffraction to associate DSC peaks with crystallizing phases and TEM to study their morphology. They report that the single DSC peak near 66.7 at. % Zr corresponds to the formation of Zr_2Ni. Crystals of the phase showed no preferred shape but a very fine internal structure which they attributed to microtwinning. The micrographs which they presented showed crystals like those in Fig. 21(c) of this report. Their attempts at associating DSC peaks with the formation of phases in the 63.5 at. % Zr alloy (the eutectic composition) met with the same difficulties as the present study. Three DSC peaks are present and it is impossible to tell for sure which phase belongs to which peak. Dong et al. saw only equilibrium phases after annealing, although they do not say which phase they observed first. At 62 at. % Zr, they attributed the two distinct DSC peaks to the crystallization of Zr_2Ni and ZrNi, respectively. Contrary to their results, the XRD results of this thesis indicate that one has to anneal well past the first DSC peak before any crystalline x-ray lines are seen. The

first line which appears belongs to the metastable phase, but after the second DSC peak, lines belonging to Zr_2Ni appear.

Altounian et al.[14] used x-ray diffraction to identify crystallizing phases in the 60, 63.5, and 67 at. % Zr alloys. Their results on 67 at. % Zragree with Dong et al. and with the results of this thesis. At 60 and 63.5 at. % Zr x-ray diffraction patterns taken after heating to just past the first DSC peak showed only the broad diffuse pattern characteristic of the glassy phase, in agreement with the results of this thesis and several other studies.[69,72,73] However, they can give no clear explanation for what process is occurring during this peak. They attribute the second DSC peak in these two alloys as corresponding to the formation of Zr_2Ni, in agreement with the results of this thesis.

Very few studies of the morphology of the crystals that form during the crystallization of Zr-Ni metallic glasses have been conducted. With respect to the composition range of this study, only micrographs of Zr_2Ni crystals have been published,[31,65] and those micrographs look like the one presented in Fig. 21(c) of this study. As stated earlier, the fine internal structure seen in Zr_2Ni crystals has been attributed to microtwinning or stacking faults.[31,65] This type of structure is common in crystals grown in metallic glasses.[18,21]

Although a eutectic occurs at 63.5 at. % Zr, Scott et al.[31] have shown that this alloy does not crystallize eutectically. Instead crystals of Zr_2Ni with identical morphology to those at 67 at. % Zr nucleated and grew in the glassy matrix. As stated in Chapter IV of this thesis, the first crystals to form from the 63.5, 65.5, and

67 at. % Zr compositions appeared to have the same morphology (see Fig. 21(c)], in support of the results of Scott et al.

Metastable Phase Formation

Since the beginning of studies on the crystallization of metallic glasses, it has been recognized that metastable phase formation could be an integral part of the crystallization process.[21,76,84,85] This is easily imaginable if one considers thermodynamic equilibria and the necessary diffusion processes for formation of equilibrium crystalline phases from the liquid-like glass phase. With reference to Fig. 1 (Chapter II), if the concentration of the glass is close to a pure component α, an intermetallic phase β, or a crystalline metastable phase M, crystallization can take place without a change in composition, requiring little or no diffusion. However, at the eutectic, long-range diffusion would be necessary in order to form the equilibrium phases. If a metastable phase occurs near the eutectic, the thermodynamics and kinetics of the system may dictate that crystallization by way of the metastable phase is easier. By making shorter atomic jumps, the metastable phase can be formed, thereby lowering the Gibbs free energy of the system. The success of this process is enhanced if the atomic configuration in the glass (i.e. short range order of the glass) is similar to that which exists in the metastable phase.

The classic example of crystallization by metastable phase formation in metallic glasses is exhibited by the Fe-B system, in which eutectic crystallization of α-Fe and a metastable tetragonal Fe_3B phase occurs in the concentration range from 17 to 24 at. % B.[18,86] The final

products of crystallization are the stable phases α-Fe and Fe_2B. Certain compositions of many other systems have been shown to crystallize through the formation of metastable phases, including Pd-Si,[17] Ag-Ge,[87] Metglas 2826A,[88] Zr-Be,[89] Zr-Si,[90] and Zr-Cu.[91] In these systems, most metastable phases are found at compositions near eutectics, although this need not always be the case.

In view of the common appearance of metastable phases during the crystallization of various metallic glass systems, including both the metal-metal and metal-metalloid systems, one should not be surprised to find one or more metastable phases participating in the crystallization of Zr-Ni metallic glasses. In fact, Buschow et al. have been studying a metastable phase at 78 at. % Zr.[64]

This study has presented evidence for a metastable phase which participates in the crystallization process in the composition range 57–63.5 at. % Zr. X-ray diffraction lines which do not belong to either the ZrNi or Zr_2Ni equilibrium phases appear after the low-temperature transformations seen in the DSC. Depending on composition within this 57–63.5 at. % Zr range, some of one of the equilibrium phases also forms during the low-temperature transformations. However after heating to above the high-temperature DSC peak, which is more than one hundred degrees above the low-temperature transformations, only ZrNi and Zr_2Ni lines are seen. The high-temperature peak is not believed to represent an oxidation effect since oxidation would affect all compositions. Also, it cannot be a quench-rate effect because melt-spun ribbons give the same response with the same composition dependence. The morphology

of the crystals shown in Fig. 21(b), which is different from that of Zr_2Ni or ZrNi, was seen in samples of 57.7, 60, and 62 at. % Zr, all of which are within the composition range where the high-temperature peak is seen. Outside the 57–63.5 at. % Zr range the morphology corresponded to that expected for ZrNi or Zr_2Ni.

Phase Separation and Chemical Short-Range Ordering in the Glass Structure

The modes of crystallization discussed in Chapter II all involve the nucleation and growth of one or more crystalline phases within the amorphous matrix. An alternative initial stage observed in some glasses is the separation of the initially homogeneous glass into two compositionally discrete glassy phases which then crystallize independently. This process allows an initially single phase glass to lower its free energy by separating into two glassy phases with compositions given by the common tangent construction. This process of phase separation is shown theoretically in Fig. 25, where it is seen that the free energy curve for the glass is initially concave downward, denoting a negative heat of mixing. Phase separation produces a composition range which exhibits a positive heat of mixing. In this composition range, from C_s to C_s' in Fig. 25, it has been shown that many glasses decompose by a spinodal mechanism,[43] in which sinusoidal fluctuations of composition appear and grow in intensity at a wavelength which depends on temperature. From C to C_s and C_s' to C', an activation barrier to phase separation occurs,[21] leading to decomposition by the nucleation and growth processes discussed in Chapter II.

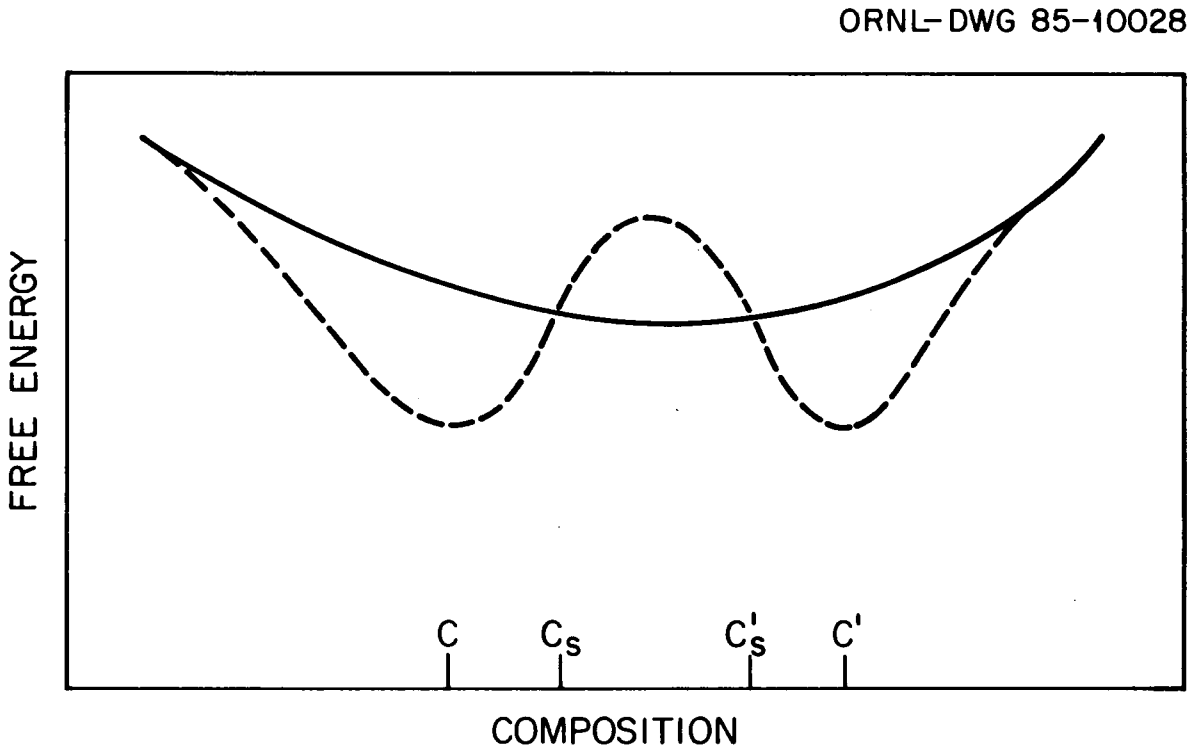

Figure 25. Theoretical free energy versus composition diagram to illustrate phase separation in a glass. The dashed line is the curve for the glass which has phase separated between compositions C and C'. For comparison, the solid line is the curve for the glass before phase separation occurs.

Phase separation is well known in oxide glasses, but its existence in metallic glasses is still being debated. The presence of two T_g's in Ni-Pd-P,[37] Ti-Be-Zr,[38] and Zr-Ni[41], two T_c's in Zr-Ni[40,41], and two SAD rings for the amorphous structure in Zr-Ni[42] have been taken as evidence for two glassy phases in these alloys. Microstructures showing two interconnecting glassy shapes in Fe-B[39] and Ti-Be-Zr[38] have been published. According to Chou and Turnbull,[43] SAXS studies on the $Pd_{82-x}Au_xSi_{18}$ system show that the 8 at. % Au alloy is single phase after quenching, but in the early stages of crystallization (after annealing near 400°C) the decomposition is by a spinodal mechanism with composition fluctuations on the order of 20 nm.

The strongest evidence for phase separation in the Zr-Ni system has been reported by van Swijgenhoven, Stals, and Buschow.[72] Because they saw a splitting of the principal SAD ring of an as-quenched 63 at. % Zr alloy, they concluded that $Zr_{63}Ni_{37}$ is phase separated during the rapid quenching process. Their comparison of d-values from the SAD rings of amorphous samples with the concentration dependence of the d-values determined from x-ray diffraction led them to infer that the glass sample is phase separated into one glass structure which is a precursor of the Zr_2Ni equilibrium crystalline phase and one which is a precursor to the ZrNi equilibrium phase. However they note that the glass phase which crystallizes into ZrNi (the first crystals to form) is richer in zirconium than expected from their analysis.

In light of these results, it seems possible that the metastable phase reported in this thesis may actually be the phase which van Swijgenhoven et al. reported as the first phase to crystallize in

$Zr_{63}Ni_{37}$. They refer to it as an off-stoichiometric ZrNi which is rich in zirconium. However it could also be a crystalline phase resulting from the crystallization of a glass structure which is near a Zr_3Ni_2 composition. This hypothesis is further supported by the results of Kroeger et al.[41] who reported evidence from low-temperature specific heat data for two superconducting glassy phases in a splat quenched 62.9 at. % Zr alloy, one phase near 67 at. % Zr and the other near 60 at. % Zr. They interpreted their results in terms of a model of the glass structure proposed by Sommer and Predel in which "associates" of unlike atoms form.[73-76]

Other researchers have recognized from investigations of the formation, stability, and properties of some amorphous intertransition metal alloys that they may represent a special class of glassy metals whose short-range structure is characterized by a random tetrahedral close-packing of atoms similar to those in the crystalline counterparts.[92] In other words, these amorphous alloys, which include Zr-Ni, may have a "crystal-like" short-range structure that deviates from the dense random packing of hard spheres (DRPHS) model proposed by Bernal[93] and is more like the chemical short-range order (CSRO) of the crystalline phase. Whether this CSRO occurs in the as-quenched alloy or is produced by the process of phase separation is not known.

Assuming that CSRO does exist in some binary glass systems, Buschow has re-evaluated a theoretical model for describing the thermal stability of amorphous alloys which he proposed earlier.[77] Without going into the thermodynamics, the earlier model was based on the kinetic approach, the crystallization temperature T_x being proportional to the

activation energy for crystallization ΔE.[63] The activation energy was taken to be proportional to the formation energy of a hole the size of the smaller atom. This model was applied successfully to many binary systems, but some systems did not show the expected T_x-ΔE relationship. It was expected that a glass which formed easily (i.e. at a deep eutectic, where the depression of the melting point from the ideal solid solution liquidus is high) would be more stable, resulting in a maximum in the concentration dependence of Tp_l at the eutectic. This does not occur in the Zr-Ni system. Instead T_{p_l} varies linearly with composition (see Fig. 9). By assuming that the Zr-Ni system exhibits a strong tendency toward CSRO and evaluating the hole model with respect to that CSRO, Buschow was able to show that the predictions of the hole model are only slightly affected by the occurrence of CSRO, thus explaining why the hole model has been applied successfully to so many alloy systems. However the strong temperature dependence of the configurational entropy expected for alloys with CSRO leads to an increase in the effective activation energy.[77] Buschow concluded that an increase in ΔE in certain composition ranges, as at the eutectic in Zr-Ni alloys, is not an indication of thermal stability, but indicates the occurrence of CSRO.

CHAPTER VI

CONCLUSIONS

From a study of the crystallization of Zr-Ni metallic glasses by means of thermal analysis, x-ray diffraction, and transmission electron microscopy, the following conclusions can be drawn:

1. From 55 to 57 at. % Zr, the ZrNi equilibrium phase forms first from the glassy structure. It probably forms by a primary crystallization process, expelling zirconium into the amorphous matrix. The Zr_2Ni phase begins forming soon after the ZrNi.

2. Above approximately 66 at. % Zr, Zr_2Ni is the predominant crystalline phase and presumably forms by a polymorphic transformation.

3. Between 57 and 66 at. % Zr, the crystallization process becomes quite complicated. Eutectic crystallization does not seem to occur. Instead the first phase which forms on the low zirconium side of the eutectic at 63.5 at. % Zr is a crystalline phase which has not been reported before. The evidence indicates that it has a different morphology than either equilibrium phase, the x-ray pattern is different, and it transforms to the equilibrium phases upon further heating. The very sharp narrow DSC peak produced by the formation of this metastable phase indicates that the crystallization of this phase needs little diffusion to proceed and may be occurring by a polymorphic transformation similar to that of Zr_2Ni. From 63.5 to 66 at. % Zr the first phase to form is believed to be Zr_2Ni. Since the eutectic composition is so far from the compound at 66.7 at. % Zr, the crystals at this composition probably form by a primary crystallization process.

4. A maximum in the activation energy of the first DSC peak between 61.2 and 65 at. % Zr indicates that the first stage of crystallization in this composition range is quite different from that of 60 or 67 at. % Zr. It is also in this range that heating into or past the first DSC peak produces XRD patterns showing only the broad diffuse peak characteristic of the amorphous structure. It is believed that this phenomenon is related to the fact that at the eutectic the glass forms more easily on quenching and produces a glass structure of less order (the atoms fall into a more random structure) than the structures produced at 60 or 67 at. % Zr. Since TEM micrographs indicate that eutectic crystals do not form at 63.5 at. % Zr, some type of process has to occur which involves diffusion of atoms and results in some degree of ordering of the glass structure before the formation of crystals can proceed. It has been debated by other researchers whether this phase separation occurs during the liquid-quenching process or upon heating of the as-quenched sample. Van Swijgenhoven et al.[72] and Schulz et al.[73] believe the samples are phase separated as-quenched. But these researchers produced their samples by the melt-spinning process which is considered to produce a slower quench than splat-quenching. The results of this study on splat-quenched samples indicate that, between 61 and 66 at. % Zr, various amounts of ordering in the glass structure occur on heating in the DSC. Since the eutectic composition is approximately midway between Zr_2Ni at 66.7 at. % Zr and the metastable phase at approximately 60 at. % Zr, it seems reasonable to assume that it phase separates into glasses of short-range order similar to those two phases. The maximum in the activation energy is a consequence of that ordering.

At 60 and 67 at. % Zr, the as-quenched glass has the short-range order it needs to proceed with crystallization.

There is much more work which could be done on this system. The structure of the metastable phase needs to be determined; the nature of the phase separation should be investigated further; and chemical analysis should be done on the first crystals which form as a function of composition to add to the information on the crystallization processes.

LIST OF REFERENCES

LIST OF REFERENCES

1. W. Klement, R. H. Willens, P. Duwez, Nature 187 (1960) 869.

2. R. M. J. Cotterill, Am. Sci. 64 (1976) 430.

3. J. J. Gilman, Phys. Today (May 1975) 46.

4. S. Takayama, J. Mater. Sci. 11 (1976) 164.

5. T. Masumoto and R. Maddin, Mater. Sci. Eng. 19 (1975) 1.

6. Y. Waseda, H. Okazaki, and T. Masumoto, J. Mater. Sci. 12 (1977) 1927.

7. P. Chaudhari and D. Turnbull, Science 199 (1978) 11.

8. R. W. Cahn, Contemp. Phys. 21(1) (1980) 43.

9. H. S. Chen, Rep. Prog. Phys. 43 (1980) 353.

10. L. A. Davis and R. Hasegawa, "Metallic Glasses: Formation, Structure and Properties," pp. 301–321, in Metallurgical Treatises, eds. J. K. Tien and J. F. Elliott, AIME, New York, 1981, Proceedings of the First Bilateral USA-China Metallurgy Conference, Beijing, China, Nov. 13–22, 1981.

11. R. W. Cahn, J. Physique C9 (1982) 55.

12. J. J. Gilman and H. J. Leamy, eds., Metallic Glasses, ASM, Metals Park, Ohio, 1978, papers presented at a Seminar of the Materials Science Division of the American Society for Metals, September 18–19, 1976.

13. F. E. Luborsky, ed., Amorphous Metallic Alloys, Butterworths, London, 1983.

14. Z. Altounian, Tu Guo-hua, and J. O. Strom-Olsen, J. Appl. Phys. 54(6) (1983) 3111.

15. R. P. Elliott, Constitution of Binary Alloys, First Supplement, McGraw-Hill, New York, 1965.

16. Y. Waseda, H. Okazaki, and T. Masumoto, J. Mater. Sci. 12 (1977) 1927.

17. M. Scott, pp. 198–213, in Proceedings of the Third International Conference on Rapidly Quenched Metals, Brighton, ed. B. Cantor, Metals Society, London, 1978.

18. U. Köster and U. Herold, pp. 225–59, in Glassy Metals I, eds. H.-J. Güntherodt and H. Beck, Vol. 46 of Topics in Applied Physics, Springer-Verlag, Berlin, 1981.

19. U. Köster, pp. 113–26, in Phase Transformations in Crystalline and Amorphous Alloys, ed. B. L. Mordike, Deutsche Gesellschaft für Metallkunde e.V., Clausthal, Germany, 1983.

20. H. W. Bergmann and H. U. Fritsch, in Ref. 4, pp. 127–44.

21. M. G. Scott, Chapter 10 of Ref. 13, pp. 144–68

22. F. Spaepen, J. Non-Cryst. Solids 31 (1978) 207.

23. T. Egami, Mater. Res. Bull. 13 (1978) 557.

24. H. H. Liebermann, C. D. Graham, Jr., and P. J. Flanders, IEEE Trans. Magn-13 (1977) 1541.

25. M. A. Marcus, Acta Metall. 27 (1979) 879.

26. H. S. Chen, J. Appl. Phys. 49 (1978) 4595.

27. H. S. Chen, L. C. Kimmerling, J. M. Poate, and W. L. Brown, Appl. Phys. Lett. 32 (1978) 461.

28. H. S. Chen, Mater. Sci. Eng. 26 (1976) 79.

29. J. L. Walter, D. G. Legrand, and F. E. Luborsky, Mater. Sci. Eng. 29 (1977) 161.

30. U. Köster and P. Weiss, J. Non-Cryst. Solids 17 (1975) 359.

31. M. G. Scott, G. Gregan, and Y. D. Dong, pp. 671–74 in Proc. Fourth Int. Conf. on Rapidly Quenched Metals, eds. T. Masumoto and K. Suzuki, Japan Institute of Metals, Sendai, 1981.

32. A. Calka, M. Madhava, D. E. Polk, B. C. Giessen, and J. Vandersande, Scripta Metall. 11 (1977) 65.

33. B. G. Bagley and D. Turnbull, Acta Metall. 18 (1970) 857.

34. R. D. Doherty p. 485 in Crystal Growth, ed R. Pamplin, Pergamon Press, London, 1980.

35. R. S. Tiwari, S. Ranganathan, and M. Von Heimendahl, Z. Metallkd. 72 (1981) 563.

36. A. L. Greer, Acta Metall. 30 (1982) 171.

37. H. S. Chen, Mater. Sci. Eng. 23 (1976) 151.

38. L. E. Tanner and R. Ray, Scripta Metall. 14 (1980) 657.

39. J. L. Walter and S. F. Bartram, pp. 307–14 in Proc. Third Int. Conf. on Rapidly Quenched Metals, ed. B. Cantor, The Metals Society, London, 1978.

40. D. M. Kroeger, C. C. Koch, C. G. McKamey, and J. O. Scarbrough, J. Non-Cryst. Solids 61 and 62 (1984) 937.

41. D. M. Kroeger, C. C. Koch, J. O. Scarbrough, and C. G. McKamey, Phys. Rev. B 29(3) (1984) 1199.

42. H. van Swijgenhoven, L. M. Stals, and K.H.J. Buschow, Phys. Status Solidi A 72 (1982) 153.

43. C. P. Chou and D. Turnbull, J. Non-Cryst. Solids 17 (1975) 169.

44. H. S. Chen and D. Turnbull, Acta Metall. 17 (1969) 1021.

45. J. W. Christian, The Theory of Transformations in Metals and Alloys, 2nd ed., Pergamon Press, Oxford, England, 1975.

46. W. A. Johnson and R. F. Mehl, Trans. AIME 135 (1939) 416.

47. M. Avrami, J. Phys. Chem. 7 (1939) 1103; J. Phys. Chem. 8 (1940) 212; J. Phys. Chem. 9 (1941) 177.

48. T. Ozawa, Polymer 12(3) (1971) 150.

49. D. W. Henderson, J. Non-Cryst. Solids 30 (1979) 301.

50. D. W. Henderson, J. Thermal Analysis 15 (1979) 325.

51. K. Matusita and S. Sakka, J. Non-Cryst. Solids 38 and 39 (1980) 741.

52. S. Ranganathan and M. von Heimendahl, J. Mater. Sci. 16 (1981) 2401.

53. H. Yinnon and D. R. Uhlmann, J. Non-Cryst. Solids 54 (1983) 253.

54. H. E. Kissinger, J. Res. Nat. Bur. Stand. 57(4) (1956) 217; Anal. Chem. 29(11) (1957) 1702.

55. A. Ravex, J. C. Lasjaunias, and O. Béthoux, Solid State Commun. 40 (1981) 853.

56. A. Ravex, J. C. Lasjaunias, and O. Béthoux, Physica 107B (1981) 395.

57. D. G. Onn, L. Q. Wang, Y. Obi, and K. Fukamichi, Solid State Commun. 46(1) (1983) 37.

58. J. C. Lasjaunias and A. Ravex, J. Phys. 13 (1983) L101.

59. Z. Altounian and J. O. Strom-Olsen, Phys. Rev. B27(7) (1983) 4149.

60. R. W. Cochrane, J. Destry, and M. Trudeau, Phys. Rev. B27(10) (1983) 5955.

61. M. G. Karkut and R. R. Hake, Phys. Rev. B28(3) (1983) 1396.

62. R. Frahm, R. Haensel, and P. Rabe, J. Phys. 14 (1984) 1029; J. Phys. 14 (1984) 1333.

63. K.H.J. Buschow and N. M. Beekmans, Phys. Rev. B19(8) (1979) 3843.

64. K.H.J. Buschow, I. Vincze, and F. van der Woude, J. Non-Cryst. Solids 54 (1983) 101.

65. Y. D. Dong, G. Gregan, and M. G. Scott, J. Non-Cryst. Solids 43 (1981) 403.

66. K.H.J. Buschow, J. Appl. Phys. 52 (1981) 3319; Solid State Commun. 43 (1982) 171.

67. R. Ray, R. Hasegawa, C. P. Chou, and L. A. Davis, Scripta Metall. 11 (1977) 973.

68. C. Cunat, M. Notin, J. Hertz, J. M. Dubois, and G. Le Caer, J. Non-Cryst. Solids 55 (1983) 45.

69. K.H.J. Buschow, B. H. Verbeek, and A. G. Dirks, J. Phys. D: Appl. Phys. 14 (1981) 1087.

70. R. Frahm, J. Non-Cryst. Solids 56 (1983) 255.

71. A. F. Polesya and L. S. Slipchenko, Russ. Metall. 6 (1973) 103–107.

72. H. van Swijgenhoven, L. M. Stals, and K.H.J. Buschow, Phys. Stat. Solidi A 72 (1982) 153.

73. R. Schulz, V. Matijasevic, and W. L. Johnson, to be published.

74. F. Sommer, Z. Metallkd. 73 (1982) 72; Z. Metallkd. 73 (1982) 77.

75. F. Sommer, K. H. Klappert, I. Arpshofen, and B. Predel, Z. Metallkd. 73 (1982) 581.

76. B. Predel, Physica 103B (1981) 113.

77. K.H.J. Buschow, J. Phys. 14 (1984) 593.

78. P. Pietrokowsky, Rev. Sci. Instrum. 34 (1963) 445.

79. D. M. Kroeger, W. A. Coghlan, D. S. Easton, C. C. Koch, and J. O. Scarbrough, J. Appl. Phys. 53(3) (1982) 1445.

80. M. K. Ferber, Department of Ceramic Engineering, University of Illinois at Urbana-Champaign, Urbana, IL 61801.

81. C. G. McKamey, D. M. Kroeger, D. S. Easton, and J. O. Scarbrough, to be submitted to J. Non-Cryst. Solids.

82. D. S. Easton, C. G. McKamey, D. M. Kroeger, and O. B. Cavin, to be submitted to Scripta Metall.

83. H. Y. Yakel, private communication.

84. T. B. Massalski, pp. 203–8, Proc. Fourth Int. Conf. on Rapidly Quenched Metals, eds. T. Masumoto and K. Suzuki, Japan Institute of Metals, Sendai, 1981.

85. E. Hornbogen, J. Mater. Sci. 18 (1983) 127.

86. J. L. Walter, S. F. Bartram, and R. R. Russell, Metall. Trans. A9 (1978) 803.

87. H.O.K. Kirchner, P. Ramachandrarao, and G. A. Chadwick, Philos. Mag. 25 (1972) 1151.

88. M. von Heimendahl and G. Maussner, J. Mater Sci. 14 (1979) 1238.

89. L. E. Tanner and R. Ray, Acta Metall. 27 (1979) 1727.

90. A. Inoue, Y. Takahashi, C. Suryanarayana, and T. Masumoto, J. Mater. Sci. 17 (1982) 3253.

91. R. L. Freed and J. B. VanderSande, J. Non-Cryst. Solids 27 (1978) 9.

92. R. Wang, Nature 278 (1979) 700.

93. J. D. Bernal, Proc. Roy. Soc. A280 (1964) 299.

94. J. R. Taylor, An Introduction to Error Analysis, The Study of Uncertainties in Physical Measurements, University Science Books, Mill Valley, Ca., 1982.

APPENDIXES

APPENDIX A

PREPARATION AND CHARACTERIZATION OF ALLOYS

Table A-I. Weights of Zr-Ni Alloys Before and After Casting

Nominal Composition (at. % Zr)	Casting Designation	Weight of Alloy (g) Beginning	Weight of Alloy (g) Final	Change in Weight (g)	Explanation for Change
52.0	ABA	19.0400	19.0400	0	
55.0	AAB	5.0270	5.0270	0	
56.7	BD	2.8302			
57.1	AAP	10.9771	10.9716	−0.0055	
57.7	ABF	16.6146	16.6175	+0.0029	
58.4	BE	3.6500	3.6140	−0.0360	Lost 3 beads after 1st melt
59.0	AAC	5.0870	5.0865	−0.0005	
59.5	AAD	7.2180	7.2160	−0.0020	
60.0	AAF	16.4275	16.4270	−0.0005	
60.6	ABG	15.7533	15.7433	−0.0100	Lost bead after 1st melt
61.2	S	1.9930	1.9910	−0.0020	
62.0	AAV	14.6250	14.6062	−0.0188	Lost bead after 1st melt
62.9	BF	3.1240	3.1210	−0.0040	
63.2	D	4.3645	4.3640	−0.0005	
63.5	AAE	17.3042	17.2428	−0.0614	Lost bead after 1st melt
63.5	AAK	14.9055	14.8392	−0.0663	Lost bead after 1st melt
64.0	AB	1.7058	1.7050	−0.0008	
64.6	I	2.6410	2.6390	−0.0020	
65.0	AAG	12.2757	12.2716	−0.0041	
65.5	T	4.7840	4.7820	−0.0020	
66.0	AAU	12.0046	11.9988	−0.0058	
66.5	AD	1.9250	1.9248	−0.0002	
67.0	AAH	14.2047	14.2043	−0.0004	
67.0	AAT	16.1710	16.1790	+0.0080	
69.0	L	2.9000	2.8950	−0.0050	
71.0	K	2.1120	2.1110	−0.0010	

Table A-II. Results of Wet Chemistry Analysis for Impurities in Ingot AAF, $Zr_{60}Ni_{40}$ Alloy

Impurity Element	Amount of Impurity (ppm wt)
H	40
N	2
O	61
Hf	200
In	~5
Cu	7
Co	3
Fe	80
Mn	0.6
Cr	1
V	≤0.1
Ca	1
K	1
Cl	1
S	10
Al	3
Mg	≤1

APPENDIX B

COMPUTER PROGRAM FOR DIGITIZATION OF DSC CURVES

The following program was used to reduce differential scanning calorimeter chart strips (DSC traces) to a size which could be more easily used. It was written by M. K. Ferber for use on a IBM-PC personal computer and allows for the entering of raw data by either digitization, from a floppy disk, or from the keyboard. After entering the data, the individual data points can be edited, allowing one to normalize the curves to the same size sample and the same calorimeter parameters. The data can be plotted on the CRT screen or up to six curves can be drawn together on the plotter. On a printer the individual data points can also be printed out in table form. The data is stored on a floppy disk.

```
530 PRINT "******THIS PROGRAM PROVIDES FOR GRAPHICAL REPRESENTATION OF RAW DATA
******"
540 PRINT"       WHICH IS ENTERED :(1) VIA A DIGITIZATION PROCESS; (2) FROM DISK
550 PRINT"       (in raw form); OR (3) FROM THE KEYBOARD.THE RESULTING GRAPHS "
560 PRINT"       (up to 6) ARE DRAWN TOGETHER AS COMPLETE PLOT.THESE PLOTS MAY BE
"
570 PRINT"       STORED ON DISK FOR LATER VIEWING."
580 PRINT:BEEP:PRINT SPACE$(15);"(PRESS ANY KEY TO CONTINUE !!)"
590 IF INKEY$="" THEN GOTO 590 ELSE CLS
600 CLS:LOCATE 8,1:PRINT"*****THE FOLLOWING INPUT OPTIONS ARE AVAILABLE*****"
610 PRINT:PRINT"      (1) ENTER RAW DATA"
620 PRINT"      (2) ENTER EXISTING PLOT FROM DISK":PRINT
630 INPUT"      ENTER 1 OR 2:",INOPT%
640 IF INOPT%=2  THEN K=1:GOSUB 2650:GOTO 1180
650 CLS:LOCATE 8,1:PRINT"*****ENTER FOLLOWING INFORMATION:*****":PRINT
660 INPUT "      (1) GENERAL HEADING:",MATL$
670 INPUT "      (2) Y-AXIS LABEL:",YLAB$
680 INPUT "      (3) X-AXIS LABEL:",XLAB$
690 INPUT "      (4) ENVIRONMENT:",ENV$
700 INPUT"      (5) COMMENTS:",COMMT$
710 GOTO 4000
720 REM*************************************************************************
730 REM     ROUTINE FOR EDITING INDIVIDUAL DATA POINTS
740 REM*************************************************************************
750 GOSUB 6680
760 PRINT:INPUT"      ENTER GRAPH NO.TO BE EDITED(zero to exit):",NDEL%
770 IF NDEL%=0 THEN GOTO 3720
780 IF NDEL%<0 OR NDEL%>NPLTS1% THEN SOUND 180,100:GOTO 3720
790 PRINT:PRINT:PRINT"      YOU MAY EITHER (1) ADD OR (2) DELETE DATA."
800 INPUT"       ENTER 1 OR 2:",OPT%
810 K=NDEL%:IF OPT%=2 THEN GOTO 890
820 CLS:LOCATE 3,6:INPUT"ENTER NO. OF POINTS TO BE ADDED:",NDEL%
830 J=N%(K)+1:N%(K)=N%(K)+NDEL%
840 FOR I=J TO N%(K):PRINT:PRINT
850 INPUT"      ENTER X-VALUE:",T!(I,K)
860 INPUT"      ENTER Y-VALUE:",EL!(I,K)
870 INPUT"      ENTER STANDARD DEVIATION:",SD!(I,K)
880 NEXT I:GOTO 3720
890 CLS:LOCATE 10,5:DIV$="YES"
900 PRINT"DELETING PROCEDURE FOR GRAPH ";K;" WILL NOW BEGIN!!"
910 FOR I=1 TO 1000:NEXT I
920 NPLTS%=K:NUM%=N%(K):XTYPE%=1:YTYPE%=1:OPT%=0
930 FOR I=1 TO 6:PTYPE%(I)=1:NEXT I
940 CLS:GOSUB 2890:GOSUB 3170:GOSUB 3260:GOSUB 3450:BEEP
950 PPOS%=0
960 LOCATE 1,10
970 PRINT"                                                                    "
980 LOCATE 1,12:BEEP:PRINT"USE ARROWS (";CHR$(26);")&(";CHR$(27);") TO ISOLATE P
OINT (D-DELETE POINT X-EXIT ROUTINE)"
990 NO%=0
1000 A$=INKEY$:IF A$="" THEN GOTO 1000
1010 IF LEN(A$)=2 THEN A$=RIGHT$(A$,1)
1020 IF A$="M"AND PPOS%<NUM% THEN NO%=-1:PPOS%=PPOS%+1:GOSUB 2090:GOTO 990
1030 IF A$="K" AND PPOS%>1 THEN NO%=1:PPOS%=PPOS%-1:GOSUB 2090:GOTO 990
1040 IF A$="X" THEN BEEP:NO%=0:GOSUB 2090:CLS:GOTO 1170
1050 IF A$="D" THEN GOTO 1060 ELSE GOTO 990
1060 NO%=0:GOSUB 2090:CIRCLE(XT%(PPOS%),YT%(PPOS%)),3,0,,,2/3
1070 LOCATE 1,10:PRINT SPACE$(70)
1080 IF PPOS%>NUM% OR PPOS%<1 THEN GOTO 960
```

```
1090 IF NUM%-1=0 THEN CLS:LOCATE 5,5:BEEP:PRINT"ALL DATA POINTS ELIMINATED STUPI
D!!!!":FOR I=1 TO 1000:NEXT:GOTO 3720
1100 LOCATE 1,20:BEEP: PRINT" DATA POINT BEING DELETED FOR POSITION:";PPOS%
1110 FOR I=1 TO 1000:NEXT I
1120 NUM%=NUM%-1:IF PPOS%=NUM%+1 THEN PPOS%=NUM%:GOTO 1150
1130 FOR I=PPOS% TO NUM%
1140 T!(I,K)=T!(I+1,K):EL!(I,K)=EL!(I+1,K):XT%(I)=XT%(I+1):YT%(I)=YT%(I+1):SD!(I
,K)=SD!(I+1,K):NEXT I
1150 LINE (XT%(PPOS%)-5,YT%(PPOS%)-5)-(XT%(PPOS%)+5,YT%(PPOS%)+5),1,B
1160 GOTO 960
1170 N%(K)=NUM%:NUM%=0:GOTO 3720
1180 DIV$="":K=1:DIV2$="":DIV3$="":BEEP:CLS:LOCATE 8,6
1190  BEEP:PRINT"YOU NOW HAVE THE FOLLOWING CHOICES:"
1200 PRINT:PRINT"      (1) IMPLEMENT SPECIAL EDITING FEATURES"
1210 PRINT"      (2) INITIATE MATH ROUTINES"
1220 PRINT"      (3) DATA PRINTOUT AND CRT PLOTTING OPTIONS"
1230 PRINT"      (4) OUTPUT GRAPHICAL DATA TO PLOTTER"
1240 PRINT"      (5) EXIT WITH DATA STORAGE OPTION":PRINT
1250 INPUT"      ENTER 1,2,3,4 OR 5:",OPT4%:ON OPT4% GOTO 3720,5790,1260,4540,186
0
1260 CLS:LOCATE 10,6:INPUT"DO YOU REQUIRE TABLE PRINTOUT (Y/N)?",A$
1270 IF A$="N" THEN GOTO 1290
1280 GOSUB 1410
1290 PRINT:INPUT"      DO YOU REQUIRE GRAPHICAL OUTPUT (Y/N)?",A$
1300 IF A$="N" THEN GOTO 1180 ELSE PRINT:INPUT"      WILL YOU BE DUMPING IMAGE TO
 PRINTER (Y/N)?",A1$
1310 NPLTS%=NPLTS1%:K=1:XTYPE%=1:YTYPE%=1:OPT%=0
1320 PRINT:INPUT"      DO YOU REQIRE SELF SCALING (Y/N)?",A$:IF A$="Y" THEN GOTO
1360
1330 CLS:LOCATE 10,6:INPUT"ENTER X-MIN AND X-MAX:",XMIN!,XMAX!
1340 LOCATE 12,6:INPUT"ENTER Y-MIN AND Y-MAX:",YMIN!,YMAX!
1350 CLS:GOSUB 4420:GOSUB 2890:GOSUB 3170:GOSUB 2940:GOSUB 3450:GOTO 1370
1360 CLS:GOSUB 4420:GOSUB 2890:GOSUB 3170:GOSUB 3260:GOSUB 3450
1370 BEEP:IF A1$="N" THEN GOTO 1400 ELSE LPRINT STRING$(12,11)
1380 IF INKEY$="" THEN GOTO 1380
1390 LPRINT CHR$(27);CHR$(55);CHR$(18);CHR$(27);CHR$(86);CHR$(0);CHR$(27);CHR$(5
0);CHR$(12)
1400 IF INKEY$="" THEN GOTO 1400 ELSE CLS:LOCATE 10,6:INPUT"DO YOU WISH TO REPLO
T DATA ON CRT(Y/N)?",A$:IF A$="Y" THEN CLS:LOCATE 10,1:GOTO 1300 ELSE GOTO 1180
1410 REM ************************************************************
1420 REM SUBROUTINE FOR PRINTING DATA!!
1430 REM************************************************************
1440 HEAD$="       GRAPHICAL DATA PRINTOUT":GOSUB 1710
1450 FOR K=1 TO NPLTS1%
1460 LPRINT:LPRINT CHR$(14);"         DATA FOR GRAPH:";K;CHR$(20)
1470 LPRINT CHR$(14);"         GRAPH NAME:";GTITLE$(K);CHR$(20):LPRINT
1480 LPRINT:LPRINT CHR$(27);CHR$(88);CHR$(0);STAR$
1490 LPRINT SPACE$(5);"DATA";SPACE$(12);"X-AXIS";SPACE$(12);"Y-AXIS";SPACE$(12);
"STANDARD"
1500 LPRINT SPACE$(6);"NO.";SPACE$(12);"VALUE";SPACE$(13);"VALUE";SPACE$(13);"DE
VIATION"
1510 LPRINT STAR$:LPRINT
1520 FOR I=1 TO N%(K)
1530 LPRINT TAB(6);I;
1540 LPRINT TAB(18):LPRINT USING "###.##^^^^";T!(I,K);:LPRINT TAB(37):LPRINT USI
NG "###.####^^^^";EL!(I,K);:LPRINT TAB(54):LPRINT USING "###.####^^^^";SD!(I,K)
1550 NEXT I:LPRINT STAR$:LPRINT:LPRINT
1560 LPRINT CHR$(12):NEXT K
```

```
1570 CLS:LOCATE 10,1:INPUT"      DO YOU WISH TO ALTER ANY OF THE MAJOR TABLE HEAD
INGS (Y/N)?",D$
1580 IF D$="N"  THEN RETURN
1590 CLS:LOCATE 10,1:PRINT"      ENTER DESIRED ALTERATIONS FOR FOLLOWING HEADINGS
":PRINT"        (leave blank if no changes are necessary)"
1600 PRINT:INPUT"      GENERAL HEADING:",D$:IF D$="" THEN GOTO 1610 ELSE MATL$=D$

1610 INPUT"      ENVIRONMENT:",D$:IF D$="" THEN GOTO 1620 ELSE ENV$=D$
1620 INPUT"      Y-LABEL:",D$:IF D$="" THEN GOTO 1630 ELSE YLAB$=D$
1630 INPUT"      X-LABEL:",D$:IF D$="" THEN GOTO 1640 ELSE XLAB$=D$
1640 INPUT"      COMMENTS:",D$:IF D$="" THEN GOTO 1650 ELSE COMMT$=D$
1650 FOR I=1 TO NPLTS1%:PRINT"      GRAPH ";I;:INPUT ":",D$
1660 IF D$="" THEN GOTO 1670 ELSE GTITLE$(I)=D$
1670 NEXT I
1680 IF DIV3$="YES" THEN RETURN
1690 CLS:LOCATE 10,1:INPUT"      DO YOU REQUIRE PRINTOUT OF MODIFIED TABLE ?(Y/N)
",D$
1700 IF D$="Y" THEN GOTO 1410 ELSE RETURN
1710 REM*************************************************************************
1720 REM   SUBROUTINE FOR HEADING PRINTOUT!!!!
1730 REM*************************************************************************
1740 CLS:LOCATE 10,1 :BEEP:PRINT"      TURN ON PRINTER AND THEN PRESS ANY KEY !!!
"
1750 A$=INKEY$:IF A$="" THEN GOTO 1750 ELSE CLS
1760 LPRINT CHR$(27);CHR$(78);CHR$(10):CLS
1770 STAR$="*************************************************************************
*********"
1780 LPRINT CHR$(27);CHR$(88);CHR$(1);CHR$(14)
1790 LPRINT CHR$(14);HEAD$;CHR$(20):LPRINT
1800 LPRINT"           HEADING:";MATL$
1810 LPRINT "           ENVIRONMENT:";ENV$
1820 LPRINT "           X-AXIS LABEL:";XLAB$
1830 LPRINT "           Y-AXIS LABEL:";YLAB$
1840 IF COMMT$="" THEN RETURN ELSE LPRINT"          ADDITIONAL COMMENTS:";COMMT$

1850 RETURN
1860 REM*************************************************************************
1870 REM    SUBROUTINE FOR WRITING DATA FILE
1880 REM*************************************************************************
1890 CLS:BEEP:LOCATE 10,1:INPUT"      DO YOU WISH TO SAVE DATA (Y/N)?",A1$
1900 IF A1$="N" THEN GOTO 2070
1910 CLS:BEEP:LOCATE 10,6:PRINT"INSERT DATA DISK INTO SIDE B!!!"
1920 PRINT"       (PRESS ANY KEY TO CONTINUE !)"
1930 IF INKEY$="" THEN GOTO 1930
1940 PRINT:INPUT"      DO YOU WISH TO VIEW FILES (Y/N)?",A1$
1950 IF A1$="N" THEN GOTO 1990
1960 CLS:LOCATE 1,6:PRINT"THE FOLLOWING FILES ARE PRESENT:"
1970 FILES"B:*.*":PRINT"      PRESS ANY KEY TO CONTINUE!"
1980 IF INKEY$="" THEN GOTO 1980
1990 CLS:LOCATE 10,6:INPUT"ENTER BOTH NAME OF STORAGE FILE AND DISC NO.:",A1$,DI
SNO%:FLNM2$=A1$
2000 OPEN "B:"+A1$ FOR OUTPUT AS #1
2010 WRITE#1,MATL$,ENV$,YLAB$,XLAB$,COMM$,NPLTS1%
2020 FOR J=1 TO NPLTS1%
2030 WRITE#1,N%(J),GTITLE$(J)
2040 FOR I=1 TO N%(J):WRITE#1,T!(I,J),EL!(I,J),SD!(I,J):NEXT I:NEXT J
2050 CLOSE#1
```

```
2060 GOSUB 1720:LPRINT:LPRINT:LPRINT"           DATA STORED IN FILE:";FLNM2$;"  D
ISK NUMBER:";DISNO%:LPRINT SPACE$(15);"DATE=";DATE$:LPRINT CHR$(12)
2070 CLS:LOCATE 12,6:INPUT"DO YOU WISH TO RESTART PROGRAM (Y/N)?",A$
2080 IF A$="Y" THEN GOTO 520 ELSE SYSTEM
2090 REM*************************************************************************
2100 REM SUBROUTINE FOR SCANNING DATA POINTS!!
2110 REM*************************************************************************
2120 IF NO%=0 THEN GOTO 2160
2130 LINE (XT%(PPOS%)-5,YT%(PPOS%)-5)-(XT%(PPOS%)+5,YT%(PPOS%)+5),1,B
2140 IF PPOS%=1 AND NO%=-1 THEN GOTO 2180
2150 IF PPOS%=NUM% AND NO%=1 THEN GOTO 2180
2160 LINE (XT%(PPOS%+NO%)-5,YT%(PPOS%+NO%)-5)-(XT%(PPOS%+NO%)+5,YT%(PPOS%+NO%)+5
),0,B
2170 CIRCLE(XT%(PPOS%+NO%),YT%(PPOS%+NO%)),3,,,,2/3
2180 RETURN
2190 REM*************************************************************************
2200 REM                SUBROUTINE FOR DIGITIZING DATA
2210 REM*************************************************************************
2220 OPEN "COM2:4800,O,7,1,CS,DS"AS#1
2230 CLS:LOCATE 2,1:BEEP
2240 PRINT"*****DIGITIZE LOWER LEFT REFERENCE POINT*****"
2250 INPUT#1,TMP$:XLL#=VAL(MID$(TMP$,2,5)):YLL#=VAL(MID$(TMP$,8,5))
2260 PRINT:INPUT"      ENTER X-VALUE AT THIS POINT:",MV1#
2270 INPUT"      ENTER Y-VALUE AT THIS POINT:",RE1#
2280 LOCATE 12,1:BEEP
2290 PRINT"*****DIGITIZE UPPER RIGHT REFERENCE POINT*****"
2300 INPUT#1,TMP$:XUR#=VAL(MID$(TMP$,2,5)):YUR#=VAL(MID$(TMP$,8,5))
2310 PRINT:INPUT"      ENTER X-VALUE AT THIS POINT:",MV2#
2320 INPUT"      ENTER Y-VALUE AT THIS POINT:",RE2#
2330 DEF FNXLOC#(X#)=((MV2#-MV1#)/(XUR#-XLL#))*(X#-XLL#)+MV1#
2340 DEF FNYLOC#(Y#)=((RE2#-RE1#)/(YUR#-YLL#))*(Y#-YLL#)+RE1#
2350 CLS:BEEP:LOCATE 2,1:PRINT"*********YOU MAY NOW DIGITIZE DATA*********"
2360 PRINT"      USE WHITE BUTTON FOR DATA ENTRY"
2370 PRINT"      USE RED BUTTON FOR DATA REMOVAL"
2380 PRINT"      USE GREEN BUTTON TO EXIT ROUTINE"
2390 PRINT"      USE YELLOW BUTTON TO INPUT STANDARD DEVIATION"
2400 PRINT:PRINT
2410 PRINT"         X-VALUE                Y-VALUE           STANDARD DEV.          DA
TA NO."
2420 PRINT"        *********              *********         **************       ***
******"
2430 INPUT#1,TMP$:X#=VAL(MID$(TMP$,2,5)):Y#=VAL(MID$(TMP$,8,5)):DTCP$=MID$(TMP$,
1,1)
2440 IF LOF(1)(100 THEN SOUND 390,3:SOUND 150,3
2450 SD!(NUM%+1,K)=0
2460 IF DTCP$="b" THEN GOTO 2600
2470 X#=FNXLOC#(X#):Y#=FNYLOC#(Y#)
2480 IF DTCP$="R" THEN GOTO 2550
2490 IF DTCP$="B" THEN NUM%=NUM%-1:GOTO 2510
2500 NUM%=NUM%+1:T!(NUM%,K)=X#:EL!(NUM%,K)=Y#
2510 LOCATE 12,1
2520 PRINT SPACE$(80):LOCATE 12,1
2530 PRINT TAB(3);T!(NUM%,K);TAB(24);EL!(NUM%,K);TAB(47);SD!(NUM%,K);TAB(70);NUM
%
2540 BEEP:GOTO 2430
2550 CLS:LOCATE 8,1:PRINT"*****YOU NOW HAVE THE FOLLOWING OPTIONS*****"
2560 PRINT:PRINT"      (1) RESET DIGITIZING LIMITS"
2570 PRINT"      (2) EXIT DIGITIZING ROUTINE"
```

```
2580 PRINT:INPUT"      ENTER OPTION NO.:",DIGOPT%
2590 IF DIGOPT%=1 THEN GOTO 2190 ELSE CLOSE #1:RETURN
2600 REM ************************************************************
2610 REM ROUTINE FOR INPUTING STANDARD DEVIATION
2620 REM ************************************************************
2630 SD!(NUM%,K)=ABS(FNYLOC#(Y#)-EL!(NUM%,K))
2640 GOTO 2510
2650 REM************************************************************************
2660 REM     SUBROUTINE FOR READING DATA FILE
2670 REM************************************************************************
2680 CLS:BEEP:LOCATE 10,6:PRINT"INSERT DATA DISK INTO SIDE B!!!"
2690 PRINT"       (PRESS ANY KEY TO CONTINUE !)"
2700 IF INKEY$="" THEN GOTO 2700
2710 PRINT:INPUT"      DO YOU WISH TO VIEW FILES (Y/N)?",A1$
2720 IF A1$="N" THEN GOTO 2760
2730 CLS:LOCATE 1,6:PRINT"THE FOLLOWING FILES ARE PRESENT:"
2740 FILES"B:*.*":PRINT"      PRESS ANY KEY TO CONTINUE!"
2750 IF INKEY$="" THEN GOTO 2750
2760 CLS:LOCATE 10,6:INPUT"ENTER NAME OF DATA FILE:",A1$
2770 OPEN "B:"+A1$ FOR INPUT AS #1
2780 IF DIV$="YES" THEN GOTO 2830
2790 IF DIV2$="YES" THEN INPUT#1,D$,D$,D$,D$,D$,NPLTS1%:GOTO 2810
2800 INPUT#1,MATL$,ENV$,YLAB$,XLAB$,COMM$,NPLTS1%
2810 IF DIV2$="YES" THEN NPLTS1%=NPLTS1%+K-1
2820 IF NPLTS1%)6 THEN CLS:LOCATE 4,6:NLPTS1%=NPLTS1%-K+1:PRINT"LIMIT ON NO. OF
GRAPHS EXCEEDED! NEW GRAPHS NOT ADDED!":CLOSE#1:SOUND 200,100:GOTO 3720
2830 FOR J=K TO NPLTS1%:INPUT#1,N%(J),GTITLE$(J)
2840 FOR I=1 TO N%(J):INPUT#1,T!(I,J),EL!(I,J),SD!(I,J):NEXT I:NEXT J
2850 NUM%=NO%:CLOSE #1:CLS:LOCATE 12,6:INPUT"DO YOU WISH TO SAVE THIS FILE (Y/N)
?",A2$
2860 IF A2$="Y" THEN RETURN ELSE KILL A1$:RETURN
2870 REM ************************************************************************
2880 REM SUBROUTINE FOR FRAMING!!!!
2890 REM ************************************************************
2900 KEY OFF:CLS:LINE (75,20)-(625,300),,B:LINE (76,21)-(626,301),,B:RETURN
2910 REM ************************************************************************
2920 REM SUBROUTINE FOR SCALING!!!!
2930 REM ************************************************************************
2940 IF YMAX!=0 THEN YMX%=-9999:GOTO 2960
2950 YMX%=INT(LOG(ABS(YMAX!))/LOG(10))
2960 IF YMIN!=0 THEN YMN%=-9999 :GOTO 2980
2970 YMN%=INT(LOG(ABS(YMIN!))/LOG(10))
2980 IF YMX%(YMN% THEN YI%=YMN% ELSE YI%=YMX%
2990 IF XMAX!=0 THEN XMX%=-9999:GOTO 3010
3000 XMX%=INT(LOG(ABS(XMAX!))/LOG(10))
3010 IF XMIN!=0 THEN XMN%=-9999:GOTO 3030
3020 XMN%=INT(LOG(ABS(XMIN!))/LOG(10))
3030 IF XMX%(XMN% THEN XI%=XMN% ELSE XI%=XMX%
3040 XI%=XI%-OPT%:YI%=YI%-OPT%
3050 YMAX1!=YMAX!/(10^YI%):YMIN1!=YMIN!/(10^YI%)
3060 XMAX1!=XMAX!/(10^XI%):XMIN1!=XMIN!/(10^XI%)
3070 IF DIV3$="YES" THEN RETURN
3080 STP!=(YMAX1!-YMIN1!)/10:YL!=YMIN1!:TICY%=300
3090 FOR I=1 TO 11:LOCATE (24-2*I),4:PRINT USING"##.##";YL!:YL!=YL!+STP!:TICY%=3
00-(I-1)*28:LINE (75,TICY%)-(85,TICY%):NEXT I
3100 STP!=(XMAX1!-XMIN1!)/10:XL!=XMIN1!:TICX%=75
3110 FOR I=1 TO 11:LOCATE 23,(7+6*(I-1)):PRINT USING"##.##";XL!:XL!=XL!+STP!:TIC
X%=75+(I-1)*55:LINE (TICX%,300)-(TICX%,293):NEXT I
```

```
3120 XSC$="(X10^"+STR$(XI%)+")":YSC$="(X10^"+STR$(YI%)+")"
3130 LOCATE 1,1:PRINT YSC$:LOCATE 24,71:PRINT XSC$;
3140 RETURN
3150 REM ************************************************************
3160 REM SUBROUTINE FOR AXIS LABELLING!!!!
3170 REM ************************************************************
3180 XLEN%=LEN(XLAB$):YLEN%=LEN(YLAB$):HLEN%=LEN(MATL$)
3190 LOCATE 1,40-INT(HLEN%/2):PRINT MATL$
3200 LOCATE 24,40-INT(XLEN%/2):PRINT XLAB$;
3210 YPOS%=11-INT(YLEN%/2):LOCATE YPOS%,2
3220 FOR I=1 TO YLEN%:LOCATE YPOS%+(I-1),2:PRINT MID$(YLAB$,I,1);:NEXT I
3230 RETURN
3240 REM ************************************************************
3250 REM SUBROUTINE FOR SELF SCALING!!!!!
3260 REM ************************************************************
3270 XMIN!=T!(1,K):XMAX!=T!(1,K):YMIN!=EL!(1,K):YMAX!=EL!(1,K)
3280 FOR J=K TO NPLTS%
3290 FOR I=1 TO N%(J)
3300 IF T!(I,J)>XMAX! THEN XMAX!=T!(I,J)
3310 IF T!(I,J)<XMIN! THEN XMIN!=T!(I,J)
3320 IF EL!(I,J)>YMAX! THEN YMAX!=EL!(I,J)
3330 IF EL!(I,J)<YMIN! THEN YMIN!=EL!(I,J)
3340 NEXT I:NEXT J
3350 IF XTYPE%=2 THEN GOTO 3380
3360 TMP1!=(XMAX!-XMIN!):TMP2!=10^INT(LOG(TMP1!)/(LOG(10)))
3370 XMIN!=(CINT(XMIN!/TMP2!)-.5)*TMP2!:XMAX!=(CINT(XMAX!/TMP2!)+.5)*TMP2!
3380 IF YTYPE%=2 THEN GOTO 3410
3390 TMP1!=(YMAX!-YMIN!):TMP2!=10^INT(LOG(TMP1!)/(LOG(10)))
3400 YMIN!=(CINT(YMIN!/TMP2!)-.5)*TMP2!:YMAX!=(CINT(YMAX!/TMP2!)+.5)*TMP2!
3410 IF DIV3$="YES" THEN SOUND 300,3:RETURN
3420 GOSUB 2940
3430 RETURN
3440 REM ************************************************************
3450 REM SUBROUTINE FOR PLOTTING DATA!!!!
3460 REM ************************************************************
3470 SCX!=550/(XMAX!-XMIN!):SCY!=280/(YMAX!-YMIN!)
3480 FOR I=K TO NPLTS%
3490 FOR J=1 TO N%(I)
3500 SD1%=INT((SD!(J,I)*SCY!))
3510 X1%=INT((T!(J,I)-XMIN!)*SCX!)+75
3520 Y1%=INT((YMAX!-EL!(J,I))*SCY!)+20
3530 XT%(J)=X1%:YT%(J)=Y1%
3540 IF DIV$="YES" THEN CIRCLE (X1%,Y1%),3,,,,2/3:GOTO 3630
3550 IF I=1 THEN CIRCLE (X1%,Y1%),3,,,,2/3:GOTO 3630
3560  IF I=2 THEN CIRCLE(X1%,Y1%),3,,,,2/3:PAINT (X1%,Y1%),1:GOTO 3630
3570  IF I=3 THEN LINE (X1%-2,Y1%)-(X1%+2,Y1%):LINE (X1%,Y1%+2)-(X1%,Y1%-2):GOTO
 3630
3580  IF I=4 THEN LINE (X1%+2,Y1%+2)-(X1%-2,Y1%-2),,B:GOTO 3630
3590  IF I=5 THEN LINE (X1%+2,Y1%+2)-(X1%-2,Y1%-2),,BF:GOTO 3630
3600  IF I=6 THEN LINE (X1%+2,Y1%-2)-(X1%-2,Y1%-2)
3610  IF I=6 THEN LINE (X1%+2,Y1%-2)-(X1%,Y1%+2)
3620  IF I=6 THEN LINE (X1%-2,Y1%-2)-(X1%,Y1%+2)
3630 IF SD1%=0 THEN GOTO 3660 ELSE LINE (X1%,Y1%-SD1%)-(X1%,Y1%+SD1%)
3640 LINE (X1%+6,Y1%+SD1%)-(X1%-6,Y1%+SD1%)
3650 LINE (X1%+6,Y1%-SD1%)-(X1%-6,Y1%-SD1%)
3660 IF PTYPE%(I)=1 OR PTYPE%(I)=3 THEN GOTO 3690
3670 IF J=1 THEN GOTO 3690
3680 LINE (XL%,YL%)-(X1%,Y1%),1
```

```
3690 XL%=X1%:YL%=Y1%:NEXT J
3700 IF PTYPE%(I)=3 THEN GOSUB 5570
3710 NEXT I:RETURN
3720 REM*************************************************************************
3730 REM SPECIAL EDITING ROUTINES
3740 REM*************************************************************************
3750 DIV$="":DIV2$="":K=1:CLS:LOCATE 2,6:DIV3$=""
3760 PRINT"*********NUMBER OF GRAPHS IN MEMORY= ";NPLTS1%;"***********":LOCATE 8
,6
3770 PRINT"THE FOLLOWING ARE THE SPECIAL EDITING ROUTINES:":PRINT
3780 PRINT"       (1) EDIT INDIVIDUAL POINTS FOR EACH GRAPH"
3790 PRINT"       (2) DELETE AN INDIVIDUAL GRAPH"
3800 PRINT"       (3) ADD AN INDIVIDUAL GRAPH"
3810 PRINT"       (4) ADD TWO GRAPHS TOGETHER"
3820 PRINT"       (5) MERGE STORED PLOT WITH ONE IN MEMORY"
3830 PRINT"       (6) EXIT SPECIAL ROUTINES AND RETURN TO MAIN MENU":PRINT
3840 INPUT"      ENTER 1,2,3,4,5 OR 6:",OPT5%:ON OPT5% GOTO 720,3850,4000,4150,42
70,1180
3850 REM*************************************************************************
3860 REM          ROUTINE FOR DELETING GRAPH
3870 REM*************************************************************************
3880 GOSUB 6680
3890 INPUT"      ENTER GRAPH NO.TO BE DELETED(zero to exit):",NDEL%
3900 IF NDEL%=0 THEN GOTO 3720
3910 IF NDEL%<0 OR NDEL%>NPLTS1% THEN SOUND 180,100:GOTO 3720
3920 IF NPLTS1%=1 THEN CLS:LOCATE 8,6:PRINT"LAST GRAPH DELETED!!!":FOR I=1 TO 10
00:NEXT I:NPLTS1%=0:GOTO 2070
3930 NPLTS1%=NPLTS1%-1
3940 IF NPLTS1%+1=NDEL% THEN GOTO 3980
3950 FOR I=NDEL% TO NPLTS1%:N%(I)=N%(I+1):GTITLE$(I)=GTITLE$(I+1)
3960 FOR J=1 TO N%(I)
3970 T!(J,I)=T!(J,I+1):EL!(J,I)=EL!(J,I+1):SD!(J,I)=SD!(J,I+1):NEXT J:NEXT I
3980 PRINT:PRINT"         GRAPH ";NDEL%;" DELETED !!!"
3990 FOR I=1 TO 1000:NEXT I:GOTO 3720
4000 REM*************************************************************************
4010 REM       ROUTINE FOR ADDING GRAPH
4020 REM*************************************************************************
4030 CLS:LOCATE 8,6
4040 IF NPLTS1%=6 THEN SOUND 180,100:PRINT"MAXIMUN NO. OF GRAPHS ALREADY PRESENT
 !!!":FOR I=1 TO 1000:NEXT I:GOTO 3720
4050 GOSUB 6680:NPLTS1%=NPLTS1%+1:PRINT
4060 PRINT"       GRAPH ";NPLTS1%;" WILL NOW BE ADDED!":PRINT
4070 INPUT"       ENTER GRAPH NAME:",GTITLE$(NPLTS1%):PRINT
4080 INPUT"       CHOOSE DATA ENTRY METHOD(1-digitization,2-disk or 3-keyboard):"
,OPT%
4090 K=NPLTS1%:NUM%=0
4100 IF OPT%=2 THEN DIV$="YES":GOSUB 2650:K=1:GOTO 3720
4110 IF OPT%=3 THEN N%(NPLTS1%)=0:K=NPLTS1%:GOTO 820
4120 PRINT"DIGITIZATION OF GRAPH ";NPLTS1%;" WILL NOW BEGIN"
4130 FOR I=1 TO 1000:NEXT I
4140 GOSUB 2190:N%(K)=NUM%:GOTO 3720
4150 REM*************************************************************************
4160 REM          ROUTINE FOR ADDING TWO GRAPHS TOGETHER
4170 REM*************************************************************************
4180 GOSUB 6680
4190 PRINT:INPUT"      ENTER NUMBERS OF 2 GRAPHS TO BE ADDED(zeros to exit):",OPT
%,OPT1%
4200 IF OPT%=0 OR OPT1%=0 THEN GOTO 3750
```

```
4210 NUM%=N%(OPT%)+1:N%(OPT%)=N%(OPT%)+N%(OPT1%):M=1
4220 FOR I=NUM% TO N%(OPT%)
4230 T!(I,OPT%)=T!(M,OPT1%)
4240 EL!(I,OPT%)=EL!(M,OPT1%)
4250 SD!(I,OPT%)=SD!(M,OPT1%)
4260 M=M+1:NEXT I:NDEL%=OPT1%:GOTO 3910
4270 REM*************************************************************************
4280 REM          ROUTINE FOR MERGING STORED PLOT WITH EXISTING ONE
4290 REM*************************************************************************
4300 DIV2$="YES":K=NPLTS1%+1:GOSUB 2650:GOTO 3720
4310 REM*************************************************************************
4320 REM        ERROR CHECKING FOR DIGITIZATION PROCESS
4330 REM*************************************************************************
4340 SOUND 171,10:LOCATE 19,3:PRINT"**********ERROR ENCOUNTERED !!!!**********"
4350 IF ERR =69 THEN PRINT"      BUFFER OVERFLOW!" ELSE GOTO 4380
4360 FOR I=1 TO 1000:NEXT I
4370 CLOSE#1:OPEN "COM2:4800,O,7,1,CS,DS"AS#1:LOCATE 20,1:PRINT SPACE$(60):RESUM
E 2350
4380 IF ERR=9 THEN PRINT"      TOO MANY DATA POINTS ENTERED!":CLOSE#1:GOTO 4400
4390 PRINT"    UNKNOWN ERROR!!":CLOSE#1
4400 FOR I=1 TO 1000:NEXT
4410 RESUME 1180
4420 REM*************************************************************************
4430 REM    SUBROUTINE FOR CHOOSING CURVE TYPE
4440 REM*************************************************************************
4450 CLS:LOCATE 6,6
4460 PRINT"YOU HAVE THE FOLLOWING PLOTTING OPTIONS:"
4470 PRINT:PRINT"      (1) DRAW POINTS ONLY"
4480 PRINT"      (2) CONNECT POINTS WITH STRAIGHT LINE"
4490 PRINT"      (3) DRAW POLYNOMIAL CURVE THROUGH POINTS"
4500 PRINT"       (*curve parameters are entered using math routines)"
4510 PRINT:PRINT:PRINT
4520 FOR I=1 TO NPLTS1%
4530 PRINT"      CHOOSE 1,2 OR 3 FOR GRAPH ";I;:INPUT ":",PTYPE%(I):NEXT I:RETURN

4540 REM*************************************************************************
4550 REM    ROUTINE FOR DUMPING GRAPHICAL DATA TO PLOTTER
4560 REM*************************************************************************
4570 CLS:LOCATE 3,3:BEEP
4580 PRINT"******YOUR DATA WILL NOW BE DRAWN ON X-Y PLOTTER !"
4590 PRINT:PRINT"    ))SET SWITCH TO PLOTTER AND LOAD PENS !!"
4600 PRINT"        (press any key to continue)"
4610 IF INKEY$="" THEN GOTO 4610
4620 LPRINT "Z":PRINT:PRINT"    ))LOAD PAPER AND THEN SELECT DESIRED ORIGIN !"
4630 PRINT"        (press any key to continue)"
4640 IF INKEY$="" THEN GOTO 4640
4650 LPRINT"@":LPRINT"J1":CLS:LOCATE 3,6
4660 PRINT"A MAXIMUM PLOT SIZE OF 7(y) BY 10(x) INCHES IS USED FOR 100% SCALING.
"
4670 PRINT:INPUT"       ENTER SCALING FACTOR FOR X-AXIS (20-100%):",PSX%
4680 PRINT:INPUT"       ENTER SCALING FACTOR FOR Y-AXIS (20-100%):",PSY%
4690 PXMAX%=INT(2540*PSX%/100):PYMAX%=INT(1780*PSY%/100)
4700 LPRINT"M0,0":LPRINT"D";PXMAX%;",0,";PXMAX%;",";PYMAX%;",0,";PYMAX%;",0,0"
4710 CLS:LOCATE 3,6
4720 PRINT"THE FOLLOWING AXES TYPES ARE AVAILABLE:"
4730 PRINT:PRINT"       (1) LINEAR"
4740 PRINT"       (2) LOG (common)"
4750 PRINT:INPUT"       ENTER X-AXIS TYPE (1 OR 2):",XTYPE%
```

```
4760 INPUT"       ENTER Y-AXIS TYPE (1 OR 2):",YTYPE%
4770 PRINT:PRINT:INPUT"       DO YOU WISH TO MODIFY ANY OF THE MAJOR HEADINGS (Y/
N):",D$
4780 DIV3$="YES":IF D$="Y" THEN GOSUB 1590
4790 CLS:LOCATE 3,6
4800 INPUT"DO YOU REQIRE SELF SCALING (Y/N)?",D$:IF D$="Y" THEN GOTO 4830
4810 INPUT"       ENTER X-MIN AND X-MAX:",XMIN!,XMAX!
4820 INPUT"       ENTER Y-MIN AND Y-MAX:",YMIN!,YMAX!
4830 IF D$="Y" THEN K=1:NPLTS%=NPLTS1%:GOSUB 3240
4840 IF XTYPE%=2 THEN XMIN!=INT(XMIN!):XMAX!=INT(XMAX!)+1
4850 IF YTYPE%=2 THEN YMIN!=INT(YMIN!):YMAX!=INT(YMAX!)+1
4860 DEF FNPX%(X#)=INT(PXMAX%*(X#-XMIN!)/(XMAX!-XMIN!))
4870 DEF FNPY%(Y#)=INT(PYMAX%*(Y#-YMIN!)/(YMAX!-YMIN!))
4880 K=10:IF XTYPE%=2 THEN K=XMAX!-XMIN!
4890 LPRINT"M0,0":LPRINT"X2,";PXMAX%;",";K
4900 TN1%=FIX(PSX%*35/100):TN2%=INT(TN1%/1.8):LPRINT"S";TN1%;",";TN2%
4910 IF XTYPE%=2 THEN GOTO 5150
4920 CLS:LOCATE 3,1:PRINT"******ENTER FOLLOWING INFORMATION FOR X-AXIS*****":LOC
ATE 6,6
4930 INPUT"NO. OF DIGITS TO BE DISPLAYED TO LEFT OF DECIMAL (1-4):",OPT%
4940 OPT%=OPT%-1:GOSUB 2920
4950 PRINT:INPUT"      NO.OF DIGITS TO BE DISPLAYED TO RIGHT OF DECIMAL (0-2):",O
PT1%
4960 OPT3%=0
4970 STP!=(XMAX1!-XMIN1!)/10:NUM%=INT(PXMAX%/K):OPT5%=FIX(-50*PSX%/100)
4980 LPRINT"M";OPT5%;",";FIX(-140*PSX%/100)
4990 K=K+1
5000 FOR I=1 TO K
5010 IF XMIN1!<0 THEN A$="-" ELSE A$=""
5020 A$=A$+STR$(ABS(FIX(XMIN1!)))+"."
5030 IF OPT1%>0 THEN OPT%=ABS(CINT((XMIN1!-FIX(XMIN1!))*10^OPT1%))
5040 IF OPT1%>0 THEN A$=A$+MID$(STR$(OPT%),2,OPT1%)
5050 LPRINT"P";A$:XMIN1!=XMIN1!+STP!
5060 IF OPT3%=1 THEN A$=STR$(FIX(OPT4%))
5070 IF OPT3%=1 THEN LPRINT"R";-TN2%;".";FIX(TN1%*.9):LPRINT"P";A$:OPT4%=OPT4%+1

5080 K=NUM%*I+OPT5%
5090 LPRINT"M";K;",";FIX(-140*PSX%/100):NEXT I
5100 IF XI%=0 THEN A$="" ELSE A$="X10^"+STR$(XI%)
5110 XLEN%=LEN(XLAB$):XLEN%=PXMAX%/2-XLEN%*TN2%*.75
5120 LPRINT"M";XLEN%;",";FIX(-290*PSX%/100):LPRINT"P";XLAB$
5130 LPRINT"R";FIX(PXMAX%/10);",0":LPRINT"P";A$
5140 GOTO 5160
5150 XI%=0:XMIN1!=10:XMAX1!=10:OPT3%=1:OPT1%=0:OPT4%=XMIN!:GOTO 4970
5160 K=10:IF YTYPE%=2 THEN K=YMAX!-YMIN!
5170 LPRINT"M0,0":LPRINT"X3,";PYMAX%;",";K
5180 IF YTYPE%=2 THEN GOTO 5410
5190 CLS:LOCATE 3,1:PRINT"******ENTER FOLLOWING INFORMATION FOR Y-AXIS*****":LOC
ATE 6,6
5200 INPUT"NO. OF DIGITS TO BE DISPLAYED TO LEFT OF DECIMAL (1-4):",OPT%
5210 OPT%=OPT%-1:GOSUB 2920
5220 PRINT:INPUT"      NO.OF DIGITS TO BE DISPLAYED TO RIGHT OF DECIMAL (0-2):",O
PT1%
5230 OPT3%=0
5240 STP!=(YMAX1!-YMIN1!)/10:NUM%=INT(PYMAX%/K):OPT5%=FIX(-50*PSY%/100)
5250 LPRINT"M";OPT5%*4;"0"
5260 K=K+1
5270 FOR I=1 TO K
```

```
5280 IF YMIN1!<0 THEN A$="-" ELSE A$=""
5290 A$=A$+STR$(ABS(FIX(YMIN1!)))+"."
5300 IF OPT1%>0 THEN OPT%=ABS(CINT((YMIN1!-FIX(YMIN1!))*10^OPT1%))
5310 IF OPT1%>0 THEN A$=A$+MID$(STR$(OPT%),2,OPT1%)
5320 LPRINT"P";A$:YMIN1!=YMIN1!+STP!
5330 IF OPT3%=1 THEN A$=STR$(FIX(OPT4%))
5340 IF OPT3%=1 THEN LPRINT"R";-TN2%;",";FIX(TN1%*.9):LPRINT"P";A$:OPT4%=OPT4%+1

5350 LPRINT"M";OPT5%*4;",";NUM%*I:NEXT I
5360 IF YI%=0 THEN A$="" ELSE A$="X10^"+STR$(YI%)
5370 YLEN%=LEN(YLAB$):YLEN%=PYMAX%/2-YLEN%*TN2%*.75
5380 LPRINT"Q1":LPRINT"M";FIX(-300*PSY%/100);",";YLEN%:LPRINT"P";YLAB$
5390 LPRINT"RO,";FIX(PYMAX%/10):LPRINT"P";A$
5400 GOTO 5420
5410 YI%=0:YMIN1!=10:YMAX1!=10:OPT3%=1:OPT4%=YMIN!:OPT1%=0:GOTO 5240
5420 K=1:NPLTS%=NPLTS1%:LPRINT"Q0":SOUND 180,10
5430 GOSUB 4430:OPT5%=FIX(TN1%*.4)
5440 FOR I=K TO NPLTS%:LPRINT"J";I
5450 LPRINT"M";FNPX%(T!(1,I));",";FNPY%(EL!(1,I))
5460 FOR J=1 TO N%(I)
5470 IF PTYPE%(I)=1 OR PTYPE%(I)=3 THEN LPRINT"M";FNPX%(T!(J,I));",";FNPY%(EL!(J
,I)):LPRINT"N";I+1;",";TN1%
5480 IF PTYPE%(I)=2 THEN LPRINT"D";FNPX%(T!(J,I));",";FNPY%(EL!(J,I)):LPRINT"N";
I+1;",";TN1%
5490 IF SD!(J,I)=0 THEN GOTO 5540
5500 LPRINT"IO,";FNPY%(SD!(J,I));",";-OPT5%;",0";2*OPT5%;",0
5510 LPRINT"M";FNPX%(T!(J,I));",";FNPY%(EL!(J,I))
5520 LPRINT"IO,";FNPY%(-SD!(J,I));",";-OPT5%;",0";2*OPT5%;",0
5530 LPRINT"M";FNPX%(T!(J,I));",";FNPY%(EL!(J,I))
5540 NEXT J
5550 IF PTYPE%(I)=3 THEN GOSUB 5570
5560 NEXT I:LPRINT"JO":GOTO 1180
5570 REM************************************************************************
5580 REM     ROUTINE FOR POLYNOMIAL PLOTTING
5590 REM************************************************************************
5600 IF NC%(I)=0  THEN RETURN
5610 TMP1!=T!(1,I):TMP2!=TMP1!
5620 FOR M=1 TO N%(I)
5630 IF T!(M,I)<TMP1! THEN TMP1!=T!(M,I)
5640 IF T!(M,I)>TMP2! THEN TMP2!=T!(M,I)
5650 NEXT M
5660 TMP2!=(TMP2!-TMP1!)/100
5670 FOR M=1 TO 101:Y#=0
5680 FOR L=1 TO NC%(I)
5690 Y#=Y#+PNC#(L-1)*TMP1!^(L-1):NEXT L
5700 IF DIV3$="YES" THEN GOTO 5760
5710 X1%=INT((TMP1-XMIN!)*SCX!)+75
5720 Y1%=INT((YMAX!-Y#)*SCY!)+20
5730 IF M=1 THEN GOTO 5750
5740 LINE(XL%,YL%)-(X1%,Y1%),1
5750 YL%=Y1%:XL%=X1%:GOTO 5780
5760 IF M=1 THEN LPRINT"M";FNPX%(TMP1!);",";FNPY%(Y#):GOTO 5780
5770 LPRINT"D";FNPX%(TMP1!);",";FNPY%(Y#)
5780 TMP1!=TMP1!+TMP2!:NEXT M:RETURN
```

```
5790 REM************************************************************************
5800 REM      SPECIAL MATH ROUTINES !!!
5810 REM************************************************************************
5820 CLS:LOCATE 3,6
5830 PRINT"THE FOLLOWING MATH ROUTINES ARE AVAILABLE:"
5840 PRINT:PRINT"       (1) ENTER POLYNOMIAL CURVE PARAMETERS"
5850 PRINT"       (2) MATHEMATICAL MODIFICATION OF X OR Y VALUES"
5860 PRINT"       (3) DETERMINE AREA UNDER THE CURVE"
5870 PRINT"       (4) HORIZONTALLY ALIGN GRAPHS(based on y-minimum"
5880 PRINT"       (5) RETURN TO MAIN MENU"
5890 PRINT:INPUT"       ENTER 1,2,3,4 OR 5:",OPT%:ON OPT% GOTO 5900,6000,6370,650
0,1180
5900 REM************************************************************************
5910 REM     ROUTINE FOR DEFINING POLYNOMIAL PARAMATERS
5920 REM************************************************************************
5930 CLS:LOCATE 6,1:IF NPLTS1%<=0 THEN SOUND 180,3:GOTO 5790
5940 FOR I=1 TO NPLTS1%
5950 PRINT"       ENTER NO.OF COEFFICIENTS FOR GRAPH ";I;
5960 INPUT" (0-9):",NC%(I):PRINT:IF NC%(I)=0 THEN GOTO 5990
5970 FOR L=1 TO NC%(I):PRINT"       ENTER COEFFICIENT ";L-1;:INPUT":",PNC#(L-1)
5980 NEXT L
5990 PRINT:PRINT:NEXT I:GOTO 5790
6000 REM************************************************************************
6010 REM    ROUTINE FOR MATHEMATICAL MODIFICATION OF X OR Y VALUES
6020 REM************************************************************************
6030 CLS:LOCATE 4,6
6040 PRINT"THERE ARE CURRENTLY ";NPLTS1%;" GRAPHS IN MEMORY."
6050 PRINT:INPUT"      ENTER GRAPH NO.TO BE MODIFIED (zero to exit):",NDEL%
6060 IF NDEL%=0 THEN GOTO 5790
6070 IF NDEL%<0 OR NDEL%>NPLTS1% THEN SOUND 180,100:GOTO 5790
6080 PRINT:INPUT"      ENTER PARAMETER TO BE MODIFIED (X OR Y):",D$
6090 CLS:LOCATE 2,6
6100 PRINT"THE FOLLOWING MODIFICATION OPTIONS ARE AVAILABLE:"
6110 PRINT:PRINT"       (1) ADD CONSTANT VALUE "
6120 PRINT"       (2) MULTIPLY BY CONSTANT"
6130 PRINT"       (3) TAKE LOG(base 10)"
6140 PRINT"       (4) TAKE LOG(base e)"
6150 PRINT"       (5) TAKE INVERSE LOG(base 10)"
6160 PRINT"       (6) TAKE INVERSE LOG(base e)":PRINT
6170 INPUT"       ENTER 1,2,3,4,5 OR 6:",OPT%
6180 IF OPT%>6 OR OPT%<1 THEN SOUND 180,3:GOTO 6000
6190 IF OPT%=2 OR OPT%=1 THEN PRINT:INPUT"       ENTER VALUE OF CONSTANT:",X#
6200 FOR I=1 TO N%(NDEL%)
6210 IF D$="Y" THEN Y#=EL!(I,NDEL%):Y5#=SD!(I,NDEL%):GOTO 6240
6220 IF D$="X" THEN Y#=T!(I,NDEL%):GOTO 6240
6230 SOUND 180,4:GOTO 6000
6240 IF D$="X" OR SD!(I,NDEL%)=0 THEN Y5#=1
6250 IF OPT%=1 THEN Y#=Y#+X#
6260 IF OPT%=2 THEN Y#=Y#*X#:Y5#=Y5#*X#
6270 IF OPT%=3 THEN Y#=LOG(Y#)/LOG(10):Y5#=LOG(Y5#)/LOG(10)
6280 IF OPT%=4 THEN Y#=LOG(Y#):Y5#=LOG(Y5#)
6290 IF OPT%=5 THEN Y#=10^Y#:Y5#=10^Y5#
6300 IF OPT%=6 THEN Y#=EXP(Y#):Y5#=EXP(Y5#)
6310 IF SD!(I,NDEL%)=0 THEN Y5#=0
6320 IF D$="X" THEN T!(I,NDEL%)=Y#:SD!(I,NDEL%)=Y5#
6330 IF D$="Y" THEN EL!(I,NDEL%)=Y#
6340 NEXT I:CLS:LOCATE 8,6
6350 INPUT"DO YOU REQUIRE FURTHER MODIFICATION (Y/N)?",D$
6360 IF D$="Y" THEN GOTO 6000 ELSE GOTO 5790
```

```
6370 REM************************************************************************
6380 REM       ROUTINE FOR DETERMINIG AREAS
6390 REM************************************************************************
6400 GOSUB 6680
6410 PRINT:INPUT"      ENTER GRAPH NO.TO BE ANALYZED (zero to exit):",NDEL%
6420 IF NDEL%=0 THEN GOTO 5790
6430 IF NDEL%<0 OR NDEL%>NPLTS1% THEN SOUND 180,100:GOTO 5790
6440 M=NDEL%:SUM!=0
6450 FOR I=2 TO N%(M)
6460 SUM!=SUM!+(T!(I,M)-T!(I-1,M))*(EL!(I,M)+EL!(I-1,M))/2:NEXT I
6470 PRINT:PRINT:BEEP:PRINT"        AREA=";SUM!
6480 PRINT:PRINT:PRINT"       (press any key to continue)"
6490 IF INKEY$="" THEN GOTO 6490 ELSE GOTO 5790
6500 REM************************************************************************
6510 REM          ROUTINE FOR HORIZONTALLY ALIGNING GRAPHS
6520 REM************************************************************************
6530 CLS:LOCATE 8,6
6540 PRINT"ALIGNMENT PROCEDURE UNDER WAY!!"
6550 AVE!=0
6560 FOR I=1 TO NPLTS1%:LOW%(I)=1:YMIN!=EL!(1,I)
6570 FOR J=1 TO N%(I)
6580 IF EL!(J,I)<YMIN! THEN LOW%(I)=J:YMIN!=EL!(J,I)
6590 NEXT J
6600 AVE!=AVE!+T!(LOW%(I),I):NEXT I
6610 AVE!=AVE!/NPLTS1%
6620 FOR I=1 TO NPLTS1%
6630 TMP!=T!(LOW%(I),I)
6640 FOR J=1 TO N%(I)
6650 T!(J,I)=(AVE!-TMP!)+T!(J,I)
6660 NEXT J:NEXT I
6670 PRINT:PRINT:PRINT"       ALIGNMENT COMPLETE!!!":FOR I=1 TO 1000:NEXT I:GOTO
5790
6680 REM************************************************************************
6690 REM          ROUTINE FOR LISTING GRAPHS
6700 REM************************************************************************
6710 CLS:LOCATE 4,6
6720 PRINT"THERE ARE CURRENTLY ";NPLTS1%;"GRAPHS IN MEMORY!"
6730 LOCATE 6,1
6740 PRINT"          GRAPH NO.                GRAPH NAME"
6750 PRINT"          ********                 **********"
6760 PRINT:FOR I=1 TO NPLTS1%:PRINT TAB(11);I;TAB(34);GTITLE$(I)
6770 NEXT I
6780 PRINT:RETURN
```

APPENDIX C

ANALYSIS OF ERRORS IN THE REPORTED THERMAL DATA

The thermal data reported in this thesis, which include transformation temperatures, activation energies, and enthalpy changes for crystallization, were obtained on a Perkin-Elmer DSC-2 differential scanning calorimeter. Before use the temperature interval for the calorimeter was calibrated between the transformation temperatures of indium (429.75 K) and potassium chromate (K_2CrO_4) (943.7 K) to within ±0.5°. Additionally, the temperatures of the melting of zinc at heating rates of 5, 10, 20, 40, and 80 K/min were measured to ±0.2° and the difference between the measured and the actual temperature (692.65 K) were used to correct the measured sample temperatures. The energy axis was calibrated using the heat given off during the melting of indium (6.80 cal/gm).

For the purposes of assessing the error in measuring temperatures off the DSC curves, the composition range of this study was further divided into regions of similar DSC peak character. The very sharp peaks, for example those at 59 or 67 at. % Zr, were measurable to within 0.2°. Near the eutectic at 63.5 at. % Zr, however, the peaks were broader and it was estimated that the temperatures were only measurable to within ±2°. This procedure, when used across the whole composition range of this study, produced Table C-I, where the estimated errors in reading the different peak temperature is presented as a function of composition.

To determine the uncertainty in the reported activation energy data, it was recognized that the error δq of a function calculated from a measured quantity y with its uncertainty δy is[94]

Table C-I. Estimated Errors in Measured DSC Peak Temperatures

Composition (at. % Zr)	Peak No.	Estimated Error (K)
55–60.6	1	±0.2
57.1	HT	±2.0
57.7–62	HT	±0.5
61.2–62	1	±0.5
	2	±0.2
62.8	1	±0.5
	2	±1.0
	3	±2.0
	HT	±1.0
63.2	1	±0.5
	2	±2.0
	3	±1.0
	HT	±2.0
63.5–64.6	1	±0.5
	2	±2.0
	3	±0.5
65	1	±0.5
	2	±1.0
	3	±0.5
65.5	1	±0.5
	2	±1.0
	3	±1.0
66	1	±0.5
	2	±1.0
66.5–71	1	±0.2

$$\delta q = \frac{dq}{dy}\,\delta y \ .$$

From eq. 20 (Chapter II), replacing R by k to determine values per atom instead of per mole,

$$q = \frac{d[\ln(\dot{T}/T^2)]}{d\ (1/T)} = -\Delta E/k \quad ,$$

and

$$\left| d(q)/dT \right| = 2 \ .$$

Therefore

$$\delta(\Delta E) = 2k\delta T$$

where k is Boltzmann's constant (8.6164×10^{-5} eV/atom K) and δT is the error in the measured value of the temperature. Using the maximum estimated uncertainty in the measurement of the temperature ($\pm 2°$), the uncertainty in ΔE is calculated to be $\pm 3.4 \times 10^{-4}$ eV/atom.

An accurate determination of the uncertainty in the enthalpy change on crystallization ΔH was much harder to calculate. The enthalpy change is a function of the area under the DSC curve and the mass of the specimen. Masses were determined by weighing on a digital microbalance and could be measured to within ± 0.003 mg on a 2 mg sample. However, to measure the area under the DSC peaks, the baseline of the DSC trace had to be determined. This could not always be done unambiguously, especially near the eutectic at $Zr_{63.5}Ni_{36.5}$ where several broad peaks appear over a fairly large temperature range. At compositions which

show sharp DSC peaks, the baseline is straight and the error can be determined as a function of the error in the area and weight measurements from[94]

$$\delta(\Delta H)/\Delta H = \sqrt{(\delta A/A)^2 + (\delta W/W)^2} \quad ,$$

where the fractional uncertainty in the area A (as measured in units of DSC chart squares) is estimated to be ±0.05 and in the weight W is ±0.002. The fractional error in ΔH is then ±0.05. The largest ΔH reported in this thesis is at 67 at. % Zr. where ΔH is 5.8 kJ/mole. Therefore the error at this composition is ±0.3 kJ/mole.

If one can assume that the baselines were always determined correctly, the fractional uncertainty of ±0.05 could be applied at all compositions and no error would be larger than ±0.3 kJ/mole. However this assumption can not be made for those composition which exhibit broad multiple peaks and one must turn to statistical methods for determining the error in this situation. Since samples of each splat were annealed in the DSC at each of four or five different heating rates (5, 10, 20, 40, and 80 K/min), each of the DSC traces produced can be used to determine an enthalpy change. For a splat of a particular composition, one can therefore report a $\overline{\Delta H}$ value which is an average of four to five experimental values. The $\overline{\Delta H}$ values reported in Table III of this thesis were determined in this way and are the mean values of four to five measured values. The standard deviation of the mean $\sigma_{\overline{\Delta H}}$, also included in Table III, represents the uncertainty in the mean value. Two sample calculations for the mean enthalpy change $\overline{\Delta H}$ and its

standard deviation $\sigma_{\overline{\Delta H}}$ are presented in Tables C-II and C-III, one for a Zr-Ni composition which gives a sharp DSC peak (59 at. % Zr) and another for one which gives a broad multiple peak pattern (63.5 at. % Zr).

Analyzing the errors by the methods just discussed has resulted in unbelievably small uncertainties for ΔE ($<\pm 4 \times 10^{-4}$ eV/atom) and large uncertainties in $\overline{\Delta H}$ at certain compositions. These uncertainties apply to individual data points in Figs. 10—12. However, two or three data points were taken at each composition, and the repeatability of the values is considered to reflect the accuracy of the methods used to gather the data.

Table C-II. Calculation of $\overline{\Delta H}$ and $\sigma_{\overline{\Delta H}}$ for the Low-Temperature DSC Peaks at 59 at. % Zr

Heating Rate (K/min)	Measured ΔH (kJ/mole)	Deviation from ΔH, d	d^2
5	4.408	−0.141	1.988×10^{-2}
10	4.510	−0.039	0.152×10^{-2}
20	4.582	+0.033	0.109×10^{-2}
40	4.667	+0.118	1.392×10^{-2}
80	4.580	+0.031	0.096×10^{-2}
	$\overline{\Delta H} = 4.549$		$\Sigma d^2 = 3.737 \times 10^{-2}$

$$\sigma_{\Delta H}^2 = \Sigma d^2/N-1 = 9.34 \times 10^{-3}$$

$$\sigma_{\Delta H} = 9.66 \times 10^{-2}$$

$$\sigma_{\overline{\Delta H}} = \frac{\sigma_{\Delta H}}{\sqrt{N}} = 4.32 \times 10^{-2}$$

$$\overline{\Delta H} = 4.55 \pm 0.04 \text{ kJ/mole}$$

Table C-III. Calculation of $\overline{\Delta H}$ and $\sigma_{\overline{\Delta H}}$ for the Low-Temperature DSC Peaks at 63.5 at. % Zr

Heating Rate (K/min)	Measured ΔH (kJ/mole)	Deviation from ΔH, d	d^2
5	5.350	−0.058	0.336×10^{-2}
10	5.155	−0.253	6.401×10^{-2}
20	5.391	−0.017	0.029×10^{-2}
40	5.450	+0.042	0.176×10^{-2}
80	5.695	+0.287	8.237×10^{-2}
	$\overline{\Delta H} = 5.408$		$\Sigma d^2 = 15.179 \times 10^{-2}$

$$\sigma_{\Delta H}^2 = \Sigma d^2/N-1 = 3.79 \times 10^{-2}$$

$$\sigma_{\Delta H} = 0.195$$

$$\sigma_{\overline{\Delta H}} = \frac{\sigma_{\Delta H}}{\sqrt{N}} = 8.72 \times 10^{-2}$$

$$\overline{\Delta H} = 5.41 \pm 0.09 \text{ kJ/mole}$$

VITA

Claudette Gail McKamey was born on February 14, 1950, in Lafollette, Tennessee. She grew up in Lake City, Tennessee, where she attended Lake City Elementary School and Lake City High School, graduating in June 1968. The following September she entered The University of Tennessee at Knoxville and completed her freshman year before dropping out to work.

During the summers of 1968 and 1969, she was employed at the Oak Ridge National Laboratory as a typist in the Metals and Ceramics Division. After working six months for M. F. Flenniken and Co., an insurance company in Knoxville, she again accepted employment at Oak Ridge National Laboratory in March 1970. She was employed as a secretary in the Metals and Ceramics Division until May 1974 and a laboratory technician in the same division from May 1974 until August 1981. During that time she continued to pursue a liberal arts degree at The University of Tennessee, continuing her studies through correspondence school, evening school, or full or part-time day school. In August 1981 she received a Bachelor of Arts degree with a major in physics.

After taking a year off to follow her husband to Los Alamos, New Mexico, she entered The Graduate School of The University of Tennessee, Knoxville, in September 1982. In November 1982, she returned to the Metals and Ceramics Division, Oak Ridge National Laboratory, as a Development Associate in the Alloying Behavior and Design Group. She received the Master of Science degree with a major in Metallurgical Engineering in June 1985.

The author is a member of Phi Beta Kappa, the American Society for Metals, and The Metals Society of the American Institute of Mining, Metallurgical, and Petroleum Engineers. She will continue to be employed at Oak Ridge National Laboratory after graduation.